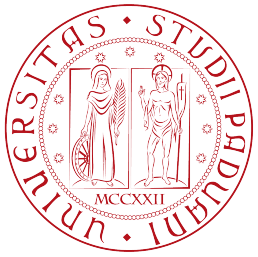

UNIVERSITÀ DEGLI STUDI DI PADOVA

Dipartimento di Fisica e Astronomia "Galileo Galilei"

Corso di Laurea Magistrale in Fisica

Tesi di Laurea

On the spectral properties of inhomogeneous Luttinger liquids

Relatore

Prof./Dr. Volker Meden

Correlatore

Prof./Dr. Luca Salasnich

Contro-relatore

Prof./Dr. Luca Dell'Anna

Laureando

Manuel Simonato

Anno Accademico 2018/2019

A Simone, che quasi sempre può capirmi senza bisogno di parole

Contents

"I just wanted to be one of The Strokes
Now look at the mess you made me make
Hitchhiking with a monogrammed suitcase
Miles away from any half-useful imaginary highway"

Introduction

The physics of one-dimensional systems of interacting fermions strongly differs from the picture offered by Fermi liquid theory [1]. The low-energy properties of metallic, paramagnetic 1D Fermi systems are well described by the Luttinger liquid (LL) theory [1, 2, 3, 4, 5]. Among other properties, the homogeneous LL is known to exhibit power-law behaviour for various correlation functions. For spin rotational invariant models, the exponents can be expressed in terms of a single parameter K_ρ. The LL parameter K_ρ is non-universal, i.e. depends on details of the model considered, such as the interaction, filling factor, and one-particle dispersion relation [6].
The LL concept emerged in the study of homogeneous systems with periodic boundary condition (PBC). In these models the bulk spectral function shows a power-law suppression at energies asymptotically close to the chemical potential μ. Theoretically this is very well understood and the exact LL parameter K_ρ is known for a set of integrable models. In the last decades however, the interest shifted towards the investigation of LLs with PBC including impurities. The fact that these systems have been shown to scale to chains with open ends led to the study of several models where open boundary condition (OBC) are introduced [7]. As the translational invariance is broken, the exponent of the power-law suppression close to the boundary differs from the one in the bulk [6].
In [6] the spectral function for diverse models of LLs with open boundaries is investigated: the Tomonaga-Luttinger model is solved using bosonization and the boundary exponent α_B is found to be linear in the interaction term. This motivates the authors to investigate the spectral properties with first order perturbation theory for the self-energy, namely the Hartree-Fock approximation (HF). Surprisingly this already gives a power-law behaviour and qualitative agreement with the exact spectral function. Also, numerically exact results are obtained with the density-matrix renormalization group (DMRG) method for two lattice models. Again, it is demonstrated that many aspects of the behaviour of the spectral function can be understood within the HF theory. Despite what one usually reads about one-dimensional interacting Fermi systems, *in the presence of the boundary* perturbation theory is already capable of providing meaningful results.

Following this approach, the present work is devoted to the study of the spectral function of two lattice models of LLs with open boundaries with the methods of perturbation theory. The models investigated are the spinless fermions model with nearest neighbour interaction and the 1D Hubbard model.
The first result is obtained employing first order perturbation for the *self-energy*. This problem is best studied in the site representation, and the real-space matrix elements of the HF self-energy are evaluated analytically. Due to the nontrivial structure though, the inversion of the full HF Hamiltonian is to be performed numerically. Within this procedure the spectral function for boundary sites obtained in both models already exhibits power-law behaviour at *two* distinct energies. This is a very interesting observation as the HF approximation for the case of PBC does not capture any of the bulk LL features [6]. The power-law boundary exponents α_B^{HF} are extracted from the numerical data and compared with the results presented in [6].
Successively, analytical results are achieved with first order perturbation for the *Green's function*. In this case it is preferable to work in k-space. Since for the OBC we do not have momentum conservation, a general two body interaction leads to a variety of different scattering vertices. They depend on different combination of the four external quantum numbers and cannot simply be parametrized by the "momentum transfer" as for PBC [6]. The HF self-energy in k-space is therefore not diagonal

and displays a distinctive *non-analytical* structure where two sharp step functions cross the diagonal in (k_F, k_F) and $(\pi - k_F, \pi - k_F)$. The introduction of an effective model then allows us to evaluate analytically the first order correction to the spectral function. This procedure yields a *logarithmic divergence* instead of power-law behaviour. Remarkably, in the spinless fermions model the prefactor of the logarithm is the correct leading order in the expansion of $\alpha_B^{\mathrm{HF}}(v)$ around $v = 0$, where v denotes the interaction term in the model. This indicates that this divergence and other ones at higher order in the perturbative expansion can be summed in a Dyson series to recover the power-law behaviour. In this work we demonstrate that perturbation theory can offer meaningful result in the study of the spectral properties of Luttinger liquids with open boundaries. The main goal is to develop an understanding of the dip appearing at an energy different from the chemical potential while proving that perturbation theory is still successful.

In Chapter 1 an introduction to the Luttinger Liquid theory is presented. Beside offering an overview on the beauty of this topic, the aim is to provide the meaningful framework to contextualise the present work. In Chapter 2 we introduce the aforementioned lattice models in the case for PBC and OBC. For one and the other the non-interacting problem is firstly studied in order to build a solid knowledge before tackling the interacting models with the HF approximation in real space. Chapter 3 offers the necessary theoretical framework to understand the central concept of spectral function. This is then computed numerically for the models of our interest and a careful characterization of its properties is given. In Chapter 4 we display the elegant connection between the spectral function and the Green's function which will enable us to extract analytical results. To do so, we need to own full knowledge of the HF self-energy in k-space and the rest of the chapter is devoted to the computation of the matrix elements for both models at different filling factors. Finally, in Chapter 5 the first order perturbation theory for the Green's function is performed with the employment of an effective model. The analytical results for the spectral function are then compared with the numerical ones obtained with the HF approximation for the self-energy.

Chapter 1

A very short introduction to Luttinger liquids

"In this book anything above one will be high dimensional"
-T. Giamarchi, footnote in *Quantum Physics in One Dimension-*

Less is more

Contrary to our friends working on string theory, we do not need to blow the number of dimensions to have fun. The physics of low dimensional systems indeed offers a plethora of interesting phenomena. The role of dimensionality comes heavily into play for systems of many interacting fermions constrained in one single spatial dimension. In this, the qualitative behaviour is drastically different from their counterparts in higher dimension.
For dimensions $d \geq 2$ a brilliant intuition by Landau led to the elegant framework of Fermi liquid theory. In one dimension this framework collapses down, leaving place for a different description, namely the Luttinger liquid theory (LL). The emergence of the Luttinger liquid concept developed from the initial works of Tomonaga (1950) and Luttinger (1963), and was finally codified by Haldane (1981) in a seminal paper [3].
As one can imagine, the subject is enormously vast and it is unfeasible to give here a comprehensive presentation. Sparkling introductions and reviews to the arguments can be found in [1, 2, 4, 5].
What is of our concern in this chapter, is to obtain an understanding of the central points in LL theory. To appreciate its emergence, one needs to understand what causes the Fermi liquid theory to breakdown in one dimension. We therefore start with a brief and mostly qualitative presentation of the Fermi liquid theory. Obviously, it is far from being exhaustive, and we refer to standard literature for further details. Understanding the role of dimensionality in this theory will allow us to look for what makes it collapse in one dimension. The LL theory is finally presented, paving the way for a deeper understanding of the present work, while providing the relevant framework to contextualise it.

1.1 Overview on Fermi liquid theory

The theory of Fermi liquids arises from the need to account for the behaviour of electrons in three-dimensional metals. It is known that in these systems the Coulomb energy is not negligible when compared to the kinetic energy, neither it is exceedingly larger than the latter. In this condition perturbation theory cannot be properly employed [2]. However, it is also common knowledge that in ordinary metals *everything goes as if* a picture of weakly interacting Fermi gas is valid. The main question to investigate then is how this is possible considering the strong interaction between fermions. Fermi liquid theory [1] provides an answer to this question and serves as a cornerstone in the understanding of interacting Fermi systems [2].

In Fermi liquids a central role is played by the adiabatic switching on of the interaction. This permits a one to one mapping between the low energy excitations of a Fermi gas and those of an interacting electron liquid [4]. These excitations are named *quasi-particles* for their peculiar nature. The high dimensionality is here crucial since it ensures large available phase space. Provided we are investigating the low energy physics of the systems, this produces a very dilute gas of excitations, where the residual interaction between these type of excitations is small. In this way we are guaranteed the 1:1 correspondence with the excitations of a Fermi gas, and the picture delineated above for the electrons in a metal becomes clearer. In a real ordinary metal the interactions are strong, but the essential degrees of freedoms turn out to be the quasiparticles. These are *weakly* interacting, and can be reasonably approximated with a non-interacting particles description. One can state that *the correlation in the electron system are weak, although the interaction may be very strong* [4].

Understanding that quasiparticles are the main characters in this act, it is interesting to analyse their properties in more detail. To this end, it is necessary to introduce the essential concept of the spectral function. A complete presentation is given in Chapter 3, where we need to evaluate this quantity for the systems of our interest. For the moment, it is sufficient to know that the spectral function $A(k,\omega)$ is the probability to find a state with a frequency ω and a momentum k. For a Fermi gas $A(k,\omega) = \delta(\omega - \xi(k))$ where $\xi(k) = \epsilon(k) - \mu$ is the energy relative to the chemical potential. This means that the excitations have a definite energy and momentum, as well as an infinite lifetime since they are exact eigenstates of the Hamiltonian. These excitations are the single-particle states with a given energy-momentum dispersion relation. In the same way, one can say that the addition or removal of a particle in k-state generates an exact eigenstate of the non-interacting system [3].

What happens when the interaction is switched on? The clever intuition by Landau is that this picture is only slightly modified. In this case the elementary particles are not the individual electrons anymore, but are electrons dressed by the density fluctuation around them. A quasiparticle then consists of an electron surrounded by a cloud of particle-hole excitations of the ground state [2].

In the spectral representation the δ-function is broadened to a Lorentzian peak, where the width is related to the strength of the interaction. One can state the quasiparticles have a "well-defined" dispersion relation $\epsilon'(k)$ so that the quasiparticle wave function has a time dependence $e^{-i\epsilon'(k)t}$. As mentioned above, we are interested in the low energy physics, and thus focus on the phase space close to the Fermi wavevector k_F [2]. In this domain we can expand the new dispersion relation to the first order around k_F

$$\epsilon'(k) \simeq \epsilon'(k_F) + \frac{k_F}{m^*}(k - k_F) \tag{1.1}$$

where m^* is the *effective mass* of the quasiparticles. The important point here is that one only needs

[1] Note the habit of physicists to use the term *gas* to denote a set of non-interacting particles and *liquid* for a set of interacting ones. This notion is employed for quantum systems at finite temperature as well as for $T = 0$. It is then clear it has nothing to do with the concept of a classical gas where equilibrium is reached through collisional processes so that interactions *are* present. Rather the term liquid simply emphasises that we are dealing with interacting quantum particles. However, notice that the notion of Fermi liquid denotes now only a particular class of high-dimensional systems of interacting fermions, as other different classes are present, the so-called non-Fermi liquids.

[2] Thanks to the Luttinger theorem applied to rotationally invariant systems, we are guaranteed that k_F for an interacting system must coincide with k_F for the non-interacting one.

to change the bare mass m to m^* to be able to make sense of a non-interacting picture, thanks to the nature of the quasiparticles. The effective mass accounts for the dressing upon the bare electron due to its interaction with the medium and for the effects on the dynamical properties.
In order to claim the quasiparticles have a particle-like nature one also need to argue the stability of these excitations. The period of oscillation $\frac{1}{\epsilon'(k)}$ is given by the linear expansion in (1.1). As we approach the Fermi energy we need the lifetime of the excitation to be greater than this value. In the opposite case the excitations would be overdamped and the picture of quasiparticles would not be valid. The remarkable point is that Landau was able to prove by simple phase space arguments in $d = 3$ that this lifetime τ_k diverges as $\frac{1}{\epsilon'(k)^2}$ when $k \to k_F$, *no matter how strong the interaction is* [2, 3]. This divergence can be tracked down to the diminishing phase space available for scattering when approaching the Fermi level [3].
This fact has evident manifestations on the quasiparticle Lorentzian peak in the spectral function. As the peaks centred around $\xi'(k) \simeq v_F^*(k - k_F)$ move towards k_F, they get sharper and sharper. The width is proportional to $\frac{1}{\tau_k} \simeq (k - k_F)^2$, so that the quasiparticles are better and better defined. The situation is nicely illustrated in figure 1.1.

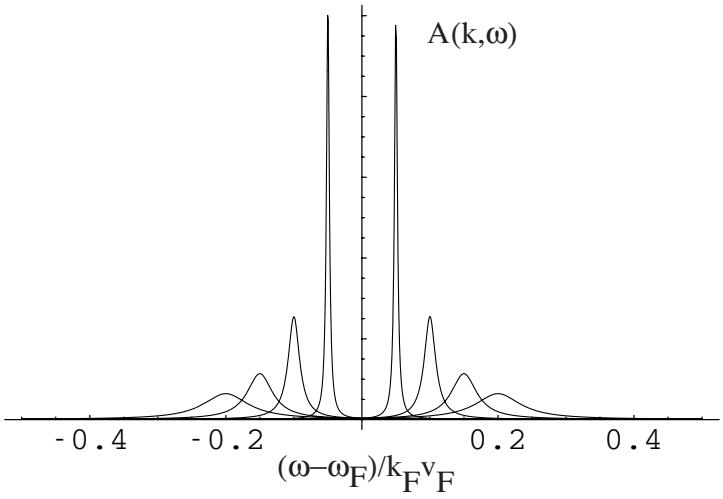

Figure 1.1: *Qualitative sketch of the zero temperature spectral function of an interacting Fermi liquid for different values of k/k_F near the Fermi surface. Here $\omega_F = \epsilon_F/\hbar$. The eight curves, from left to right, correspond to $k/k_F = 0.8, 0.85, 0.9, 0.95, 1.05, 1.1, 1.15, 1.2$. The peak at $k = k_F$ is infinitely sharp and for this reason has not been plotted. Figure taken from [3].*

To have a deeper understanding of the situation we described, it is appreciable to look at the problem from a microscopic point of view. We make use of a important relation for the spectral function which will be clear in Chapter 4

$$A(k,\omega) = -\frac{1}{\pi} \frac{\operatorname{Im}\Sigma(k,\omega)}{\Big[\omega - \epsilon(k) - \operatorname{Re}\Sigma(k,\omega)\Big]^2 + \Big[\operatorname{Im}\Sigma(k,\omega)\Big]^2} \tag{1.2}$$

where Σ denotes the retarded self-energy, $\hbar = 1$ and the spin subscript has been dropped for simplicity. The validity of the Fermi liquid theory requires that [3]

$$\epsilon'(k) = \epsilon(k) + \operatorname{Re}\Sigma\big(k, \epsilon'(k)\big) \tag{1.3}$$

and

[3] It is also interesting to notice that any power which could guarantee this situation would lead to a Fermi liquid, although an unconventional one [3].

$$\operatorname{Im}\Sigma\big(k,\epsilon'(k)\big) \simeq -(k-k_F)^2 \tag{1.4}$$

This two conditions guarantee the spectral function to have the aforementioned Lorentzian peak. This is more evident when we expand to the first order in $\omega - \epsilon'(k)$

$$\omega - \epsilon'(k) \simeq \frac{\omega - \epsilon'(k)}{Z_k} \tag{1.5}$$

where

$$Z_k = \frac{1}{1 - \frac{\partial}{\partial\omega}\operatorname{Re}\Sigma(k,\omega)\Big|_{\epsilon'(k)}} \tag{1.6}$$

while simply evaluating the imaginary part in $\epsilon'(k)$. With the definition of lifetime

$$\frac{1}{2\tau_k} = Z_k \big|\operatorname{Im}\Sigma(k,\epsilon'(k)\big| \tag{1.7}$$

we can recast the spectral function in the form

$$A(k,\omega) \simeq \frac{Z_k}{\pi}\frac{\frac{1}{2\tau_k}}{\big[\omega - \epsilon'(k)\big]^2 + \big[\frac{1}{2\tau_k}\big]^2} \tag{1.8}$$

The quantity Z_k is the strength of the Lorentzian peak and represents the fraction of the electron that remains in the quasiparticle state. The remaining $1 - Z_k$ is distributed to a structureless background, which can be safely ignored compared to the well-defined peaks [2].
Before leaving this section, a few last remarks are important. Indeed the quasiparticle is not the only type of excitation at play in an interacting Fermi system. As we know collective excitations as plasmons and zero sound modes could be present. Further details about this interesting topics are nicely illustrated in [8, 9]. Also we report the fact that a residual interaction between quasiparticles is still present. This interaction is described in Fermi liquid theory by the Landau parameters. Again we do not enter this discussion and refer for example to [10]. Finally, a subtle but very important consideration. The quasiparticle states *are not* the exact eigenstates of the interacting Hamiltonian. They are in fact made of a very large number of exact eigenstates of the interacting system. The separation in energy of these states is exponentially small in the system size L and thus irrelevant physically, for reasonable systems. The cluster of all these states form the quasiparticle with its average energy and lifetime (inverse of the broadening in energy) [2].

1.2 Breakdown of Fermi liquid theory in 1D

We report here purely qualitative arguments as presented in [2, 3], which have the favour of being strikingly intuitive. Clearly, these must be complemented by more mathematical considerations when one seeks to gain a profound comprehension of the topic.
In higher dimension the electron can move through the medium while knocking out other electrons around him, thus giving rise to the aforementioned cloud of particle-hole excitations. In one dimension this is not possible since an electron that tries to propagate has to push its neighbours in the *same spatial dimension*. Any attempt to produce an individual excitation would in fact trigger the motion

of all the particle in the system, giving rise to a *collective* excitation [4]. This qualitative consideration is enough to convince ourselves that there is no possibility to have Fermi liquid theory to work. The main degrees of freedom are collective excitations that are bosonic in nature, conversely to the fermionic quasiparticles we described above.
A fascinating phenomenon occurs when we consider fermions with spin. Since only collective excitations can exist, it implies that a single fermionic excitation has to split into a collective one carrying charge (like a sound wave) and a collective one carrying spin (like a spin wave). These two excitations have in general different velocities so that they "break" into two separated elementary excitations [2]. This qualitatively describes the exotic spin-charge separation, which is one of the essential characteristics of LLs.
The underlying physical picture is that the coupling of quasiparticles to collective excitations is small in 3D but large in 1D, no matter how small the interaction: *correlation are strong even for weak interactions!* [4]. At the heart of this relies the so-called *orthogonality catastrophe*. When adding an electron into the ground state of a strongly correlated N-electrons system it is clear we do not generate an eigenstate of the $N+1$-interacting Hamiltonian. The point is that in one dimension this new state does not even entails a considerable overlap with the previous one. Since the new injected electron lack the proper correlation with the preexisting many-body electron state, the new state of $N+1$-electrons system is essentially orthogonal to the original ground state [3]. In a more profound analysis the quantity Z_k defined for Fermi liquids turns out to be the squared overlap between the two states before and after the injection. This constant now vanishes in thermodynamic limit [3] and therefore destroys any possibility to have a quasiparticle Lorentzian peak in the spectral function.
The last peculiarity we observe is the role of particle-hole excitations in a system of interacting fermions. For an homogeneous system where the notion of momentum is valid, an electron of momentum k is destroyed underneath the Fermi surface and one with momentum $k+q$ is created above the Fermi surface, so that the momentum of the excitation is well fixed and equal to q. In high dimensions the energy of such an excitation depends on *both* k and q [2]. For $q < 2k_F$ one can create particle-hole pairs by removing an electron just below the Fermi surface and creating one just above the Fermi surface at another point. In $d = 3$ for example, the Fermi sphere is *indeed* a sphere, while in $d = 1$ it reduces to two points $\pm k_F$. This very fact implies that in $d = 3$ the spectrum of particle-hole excitation is a continuum extending to zero energy for all $q < 2k_F$. In $d = 1$ this is not possible since the only points in phase space where the excitation energy can reach zero is for $q = 0$ or $q = 2k_F$. Notice that this is the *only* way to produce the low-energy excitations we are interested in [2].
It can be shown that these excitations are well-defined particles, in the sense that the average energy only depends on the momentum q and the dispersion on the average energy goes to zero faster that the average itself for $q \to 0$ [2]. These density fluctuations consist in annihilation and creation of fermions and are therefore bosonic in nature. This bosonic excitations will described the collective modes we mentioned above, and are in fact the elementary excitations in a one-dimensional system of interacting fermions.

1.3 Luttinger liquid theory

Understanding the breakdown of FL theory in one dimension already endowed us with a first qualitative idea of what a Luttinger liquid is. We now give a rigorous definition and then proceed with a brief tour on the main properties characterizing this concept.
A Luttinger liquid is a paramagnetic one-dimensional metal without Landau quasiparticle excitations [4]. Paramagnetic and metal require that the spin and charge excitations are gapless, more precisely with dispersion relation $\omega_\nu(q) = v_\nu|q|$ for small $|q|$, where the subscript $\nu = \rho, \sigma$ denotes charge and spin respectively. As we already pointed out this two velocities are in general different, leading to two

[4] To some extent this is similar to the case of university students sitting in the usual narrow row while attending a lecture. When someone in the middle needs to go out, at least half of the row must stand and slide out to let him/her pass. Of course the motion of electrons is much more correlated than university students and the whole system is involved in the excitation.

different types of *bosonic* excitations, namely the *holons* and the *spinons*, which have different excitation energies [4]. Beside spin-charge separation it is important to mention other interesting features that characterize the LL phase:

> At $T = 0$ the system is at a (quantum) critical point, with power-law correlations, and the scaling relations between the exponents of its correlation functions are parametrised by renormalized coupling constants K_ν. For Luttinger liquids, K_ν is the equivalent of the Landau parameters. [...] The K_ν therefore only depend on the low-energy properties of the Hamiltonian. Two parameters per degree of freedom, K_ν and v_ν, completely describe the physics of a Luttinger liquid [4].

We are not going to investigate this topic further and refer to the detailed reviews [1, 4] for a complete analysis. However, a short comment about the widely employed method of *bosonization* is important, as this one emphasises the bosonic nature of the problem. We understood the elementary low-energy excitations are stable particles, i.e. they have a well-defined energy-momentum dispersion relation $\omega_\nu(q) = v_\nu|q|$. True bosons - in the mathematical sense - can be obtained as linear combination of particle-hole excitations. The main advantage is that any Hamiltonian of interacting fermions in 1D can be recast in the form of uncoupled harmonic oscillators [4]. For a *strictly linear* dispersion relation $\epsilon_n = v_F k_n$, the Hamiltonian for a system of non-interacting fermions [5] is refashioned using the *exact operator identity (Kronig identity)* [5]

$$H_0 = \sum_{n=1}^{\infty} v_F k_n c_n^\dagger c_n = \frac{v_F \pi}{L} \sum_{l=1}^{\infty} \left[l b_l^\dagger b_l + \frac{1}{2} N(N+1) \right] \tag{1.9}$$

where the operators b_l are defined as

$$b_l = \frac{1}{\sqrt{l}} \sum_{m=1}^{\infty} c_m^\dagger c_{m+l} \tag{1.10}$$

v_F is the Fermi velocity and N the total particle number operator

$$N = \sum_{n=1}^{\infty} c_n^\dagger c_n \tag{1.11}$$

The operators b_l and $b_l^\dagger$ create a linear combination of particle-hole excitations. The interesting point is that they obey *bosonic commutation relations* in the subspace of all possible N-particle states [5], and represent therefore true bosonic excitations. What happens when the interaction is turned on? If we are guaranteed a gapless dispersion relation in both charge and spin sector is preserved, we have a Luttinger liquid [4]. Remarkably, the Hamiltonian for the interacting fermions is still a quadratic form in the bosons operator [5]. For fermions with spin it can be shown [1, 4, 5] that the interaction between electrons lifts the degeneracy by making $v_\rho \neq v_\nu \neq v_F$, leading to spin-charge separation.
Diverse models have been involved in the study of LL phenomenology. Historically, the main model that has been investigated is the Tomonaga-Luttinger model (TL), as it exhibits all the interesting features of the general Luttinger liquid paradigm. In fact, as exceptionally nicely phrased in [3]

> [..] one may say that the TL model is to the Luttinger liquid concept what the Fermi gas is to the normal Landau Fermi liquid. These two exactly solvable models serve as archetypes for two qualitatively different classes of systems - Fermi liquids and Luttinger liquids: a perturbative connection exists only between two systems in the same class, but not between two systems in different classes.

The model Hamiltonian is not presented here, since it is out of the scope of this introduction. A formal derivation and its solution can be found in [3, 5]. Without entering the details we recall that

[5] This is the case for spinless fermions with open boundary condition where $k_n = n\frac{\pi}{L}$, and it will be illustrated in detail in the next chapter. For the moment it suffices to promote our qualitative considerations up to a more formal level.

the exact solution to this model can be obtained using Ward identities as well as bosonization [5]. Beside this model, integrable lattice models played a prominent role in the emergence of the general Luttinger liquid concept. They can be exactly solved by Bethe ansatz [5]. The two most important models are the spinless fermions with nearest neighbour interaction and the one dimensional Hubbard model. These model are at the very centre of the present work and will be presented in detail in the next chapters.

1.4 On the experimental verification of LL behaviour

After this introduction on the properties LLs, it is natural to ask whether this exotic behaviour is effectively realized in Nature, or purely remains an elegant abstract concept. Indeed huge efforts have been made in the last decades to attempt to verify (approximately) the physics of Luttinger liquids [5]. It is clear that strictly one dimensional system cannot be realized, but luckily there is no need for that. Experimental verification of LL behaviour can be obtained for systems where the predominant character is one dimensional. Following the presentation given in [5], we display here a brief list with the most important systems [6].

- Highly anisotropic "quasi-one-dimensional" conductors: extensive work has been performed on organic conductors, such as the Bechgaard salts as well as the inorganic materials.
- Artificial quantum wires: the two most important types of realizations are quantum wires in *semiconductor heterostructures* and quantum wires on *surface substrates*.
- Carbon nanotubes: these consist of long cylindrical fullerenes (i.e. long carbon-based cylinders) and are therefore quantum wire as well. Listing them separately emphasises their importance in future applications like *molecular electronics*.
- Fractional quantum Hall fluids: electrons at the edges of a two-dimensional fractional quantum Hall system can be described as a *chiral Luttinger Liquid*.

An important note is to be made upon the experimental techniques involved in the aforementioned verifications. Promising ones are high resolution photoemission and the characterization of transport and optical properties. The angular integrated photoemission of the Bechgaard salt $(TMTSF)_2PF_6$ for example showed a power-law suppression at the chemical potential. It is still to be understood whether this behaviour can be simply explained by LL theory and the question remains open. It is clear that the experimental verification of Luttinger liquid phenomenology requires to overcome very subtle problems for both theoreticians and experimentalists. For a great and exhaustive review on this topic the interested reader is referred to [11].

[6] For further details and complete references we refer directly to the cited review.

Chapter 2

The models

"A mathematical model is a compromise between the overwhelming complexity of reality and the elegant abstract constructions of mathematics."
-S. Salsa, *opening a lecture on PDEs-*

We introduce here the lattice models exhibiting the fascinating LL behaviour described in the previous chapter. Before analysing the full interacting problem, a complete description of the non-interacting case is given for both the models. All the systems in this work will be studied for $T = 0$.
The homogeneous problem is firstly presented where periodic boundary conditions are employed. Once a solid knowledge is achieved, we proceed with the introduction of open boundary conditions. In this case translational invariance is broken and we are therefore dealing with an *inhomogeneous* Luttinger liquid. It is known [6] that this class exhibits interesting spectral properties close to boundaries, which differs from the one in the bulk. Here and throughout the whole work the method employed to tackle the interacting problem is the machinery of perturbation theory. It has already been proved capable of providing meaningful results [6] and we will exploit this method in detail.

2.1 Non-interacting spinless fermions

2.1.1 Fermions on a necklace

The principle model we are going to investigate is the spinless fermions model [1] defined on a one dimensional lattice with nearest neighbour interaction. The case of an infinite homogeneous system is modelled by the introduction of periodic boundary condition (PBC). Labelling with the index j the sites in our lattice, this condition allows us to picture our model as a ring or a necklace, where we identify the site $j = 0$ with the one $j = L$. Fermions can hop back and forth from one site to another with a hopping energy t, while the lattice constant a is set to unity. The free Hamiltonian in PBC then is

$$H_0 = -t \sum_{j=0}^{L-1} c_{j+1}^\dagger c_j + \text{h.c.} \tag{2.1}$$

where $c_j^\dagger$ (c_j) denotes the creation (annihilation) operator at site j. The eigenstates of this Hamiltonian are easily found thanks to the symmetry of the system.

[1] In the literature, it may be sometimes addressed as *hardcore boson model*.

We introduce the orthonormal set of basis functions $|n\rangle$, eigenstates of the lattice momentum operator. The overlap to the real space basis $|j\rangle$ reads

$$\langle n|j\rangle = \frac{1}{\sqrt{L}} e^{ik_n j} \tag{2.2}$$

Due to the boundary condition it is easy to verify that k_n must be quantized as $k_n = \frac{2\pi}{L} n$, where n is an integer number between 0 and $L-1$. Introducing the creation and annihilation operator in momentum space

$$c_j = \sum_{n=0}^{L-1} \langle n|j\rangle \, c_n \qquad \text{and} \qquad c_j^\dagger = \sum_{n=0}^{L-1} \langle j|n\rangle \, c_n^\dagger$$

we can recast the free Hamiltonian in the form:

$$H_0 = -\frac{t}{L} \sum_{j=0}^{L-1} \sum_{n,n'=0}^{L-1} e^{-i\frac{2\pi}{L} n(j+1)} e^{i\frac{2\pi}{L} n' j} c_n^\dagger c_{n'} + \text{h.c.}$$

The sum in j is easily performed and gives $\delta_{n,n'} L$ so we obtain:

$$H_0 = -2t \sum_{n=0}^{L-1} \cos(k_n) n_{k_n} \tag{2.3}$$

where $n_{k_n} = c_n^\dagger c_n$ indicates the number operator in state $|n\rangle$. As we expected, plane waves are suitable functions to diagonalize the free Hamiltonian. From the dispersion relation in (2.3) it is clear the system forms a band with bandwidth equal to $4t$. We can choose the index n to run from $\frac{-L}{2}$ to $\frac{L-1}{2}$ thanks to the transational symmetry. If N_F denotes the number of particle in the system, the ground state is obtained by filling the one particle states from $\frac{-N_F}{2}$ to $\frac{N_F}{2}$.

2.1.2 Fermions on an open chain

As previously mentioned, the case of interest in this work is the inhomogeneous system. In general, the role of inhomogeneity can be played both by impurities in the lattice and by the finite size of the lattice, taken into account imposing open boundary condition (OBC). Here we are going to focus on the second case. In this case our 1D lattice can be thought of as an open chain rather than a necklace, upon which fermions can hop from site j to $j+1$ and vice versa. For practical convenience we label the two extremes of the chain with $j = 1$ and $j = L-1$, resulting with $L-1$ accessible lattice sites, and thus a maximum of $N = L-1$ fermions in the system. The free Hamiltonian for spinless fermions with open boundary condition then reads:

$$H_0 = -t \sum_{j=1}^{L-2} c_{j+1}^\dagger c_j + \text{h.c.} \tag{2.4}$$

Since our system is not transational invariant anymore, plane waves surely do not provide a suitable basis to diagonalize this Hamiltonian. Instead, we can make use of a set of sine functions, constrained to zero at the extremes of our lattice by the boundary condition. We introduce then a new (finite) orthonormal basis $|n\rangle$ with overlap to the real space basis given as:

$$\langle n|j\rangle = \sqrt{\frac{2}{L}} \sin(k_n j) \tag{2.5}$$

Due to the open boundary condition we are dealing with, k_n must be quantized as $k_n = \frac{\pi}{L}n$, where n is a positive integer number $n = 1, ..., L-1$. The factor $\sqrt{\frac{2}{L}}$ guarantees the correct normalization:

$$\begin{aligned}
\sum_{j=1}^{L-1} |\langle n|j\rangle|^2 &= \frac{2}{L}\sum_{j=1}^{L-1} \sin^2\Big(\frac{\pi}{L}nj\Big) \\
&= -\frac{1}{2L}\sum_{j=1}^{L-1}\Big(e^{i\frac{2\pi}{L}nj} - e^{-i\frac{2\pi}{L}nj}\Big)^2 \\
&= -\frac{1}{2L}\sum_{j=1}^{L-1}\Big(e^{i\frac{2\pi}{L}nj} + e^{-i\frac{2\pi}{L}nj} - 2\Big) \\
&= -\frac{1}{2L}\left[\frac{1-e^{i2\pi n}}{1-e^{i\frac{2\pi}{L}nj}} - 1 + \frac{1-e^{-i2\pi n}}{1-e^{-i\frac{2\pi}{L}nj}} - 1 - 2(L-1)\right] \\
&= -\frac{1}{2L}\big[-2-2(L-1)\big] = 1
\end{aligned}$$

This new set of basis functions is our best candidate to diagonalize the Hamiltonian in (2.4). The operators in real space can now be represented as linear combination of operators c_n and $c_n^\dagger$, respectively annihilating and creating a fermion in state $|n\rangle$:

$$c_j = \sqrt{\frac{2}{L}}\sum_{n=1}^{L-1}\sin\Big(\frac{\pi}{L}nj\Big)c_n \qquad c_j^\dagger = \sqrt{\frac{2}{L}}\sum_{n=1}^{L-1}\sin\Big(\frac{\pi}{L}nj\Big)c_n^\dagger$$

We plug this representation into the expression for the free Hamiltonian in (2.4) to obtain:

$$\begin{aligned}
H_0 &= -t\frac{2}{L}\sum_{j=1}^{L-2}\sum_{n,n'=1}^{L-1}\sin\Big(\frac{\pi}{L}n(j+1)\Big)\sin\Big(\frac{\pi}{L}n'j\Big)c_n^\dagger c_{n'} + \text{h.c.} \\
&= -t\frac{2}{L}\sum_{n=1}^{L-1}\sum_{n'=1}^{L-1}c_n^\dagger c_{n'}\sum_{j=1}^{L-2}\sin\Big(\frac{\pi}{L}n(j+1)\Big)\sin\Big(\frac{\pi}{L}n'j\Big) + \text{h.c.}
\end{aligned}$$

We have to perform the sum over the real space index j. The first and last indexes can be extended, since we are guaranteed to introduce two vanishing terms by the condition imposed on k_n. Introducing the exponential representation then we get:

$$-t\frac{2}{L}\sum_{j=1}^{L-2}\sin\Big(\frac{\pi}{L}n(j+1)\Big)\sin\Big(\frac{\pi}{L}n'j\Big) = t\frac{2}{L}\sum_{j=0}^{L-1}\left[e^{i\frac{\pi}{L}\left(n(j+1)+n'j\right)} - e^{i\frac{\pi}{L}\left(n(j+1)-n'j\right)}\right] + \text{c.c.}$$

$$= -t\frac{2}{L}\left[-e^{i\frac{\pi}{L}n}\delta_{nn'}L - e^{i\frac{\pi}{L}n}(1-\delta_{nn'})\frac{1-e^{i\pi(n-n')}}{1-e^{i\frac{\pi}{L}(n-n')}} + e^{i\frac{\pi}{L}n}\frac{1-e^{i\pi(n+n')}}{1-e^{i\frac{\pi}{L}(n+n')}}\right] + \text{c.c.}$$

$$= -t\cos\Big(\frac{\pi}{L}n\Big)\delta_{nn'} + \frac{t}{2L}\left[\frac{1-(-1)^{(n+n')}}{1-\cos(\frac{\pi}{L}(n+n'))} - \frac{1-(-1)^{(n-n')}}{1-\cos(\frac{\pi}{L}(n-n'))}\right]\left[\cos\big(\frac{\pi}{L}n\big) - \cos\big(\frac{\pi}{L}n'\big)\right]$$

$$= -t\cos\Big(\frac{\pi}{L}n\Big)\delta_{nn'} + f(n,n')$$

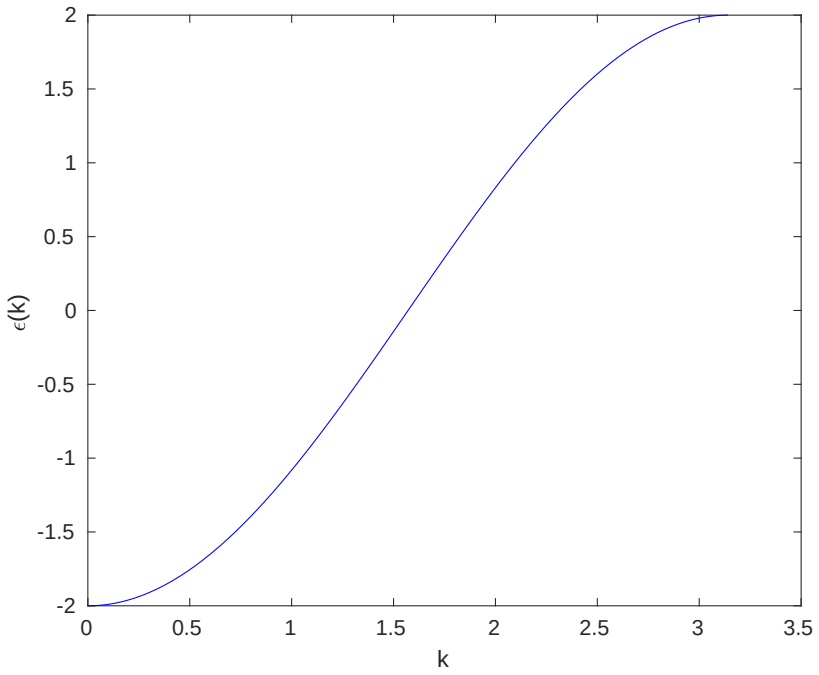

Figure 2.1: *Eigenvalues for the non interacting system with OBC. Here* $L-1=4000$ *and* $N_F=2000$.

So far we did not take into account the hermitian conjugate term in the free Hamiltonian. The sum we have to compute though is nothing but the same we already did, provided we swap the index n with n'. Luckily, the function $f(n,n')$ is antisymmetric under exchange of indexes

$$f(n,n') = -f(n',n)$$

while the first term is not. Once we add the two results together then, those terms cancel out and we are left with:

$$H_0 = -2t\sum_{n=1}^{L-1}\cos\left(\frac{\pi}{L}n\right)c_n^\dagger c_n \tag{2.6}$$

We have succeeded in diagonalizing the free Hamiltonian, making use of new, physically motivated, basis functions. These functions are the eigenstates of the non interacting system we are studying, with eigenenergies

$$\epsilon_{k_n} = -2t\cos\left(\frac{\pi}{L}n\right) \tag{2.7}$$

We conclude that for the free OBC case the dispersion relation is formally equivalent to the free PBC case, provided we introduce the right quantization condition on k. In figure 2.1 we plot the eigenvalues ϵ as a function of k_n for half filling. Here and throughout the whole work we set $t=1$ in the numerical results.

2.2 Interacting spinless fermions: mean field approach

Things get more interesting when interaction is turned on. Double occupancy on a single site j is forbidden for spinless fermions so that we introduce the nearest neighbour interaction

$$H_I = v \sum_j n_j n_{j+1} \tag{2.8}$$

The Hamiltonian can be recast into the more incisive form

$$H = -t \sum_j c_{j+1}^\dagger c_j + \text{h.c.} + v \sum_j c_j^\dagger c_{j+1}^\dagger c_{j+1} c_j = H_0 + H_I \tag{2.9}$$

Such a model is known from the literature to share the characteristics of a LL for $|v| < 2|t|$ [5, 6]. To tackle the full Hamiltonian, we follow in this work the approach delineated in [6] and study the interacting system in the mean field approximation. In perturbation theory this is also referred to as Hartree-Fock approximation[2](HF). We are going to see that this approximation already gives meaningful results for the spectral properties we are interested in. The interacting HF Hamiltonian in real space then is

$$H_I^{\text{HF}} = \underbrace{\sum_j v \langle n_{j+1} \rangle c_j^\dagger c_j + \sum_j v \langle n_j \rangle c_{j+1}^\dagger c_{j+1}}_{\text{direct}} \underbrace{- v \sum_j \langle c_{j+1}^\dagger c_j \rangle c_j^\dagger c_{j+1} - v \sum_j \langle c_j^\dagger c_{j+1} \rangle c_{j+1}^\dagger c_j}_{\text{exchange}} \tag{2.10}$$

where the brackets denotes the expectation value with respect to the non-interacting ground state. As we did before, we first face the homogeneous case, and then proceed with the inhomogeneous one.

2.2.1 Periodic Boundary Condition

Investigating the mean field approach in the PBC case will serve as solid grounds for a better understanding of the OBC case, while underlying similarities and differences. We better make use of the basis $|n\rangle$, where the free Hamiltonian is diagonal. For the off-diagonal terms we have:

$$c_{j+1}^\dagger c_j = \sum_{n=0}^{L-1} \langle j+1|n\rangle c_n^\dagger \sum_{n'=0}^{L-1} \langle n'|j\rangle c_{n'} = \frac{1}{L} \sum_{n=0}^{L-1} \sum_{n'=0}^{L-1} c_n^\dagger c_{n'} e^{-i\frac{2\pi}{L}n} e^{-i\frac{2\pi}{L}j(n-n')}$$

We have to compute the expectation value of this operator with respect to the non interacting ground state, this being the antisymmetrized tensor product of single particle eigenstates $|n\rangle$. The "Fermi sphere", which is a one dimensional interval, is filled up to a momentum $k_F = \frac{2\pi}{L} N_F$, with N_F the number of fermions in our model. This gives

$$\langle c_n^\dagger c_{n'} \rangle = \delta_{nn'} n_{k_n} \tag{2.11}$$

Where n_k is the expectation value for the particle number operator in the state $|n\rangle$. For N_F even we have then:

[2]To be more precise this is the non self-consistent Hartree-Fock approximation

$$\langle c^\dagger_{j+1} c_j \rangle = \frac{1}{L} \sum_{n=-N_F/2}^{N_F/2-1} e^{-i\frac{2\pi}{L}n} = \frac{1}{L} \sum_{n=0}^{N_F-1} e^{-i\frac{2\pi}{L}(m-N_F/2)}$$
$$= \frac{1}{L} e^{i\frac{2\pi}{L}N_F/2} \frac{1-e^{-i\frac{2\pi}{L}N_F}}{1-e^{-i\frac{2\pi}{L}}} = \frac{1}{L} \frac{e^{i\pi\eta} - e^{-i\pi\eta}}{1-e^{-i\frac{2\pi}{L}}}$$

where we explicitly introduced the number density $\eta = N_F/L$, sometimes referred to as filling factor. In the thermodynamic limit $L \to \infty$ while η is kept finite:

$$\langle c^\dagger_{j+1} c_j \rangle =: \frac{t_0}{v} \longrightarrow \frac{\sin(\pi\eta)}{\pi} \tag{2.12}$$

For odd N_F analogous computation leads to

$$\frac{t_0}{v} = \frac{2}{L} \frac{\sin(\pi\eta)\sin(\frac{\pi}{L})}{1-\cos(\frac{2\pi}{L})} \longrightarrow \frac{\sin(\pi\eta)}{\pi}$$

The expectation value of the hermitian conjugate term in the HF Hamiltonian leads to the same expression when taking the thermodynamic limit. As a result of the interaction between fermions, an effective *homogeneous* hopping term t_0 appears. We can therefore define a *renormalized*, filling-dependent hopping term

$$t' = t + t_0 = t + v\frac{\sin(\pi\eta)}{\pi} \tag{2.13}$$

We now take care of the diagonal terms in (2.10). We have to compute the expectation value of the number density operator with respect to the non-interacting ground state. It is thus clear that this value must be equal to η. For the sake of completeness though:

$$\langle n_j \rangle = \frac{1}{L} \sum_{n,n'=0}^{L-1} e^{-i\frac{2\pi}{L}j(n-n')} \langle c^\dagger_n c_{n'} \rangle = \frac{1}{L} \sum_{\frac{N_F}{2}}^{\frac{N_F}{2}-1} 1 = \frac{N_F}{L} = \eta \tag{2.14}$$

Still this is an *homogeneous* term, as expected from the translational symmetry of the problem. Since the same result holds for the term $\langle n_{j+1} \rangle$ we conclude that the direct term in our first order approximation is nothing but a constant on-site energy over the whole chain, whose value is proportional to the strength of the interaction v. Defining $u = 2v\eta$ the mean-field Hamiltonian now reads:

$$H^{\mathrm{HF}} = -t' \sum_{j=0}^{L-1} c^\dagger_{j+1} c_j + \mathrm{h.c} + u \sum_{j=0}^{L-1} c^\dagger_j c_j \tag{2.15}$$

Indeed this Hamiltonian is diagonalized by the non interacting eigenstates $|n\rangle$, our dear old plane waves, as it can be easily verified.

$$H^{\mathrm{HF}} = \sum_{n=0}^{L-1} \epsilon'(k) c^\dagger_n c_n \qquad \text{where} \qquad \epsilon'(k) = u - 2t'\cos\left(\frac{2\pi}{L}n\right) \tag{2.16}$$

As we can infer from new dispersion relation in (2.16) the interaction between fermions modifies the bandwidth from $4t$ to $4t'$. In figure 2.2 we show how the band has been stretched due to the repulsion for $v > 0$ and different values of the filling. The diagonal term in (2.15) leads to a shift in the chemical

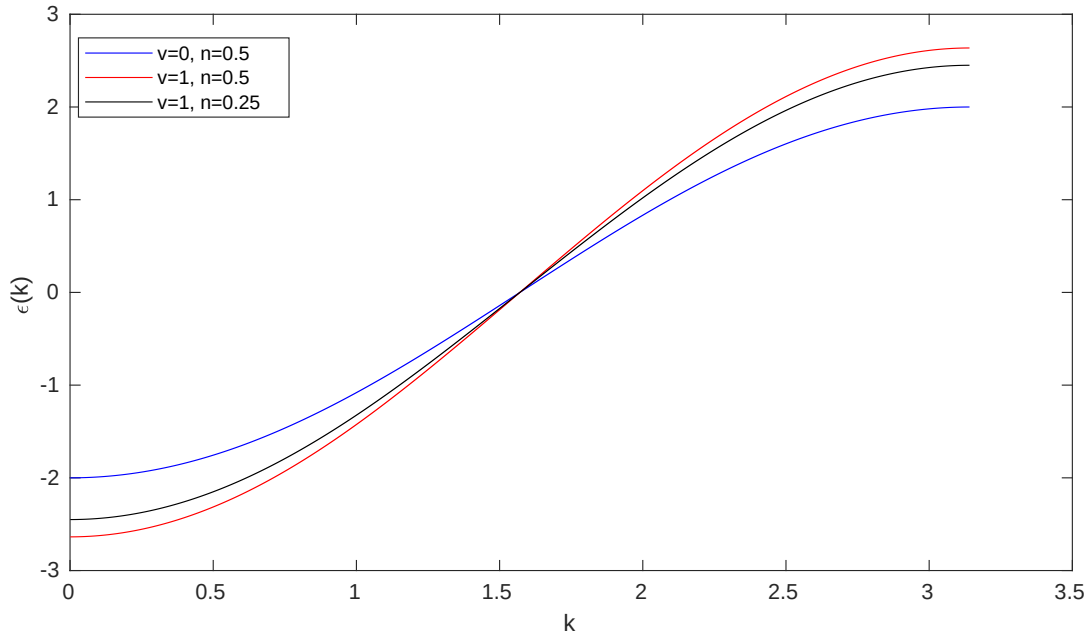

Figure 2.2: *Eingenvalues for the interacting case in PBC, with L-1=4000. In order to keep the comparison with the OBC clear, we only plot the positive k branch of the dispersion relation. For details see the text.*

potential $\delta\mu$ due to the interaction. As for our purpose this is not important, it has been set to zero in the previous plot. This choice will be employed for all the subsequent plots presented in this work[3].

2.2.2 Open Boundary Condition

We now want to see how the matrix elements in equation (2.10) look like in the case of open boundary conditions. Again we represent the operator in the basis $|n\rangle$, eigenstates of the free Hamiltonian with OBC. With k being $\frac{\pi}{L}n$ and analogously for k' we have for the off-diagonal terms:

$$\begin{aligned}
\langle c_j^\dagger c_{j+1}\rangle = \sum_{n,n'=0}^{L-1} \frac{2}{L}\sin(kj)\sin\left[k'(j+1)\right]\langle c_n^\dagger c_{n'}\rangle &= \frac{2}{L}\sum_{n=1}^{n=N_F}\sin(kj)\sin\left[k(j+1)\right] \\
&= -\frac{1}{2L}\sum_{n=1}^{n=N_F}\left(e^{ikj}-e^{-ikj}\right)\left(e^{ikj}e^{ik}-e^{-ikj}e^{-ik}\right) \\
&= -\frac{1}{2L}\sum_{n=1}^{n=N_F}\left(e^{ik(2j+1)}-e^{-ik(2j+1)}-e^{ik}-e^{-ik}\right) \\
&= -\frac{1}{2L}\sum_{n=1}^{n=N_F}\left(e^{i\frac{\pi}{L}(2j+1)}-e^{-i\frac{\pi}{L}(2j+1)}-e^{i\frac{\pi}{L}}-e^{-i\frac{\pi}{L}}\right)
\end{aligned}$$

Making use of the the partial sum of the geometric series we obtain:

$$\langle c_j^\dagger c_{j+1}\rangle = -\frac{1}{2L}\left[\frac{1-e^{i\frac{\pi}{L}(N_F+1)(2j+1)}}{1-e^{i\frac{\pi}{L}(2j+1)}}-\frac{1-e^{i\frac{\pi}{L}(N_F+1)}}{1-e^{i\frac{\pi}{L}}}+\text{c.c.}\right] \tag{2.17}$$

[3]Technically, that is to say we chose to work with an effective HF Hamiltonian $\tilde{H}^{\text{HF}} = H^{\text{HF}} - \delta\mu\mathbb{I}$, where the diagonal contribution leading to a shift in μ is subtracted.

In order to keep the derivation as clear as possible, we set now $\beta = \frac{\pi}{L}$ and $\alpha = \beta(2j+1)$:

$$\langle c_j^\dagger c_{j+1} \rangle = -\frac{1}{2L}\Big[g(\alpha) - g(\beta)\Big] \tag{2.18}$$

with the function $g(\alpha)$ defined as

$$g(\alpha) = \frac{1 - e^{-i\alpha} - e^{-i\alpha(N_F+1)} + e^{i\alpha N_F} + \text{c.c.}}{2(1-\cos\alpha)} \tag{2.19}$$

$$\begin{aligned}
\langle c_j^\dagger c_{j+1} \rangle &= -\frac{1}{2L}\left[\frac{1 - \cos\alpha + \cos(\alpha N_F) - \cos\big(\alpha(N_F+1)\big)}{2(1-\cos\alpha)} - g(\beta)\right] \\
&= -\frac{1}{2L}\left[1 + \frac{-\cos\big(\alpha(N_F+1)\big) + \cos(\alpha N_F)}{1-\cos\alpha} - g(\beta)\right] \\
&= -\frac{1}{2L}\left[\frac{2\sin\big(\frac{\alpha(2N_F+1)}{2}\big)\sin(\frac{\alpha}{2})}{2\sin^2(\frac{\alpha}{2})} - g(\beta)\right]
\end{aligned}$$

Finally, by simplifying and restoring the real value of α and β we are left with

$$\langle c_j^\dagger c_{j+1} \rangle = -\frac{1}{2L}\left[\frac{\sin\big(\frac{\pi}{2L}(2N_F+1)(2j+1)\big)}{\sin\big(\frac{\pi}{2L}(2j+1)\big)} - \frac{\sin\big(\frac{\pi}{2L}(2N_F+1)\big)}{\sin\big(\frac{\pi}{2L}\big)}\right] \tag{2.20}$$

We put now everything together to obtain the renormalized hopping term with open boundaries

$$t'_j = t + t_1(j) + t_0 = t - \frac{v}{2L}\left[\frac{\sin\big(\frac{\pi}{2L}(2N_F+1)(2j+1)\big)}{\sin\big(\frac{\pi}{2L}(2j+1)\big)}\right] + \frac{v}{2L}\left[\frac{\sin\big(\frac{\pi}{2L}(2N_F+1)\big)}{\sin\big(\frac{\pi}{2L}\big)}\right] \tag{2.21}$$

Equation (2.21) shows that the renormalized hopping is now split into a homogeneous component and an inhomogeneous one. The interaction between fermions in the case of OBC is responsible for the appearing of a spatial dependence in the hopping term. Naturally the system cannot distinguish, for example, between the "left" and "right" extreme on the chain. That is, it is still invariant under point reflection through the centre of the lattice, since nothing we introduced can break this symmetry[4]. This is evident in the hopping term we found: given the mapping $j \longrightarrow L-1-j$, it is trivial to show that t'_j is left unchanged. In a similar fashion for the Hartree terms on the diagonal we compute:

$$\langle c_j^\dagger c_j \rangle = \frac{2}{L}\sum_n^{N_F} \sin^2(\frac{\pi}{L}nj) = -\frac{1}{2L}\sum_n^{N_F}\Big(e^{i\frac{\pi}{L}nj} - e^{-i\frac{\pi}{L}nj}\Big)^2 = -\frac{1}{2L}\Big(2N_F + g(\gamma)\Big) \tag{2.22}$$

Where in the last equality we defined $\gamma = \frac{2\pi}{L}j$ and we took advantage of the definition of the function g as given in (2.19). Recasting the latter in the more appealing form we already derived one gets:

$$\langle c_j^\dagger c_j \rangle = -\frac{1}{2L}\left[2N_F + 1 + \frac{\sin\big(\frac{\pi}{L}j(2N_F+1)\big)}{\sin\big(\frac{\pi}{L}j\big)}\right] \tag{2.23}$$

[4]We observe this is nothing but *parity* symmetry in 1D.

When adding the other diagonal term and recovering the interaction parameter v, the on-site energy at site $2 \leq j \leq L-2$ reads:

$$v'_j = -\frac{v}{2L}\left[\frac{\sin\left(\frac{\pi}{L}(j-1)(2N_F+1)\right)}{\sin\left(\frac{\pi}{L}(j-1)\right)} + \frac{\sin\left(\frac{\pi}{L}(j+1)(2N_F+1)\right)}{\sin\left(\frac{\pi}{L}(j+1)\right)}\right] + \frac{v}{L}\left(2N_F+1\right) \tag{2.24}$$

and

$$v'_1 = v'_{L-1} = -\frac{v}{2L}\left[\frac{\sin\left(\frac{2\pi}{L}(2N_F+1)\right)}{\sin\left(\frac{2\pi}{L}\right)}\right] + \frac{v}{2L}\left(2N_F+1\right) \tag{2.25}$$

As for the off-diagonal terms, the on-site energy in mean field approximation is split into a homogeneous term and an inhomogeneous one. In equation (2.24) the explicit dependence of the direct term is given: a fermion occupying the site j "feels" the average charge density at site $j-1$ and $j+1$, which now depends on j due to the distortion introduced by the finite size of the chain. Notice that a particle at the boundary only interacts with one neighbour site. Again, parity symmetry is preserved, as it can be easily worked out from the expression of v'_j.
It is interesting to investigate the behaviour of the elements t'_j and v'_j under particle-hole number exchange, i.e. under the mapping: $N_F \longrightarrow L-1-N_F$. Plugging it into equation (2.21) we see that the hopping term is left untouched. The on-site energy instead picks up an overall minus sign.

2.2.3 Algebraic decay and Friedel oscillation

In figure 2.3 we plot the the value of the matrix elements t'_j close to one edge of the lattice. From equation (2.21) we see that the spatial frequency of the oscillation is $2k_F$. As it can be seen, the oscillation decays while moving from the boundary towards the bulk. This decaying has been found to be *algebraic*, both analytically and numerically, for every value of interaction v and filling factor η.

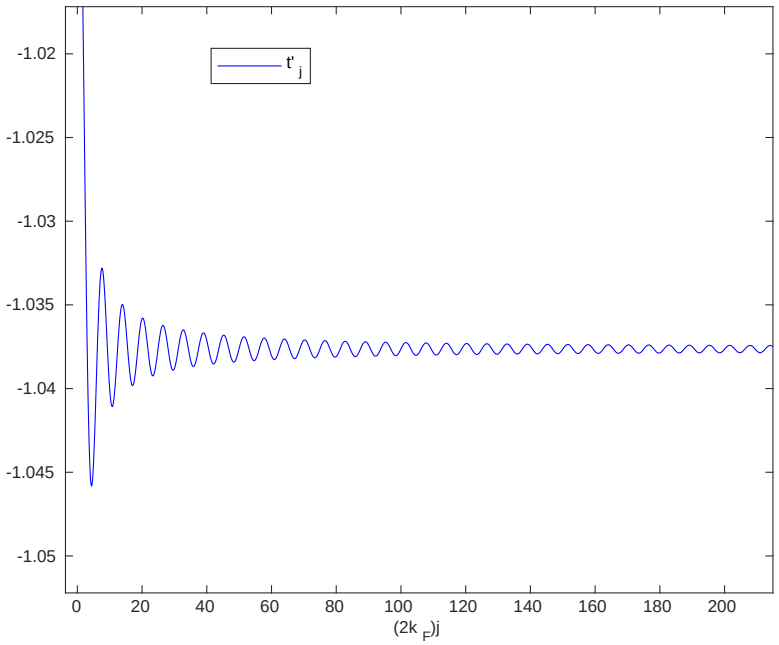

Figure 2.3: *Hopping term in the mean field approximation for OBC close to the boundary. Here v=1.5,* $N_F = 100$ *while* $L-1 = 4000$.

Analytical result can be achieved when performing the proper limit on the expression we found for the matrix elements. We are interested in the inhomogeneous term:

$$-t_1(j) = \frac{v}{2L} \frac{\sin\left(\frac{\pi}{2L}(2N_F+1)(2j+1)\right)}{\sin\left(\frac{\pi}{2L}(2j+1)\right)} \tag{2.26}$$

For a fixed value of j we take the limit for $L \to \infty$ while keeping η constant

$$-t_1(j) \longrightarrow \frac{v}{2L} \frac{\sin\left(2k_F j\right)}{\frac{\pi}{2L}(2j+1)} = v \frac{\sin\left(2k_F j\right)}{\pi(2j+1)} \tag{2.27}$$

For large j then, the oscillations decay as

$$-t_j \longrightarrow v \frac{\sin\left(2k_F j\right)}{2\pi j} \tag{2.28}$$

As mentioned above, we found an algebraic decay in the first power of j. With a quick look at equation (2.24) one realizes that taking the same limit will lead to a $\frac{1}{j}$ decay as well. As the diagonal matrix elements are nothing but the expectation value of the number density operator with respect to the non-interacting ground state, this behaviour is showing us *Friedel oscillation* in one dimension [6]. In the finite lattice model of interacting fermions we are investigating, the open boundary is the inhomogeneity causing this type of density oscillation. This behaviour has been successfully checked numerically and the results are shown for the hopping term in figures 2.4 and2.5.

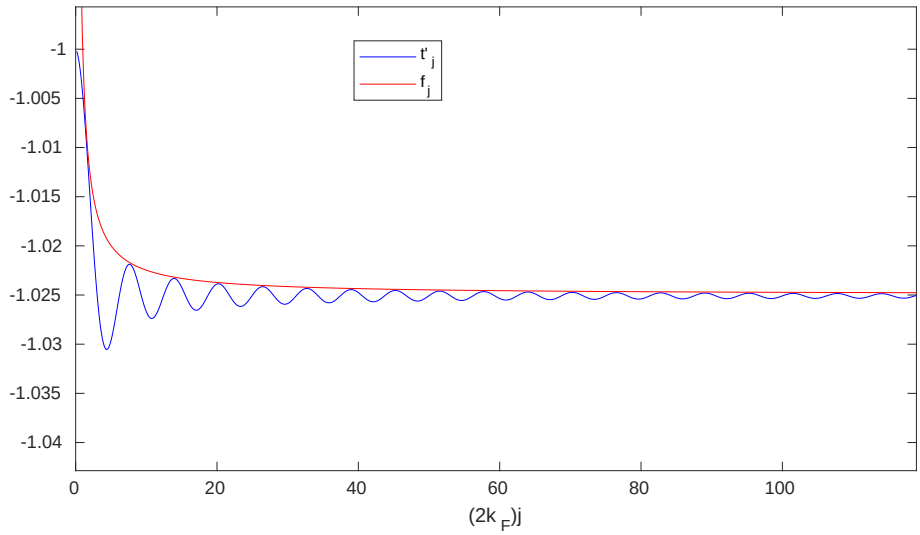

Figure 2.4: *Algebraic decay of oscillation in the hopping matrix elements in OBC. Here* $v = 1$, $N_F = 100$, $L - 1 = 4000$. *The function* $f_j = \frac{v}{2\pi j} - t - \frac{v \sin(\pi\eta)}{\pi}$ *is the sum of the amplitude of the oscillation as derived analytically and the homogeneous shift.*

For a site j far from the inhomogeneity we expect to recover the bulk properties, i.e. to loose track of the effects of the boundary. In this limit in fact, both the hopping energy as well as the on-site energy in the OBC coincide with the ones in PBC. The inhomogeneous hopping component vanishes and the homogeneous one is easily seen to coincide with the PBC we already found

$$\frac{v}{2L} \frac{\sin\left(\frac{\pi}{2L}(2N_F+1)\right)}{\sin\frac{\pi}{2L}} \xrightarrow[L\to\infty]{} \frac{v\sin(\pi\eta)}{\pi}$$

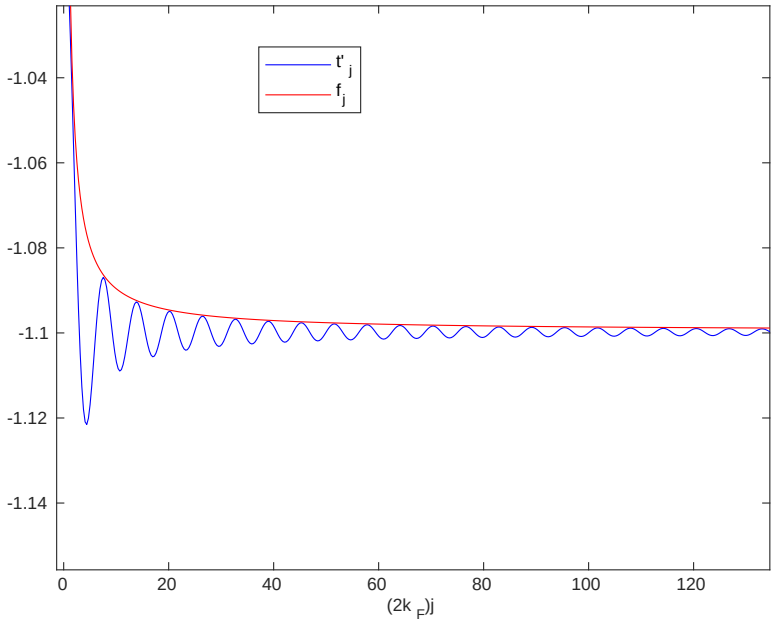

Figure 2.5: *Algebraic decay of oscillation in the hopping matrix elements in OBC. Here* $v = 2$, $N_F = 200$, $L - 1 = 4000$. *The function* $f_j = \frac{v}{2\pi j} - t - \frac{v \sin(\pi\eta)}{\pi}$ *is the sum of the amplitude of the oscillation as derived analytically and the homogeneous shift.*

Naturally, identical consideration follows for the diagonal terms v'_j: the inhomogeneous term disappears and we are left with the homogeneous one

$$\frac{v}{L}\big(2N_F + 1\big) \longrightarrow 2v\eta = u$$

2.2.4 Numerical diagonalization

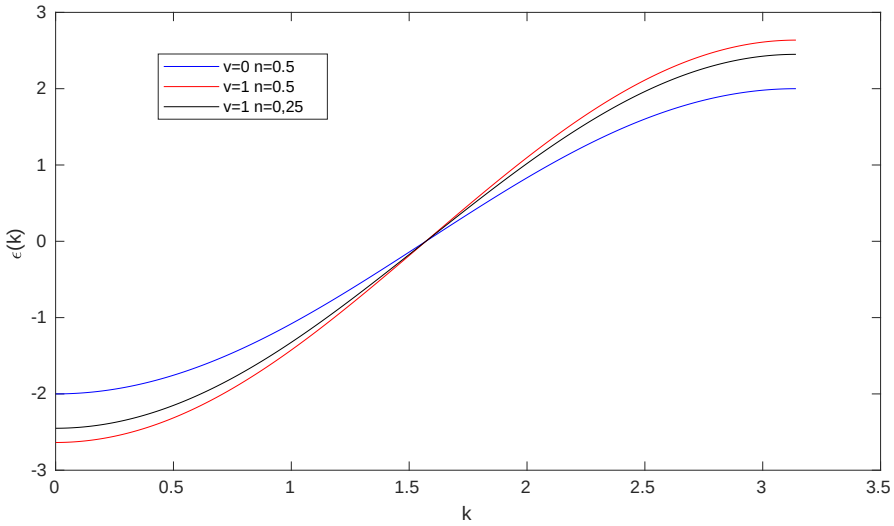

Figure 2.6: *Eigenvalues in the mean field approximation for OBC. Here* $L - 1 = 4000$

Given the nontrivial behaviour of the matrix elements in equations (2.21) and (2.24,) there is no chance to invert the HF Hamiltonian analytically. In order to investigate the properties of the finite size interacting system we proceed with the numerical diagonalization. The eigenvalues we obtain are

plotted in figure 2.6. From this plot it can be inferred that the effect of the inhomogeneous terms on the band shape is negligible. The band shares the same features of the one in PBC. The largest difference between the eigenvalues in the two cases is found at the two extremes of the band and is of the order 10^{-4} in our simulations. Concerning the eigenvectors, the meaningful comparison to work out is with the non-interacting eigenvectors in OBC. The low energy eigenstates are not distorted by the interaction. This fact can be tracked down to the Pauli exclusion principle, since the states deep below the Fermi energy are frozen inside the Fermi sea. Conversely, the main deviation from the non interacting eigenstates appears for eigenstates corresponding to the chemical potential. In real space representation, the deviation has been found to be bigger at the boundaries of the lattice, and this precise feature will be responsible of the peculiar spectral properties of the edge sites.

2.3 The Hubbard model

The second model we analyse is the one-dimensional Hubbard model. The kinetic energy term is fully analogous to the spinless fermions model. The study of the non-interacting Hamiltonian is therefore identical and we directly tackle the interacting problem. Moreover, as the main focus of this work is the investigation of inhomogeneous LLs, we only analyse the case with open boundary conditions. With the same prescription on the labelling of the real lattice sites given for the previous model, the Hamiltonian reads

$$H = \sum_{\sigma} \sum_{j=1}^{L-2} c^{\dagger}_{j+1,\sigma} c_{j\sigma} + \text{h.c.} + u \sum_{j=1}^{L-1} n_{j\uparrow} n_{j\downarrow} \tag{2.29}$$

where σ denotes the two possible spin projections - $\uparrow$,$\downarrow$ - upon a chosen axis for a spin $\frac{1}{2}$ particle, and $n_{j,\sigma}$ the particle number operator at site j and spin component σ. In this case double occupancy on the same site is not forbidden for fermions with opposite spin. The interaction term is here the on-site repulsion between particles with opposite spin.
The half-filled band case is metallic (gapless charge excitations) only for $u = 0$. For $u \gg t$ the Coulomb energy overwhelms the kinetic one and every site is singly occupied. The charge degrees of freedom are frozen so that the spin is the only relevant degree of freedom and the model can be mapped to a spin-$\frac{1}{2}$ Heisenberg ferromagnet [5]. For a different filling factor the model is known to be a LL with $K_s = 1$ [5]. We will therefore focus our investigation away from half-filling[5], i.e. for $\eta \neq 1$.

2.3.1 Hartree-Fock approximation in real space

We perform now the same perturbative analysis that has been carried out for the previous model, namely the HF approximation in real space. Successively, the numerical diagonalization is performed and a brief discussion is given. The interacting Hamiltonian in the HF approximation gives

$$\begin{aligned} u \sum_{j=1}^{L-1} n_{j\uparrow} n_{j\downarrow} &= u \sum_{j=1}^{L-1} c^{\dagger}_{j\uparrow} c^{\dagger}_{j\downarrow} c_{j\downarrow} c_{j\uparrow} \\ &= u \sum_{j=1}^{L-1} c^{\dagger}_{j\uparrow} \langle c^{\dagger}_{j\downarrow} c_{j\downarrow} \rangle c_{j\uparrow} + u \sum_{j=1}^{L-1} c^{\dagger}_{j\downarrow} \langle c^{\dagger}_{j\uparrow} c_{j\uparrow} \rangle c_{j\downarrow} \\ &= u \sum_{j=1}^{L-1} \Big[\langle n_{j\downarrow} \rangle n_{j\uparrow} + \langle n_{j\uparrow} \rangle n_{j\downarrow} \Big] \end{aligned}$$

[5] As we are allowed to put *two* fermions in each site, the filling factor can now span from 0 to 2.

where the brackets indicate the expectation value with respect to the non-interacting ground state. As it is clear, only the direct terms appear in the expansion. In this model in fact, there is no exchange term since the interaction is *local*, and the Fock contribution vanishes.
Considering the structure of the free Hamiltonian, the whole problem now simply splits into two identical ones. For every spin population we have to evaluate:

$$\langle n_{j\uparrow} \rangle = \langle n_{j\downarrow} \rangle = \sum_{n}^{N_F} |\langle n|j \rangle|^2 = \frac{2}{L} \sum_{n}^{N_F} \sin^2 \left(\frac{\pi}{L} nj \right)$$

where the same notation of the previous model has been employed since the non-interacting eigenstates are identical. This sum has already been performed for the Hartree term in the spinless fermions model. We thus end up with

$$u \langle n_{j\downarrow} \rangle = \frac{u}{2L}(2N_F + 1) - \frac{u}{2L} \frac{\sin\left(\frac{\pi}{L}(2N_F+1)j\right)}{\sin(\frac{\pi}{L}j)} \tag{2.30}$$

Again the interaction is split into a homogeneous component and an inhomogeneous one. Each spin population then interacts with the average potential generated by the population with opposite spin. The same considerations on the matrix elements made in the previous section are valid and we can directly proceed with the numerical inversion.

2.3.2 Numerical results

In figure 2.7 we plot the eigenvalues for both the non-interacting and the interacting Hubbard case. It is clear that the inhomgeneous component in the diagonal vanishes in the thermodynamic limit as it happened for the spinless fermions model. Only a constant homogeneous shift in energy is left in the diagonal, which for our purpose can be safely set to zero. The hopping energy is not renormalized as we now lack the exchange contribution coming from the Fock term. This suffice to explain the total overlap of the bands in the non-interacting and interacting case.

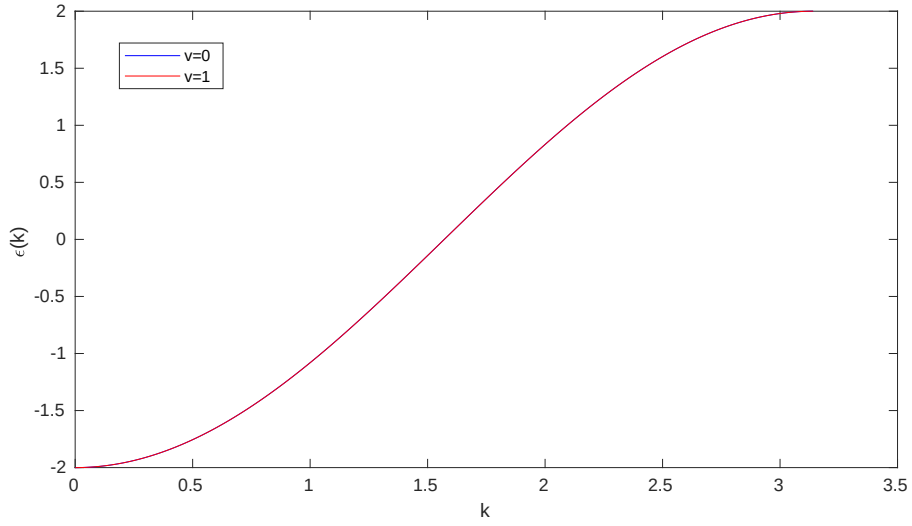

Figure 2.7: *Eigenvalues in the mean field approximation for the OBC Hubbard model. Here* $L - 1 = 4000$ *and* $\eta = 0.25$. *One can observed a perfect overlap of the band for* $u = 0$ *and* $u = 1$ *once the homogeneous shift is set to zero.*

Chapter 3

The spectral function

"The best grammar for thinking about the world is that of change, not of permanence. Not of being, but of becoming."
-C. Rovelli, in *The order of time-*

Before we set off investigating the spectral properties of our systems by means of numerical and analytical tools, it is necessary to introduce a rigorous definition of the mathematical object we are going to work with. We first give a brief recall of the well known concept of density of states. Subsequently, we illustrate the more rich structure of the spectral function (or spectral density) in the framework of many-body theory. Once we settle the important maths, analytical (where possible) and numerical results for the systems we are studying are presented. The spectral properties of interacting spinless fermions with open boundaries will show the very peculiar behaviour we are mainly focused in this work.

3.1 Theoretical framework

3.1.1 The density of states

As it is customary in many-body theory, we suppose to own the full knowledge on the exact *single-particle* eigenstates and eigenenergies of the Hamiltonian we are interested in, respectively $|n\rangle$ and ω_n[1]. With this in mind, we can compute the density of states per unit energy, which is evidently given by the definition:

$$D(\omega) = \sum_n \delta(\omega - \omega_n) \tag{3.1}$$

From this definition and the properties of the Dirac δ it is easy to prove

$$\int d\omega D(\omega) = N \tag{3.2}$$

Where in this case N denotes the number of accessible states in the system.
It is now instructive to compute the density of states for the spinless fermions model. This can be

[1]We assume for simplicity $\hbar = 1$, so that the energy coincides with the frequency, denoted by the letter ω

done analytically for the non interacting case $v = 0$. The expression of the eigenvalues, namely the dispersion relation, is formally the same for PBC and OBC, provided we use the proper definition of k_n. As an example we chose to compute $D(\omega)$ for the OBC case. In the thermodynamic limit the spacing between eigenstates vanishes, and we can trade the sum over the index n, labelling the discrete set of eigenvalues, for and integral over the continuum variable k. We have[2]

$$D(\omega) = \sum_n \delta\big(\omega + 2t\cos(k_n)\big) = \frac{L}{\pi}\int_0^\pi dk\delta\big(\omega + 2t\cos(k)\big) = \frac{L}{\pi}\int_0^\pi dk \sum_{k_0} \frac{\delta(k-k_0)}{|\omega'(k_0)|}$$

Here k_0 denotes the zeros of the function $\omega + 2t\cos(k)$, namely $k_0 = \arccos(-\frac{\omega}{2t})$ in the domain of interest, and $\omega'(k)$ the first derivative of the dispersion relation function.

$$D(\omega) = \frac{L}{2\pi}\frac{1}{t\sin k_0} = \frac{L}{2\pi t}\frac{1}{\sqrt{1-\cos\big(k_0(\omega)\big)}} = \frac{L}{2\pi t}\frac{1}{\sqrt{1-\frac{\omega^2}{4t^2}}} = \frac{L}{\pi}\frac{1}{\sqrt{4t^2-\omega^2}} \tag{3.3}$$

As it can be easily inferred from equation (3.3), the result is consistent as the function we computed is only defined in the energy region $-2t < \omega < 2t$. A quick computation shows that the sum rule in (3.2) is satisfied.

3.1.2 The spectral function

We now give the formal definition of the spectral function. In this introduction we mainly follow the presentation given in the enlightening book of Giuliani and Vignale [3].
We start by considering the N-particle system in its ground state, denoted by $|\phi_0^N\rangle$. When a particle is added in the generic state $|\alpha\rangle$, the $N+1$ particle system does not have a definite energy, provided we do not choose $|\alpha\rangle$ to be an eigenstate $|\phi_n^{N+1}\rangle$ of the $N+1$ particle Hamiltonian. Nevertheless, we can surely decompose this state as a linear combination of the eigenstates $|\phi_n^{N+1}\rangle$

$$c_\alpha^\dagger\,|\phi_0^N\rangle = \sum_n u_{n,N+1}^\alpha\,|\phi_n^{N+1}\rangle$$

where $|\phi_n^{N+1}\rangle$ is the n-th excited eigenstate of the N+1 particle Hamiltonian and the coefficient is given by the overlap

$$u_{n,N+1}^\alpha = \langle\phi_n^{N+1}|c_\alpha^\dagger|\phi_0^N\rangle$$

The interesting point is understanding the probability to find the $N+1$ particle system at the energy ω_n of the n-th exact eigenstate of the $N+1$ particle Hamiltonian. Requiring it to be normalised, this is given by

$$\frac{|u_{n,N+1}^\alpha|^2}{\sum_n |u_{n,N+1}^\alpha|^2}$$

In the thermodynamic limit where the eigenenergies condense into a continuum, it is more meaningful to look for the probability that the system is found in an energy interval between $E_0^N + \omega$ and $E_0^N + \omega + d\omega$. This is realized by the function

[2]Here we make use of the property $\delta\big[f(x)\big] = \sum \frac{1}{|f'(x_0)|}\delta(x-x_0)$ where the sum is over any simple zero x_0 of the function $f(x)$. This useful relation will be widely employed through the text.

$$\rho^{>}(\alpha,\omega) = \sum_n |\,\langle\phi_n^{N+1}|c_\alpha^\dagger|\phi_0^N\rangle\,|^2 \delta\Big(\omega - (E_n^{N+1} - E_0^N)\Big) \tag{3.4}$$

Using the resolution of identity in terms of exact eigenstates, the normalization integral is found to be

$$\int d\omega \rho^{>}(\alpha,\omega) = 1 - n_\alpha$$

with n_α the expectation value of the particle number operator in the single particle state $|\alpha\rangle$ onto the ground state. In exactly the same way, we can work out the probability for a particle to be *removed* from the system

$$\rho^{<}(\alpha,\omega) = \sum_n |\,\langle\phi_n^{N-1}|c_\alpha|\phi_0^N\rangle\,|^2 \delta\Big(\omega + E_n^{N-1} - E_0^N\Big) \tag{3.5}$$

where the normalization integral is now

$$\int d\omega \rho^{<}(\alpha,\omega) = n_\alpha$$

The sum of the two probability densities define the total spectral function

$$\rho(\alpha,\omega) = \rho^{<}(\alpha,\omega) + \rho^{>}(\alpha,\omega) \tag{3.6}$$

It is straightforward to verify this object is properly normalized and satisfies all the requirements to be a probability density. The powerful effectiveness of this tool will be evident when applied to a system of interacting particles. For instance, $\rho^{>}(\alpha,\omega)$ describes in which way the spectral weight carried by the state $c_\alpha^\dagger|\phi_0^N\rangle$ is spread out over the continuum of many-body interacting states $|\phi_n^{N+1}\rangle$. In this sense we are having information on the spectral region explored by the state $|\alpha\rangle$.

Intermezzo: Fermi gas and Fermi liquid

It is instructive to look at the spectral function for a system of non-interacting particles when $|\alpha\rangle$ is chosen to be an eigenstates $|k\rangle$ of the Hamiltonian, with eigenvalue $\omega(k)$. In the case we are adding a particle above the Fermi surface, from the definition in (3.4) it is clear that the sum over the index n collapses thanks to orthogonality and the difference $E_n^{N+1} - E_0^N = \omega(k)$ is nothing but the *single particle* energy of the particle we inject in the state $|k\rangle$. The same result holds when removing a particle in state $|k\rangle$ underneath the Fermi surface, and we simply obtain:

$$\rho(k,\omega) = \delta\big(\omega - \omega(k)\big) \tag{3.7}$$

Clearly, when the particle is added in (or removed from) an exact eigenstate, the spectral weight is concentrated on the precise corresponding eigenenergy. In a Fermi liquid, this δ-function is broadened to a Lorentzian peak by the interaction between fermions. The spectral weight of a particle injected in a non-interacting single-particle eigenstate $|k\rangle$ is spread out over a small energy range around the quasiparticle energy. The point to be stressed is that in "high dimensions" this is the only big difference in the spectral domain, such that it is meaningful to talk about quasiparticles. A description of the low energy excitations above the Fermi surface as a dilute gas of weakly interacting quasiparticles is valid and gives rise to the concept of Fermi liquid as illustrated in Chapter 1.

3.1.3 From many-body description to single-particle properties

In this work we want to investigate the structure of the spectral function at a site $|j\rangle$ of the real lattice. This is also referred to as *local spectral function* [3]. We have to perform

$$\rho^{<}(j,\omega) = \sum_n |\langle \phi_n^{N-1}|c_j|\phi_0^N\rangle|^2 \delta\Big(\omega + E_n^{N-1} - E_0^N\Big) \tag{3.8}$$

$$\rho^{>}(j,\omega) = \sum_n |\langle \phi_n^{N+1}|c_j^\dagger|\phi_0^N\rangle|^2 \delta\Big(\omega - E_n^{N+1} + E_0^N\Big) \tag{3.9}$$

Analytical results can be achieved in the case of a free Hamiltonian for both PBC and OBC. Before we set off to compute though, a few considerations must be done. We can reduce this many-body construction to a single-particle one. As an example, we work with $\rho^{>}(j,\omega)$, the result for $\rho^{<}(j,\omega)$ being totally analogous. We start by focusing on the term

$$|\langle \phi_n^{N+1}|c_j^\dagger|\phi_0^N\rangle|^2 = \langle \phi_0^N|c_j|\phi_n^{N+1}\rangle \langle \phi_n^{N+1}|c_j^\dagger|\phi_0^N\rangle$$

We represent the creation operator in the basis of single particle eigenstates of the $N+1$-particle Hamiltonian $|m\rangle$:

$$\begin{aligned}
\langle \phi_0^N|c_j|\phi_n^{N+1}\rangle \langle \phi_n^{N+1}|c_j^\dagger|\phi_0^N\rangle &= \langle \phi_0^N| \sum_{m'} \langle m'|j\rangle\, c_{m'}|\phi_n^{N+1}\rangle \langle \phi_n^{N+1}| \sum_m \langle j|m\rangle\, c_m^\dagger|\phi_0^N\rangle \\
&= \sum_m \sum_{m'} \langle m'|j\rangle \langle j|m\rangle \langle \phi_0^N|c_{m'}|\phi_n^{N+1}\rangle \langle \phi_n^{N+1}|c_m^\dagger|\phi_0^N\rangle \\
&= \sum_m \sum_{m'} \langle m'|j\rangle \langle j|m\rangle\, \Theta(m'-N_F)\Theta(m-N_F) \langle \phi_{l'}^{N+1}|\phi_n^{N+1}\rangle \langle \phi_n^{N+1}|\phi_l^{N+1}\rangle
\end{aligned}$$

where we denoted with $|\phi_l^{N+1}\rangle$ the l-th eigenstate of the $N+1$ particle Hamiltonian obtained by adding a particle in the single-particle state m, and respectively for $|\phi_{l'}^{N+1}\rangle$. This operation is permitted only for particle states lying above the Fermi number, thus the step function. The matrix elements are non vanishing only if the general n-th excited state coincide with the many-body eigenstate we created by adding one particle.

$$\begin{aligned}
\langle \phi_0^N|c_j|\phi_n^{N+1}\rangle \langle \phi_n^{N+1}|c_j^\dagger|\phi_0^N\rangle &= \sum_m \sum_{m'} \langle m'|j\rangle \langle j|m\rangle\, \Theta(m'-N_F)\Theta(m-N_F)\delta_{\phi_n\phi_{l'}}\delta_{\phi_n\phi_l} \\
&= \sum_m \sum_{m'} \langle m'|j\rangle \langle j|m\rangle\, \Theta(m'-N_F)\Theta(m-N_F)\delta_{mm'}\delta_{\phi_n\phi_l} \\
&= \sum_{m>N_F} |\langle j|m\rangle|^2 \delta_{\phi_n\phi_l}
\end{aligned}$$

The energy of this new eigenstate is clearly

$$E_l^{N+1} = E_0^N + \omega_m \tag{3.10}$$

where ω_m is the *single particle* energy in the state $|m\rangle$. Plugging this result back into equation (3.4) the sum over index n collapses and we are left with

[3] Only in the case of non-interacting systems the notion *local density of states* can be employed.

$$\rho^{>}(j,\omega) = \sum_{m>N_F} |\langle j|m\rangle|^2 \delta\big(\omega - \omega_m\big) \tag{3.11}$$

In a similar manner we compute $\rho^{<}(j,\omega)$ and obtain

$$\rho^{<}(j,\omega) = \sum_{m<N_F} |\langle j|m\rangle|^2 \delta\big(\omega - \omega_m\big) \tag{3.12}$$

Adding together the last equations we have an expression for the local spectral function in terms of single particle properties

$$\rho(j,\omega) = \sum_{m} |\langle j|m\rangle|^2 \delta\big(\omega - \omega_m\big) \tag{3.13}$$

3.2 Spectral function for the spinless fermions model

3.2.1 Free spinless fermions

We can now compute the local density of states in a generic state $|j\rangle$ for PBC. In this case the computation is rather simple since

$$|\langle j|m\rangle|^2 = \frac{1}{L}$$

for the normalized plane waves as given in equation (2.2). Denoting with ω_n the dispersion relation, we obtain:

$$\rho_0(j,\omega) = \frac{1}{L}\sum_n \delta(\omega - \omega_n) \tag{3.14}$$

As we expected in the homogeneous case, the local density of states does not depend on the site j we are looking at, and it is simply given by the total density of states divided by the number of accessible sites.
More interesting is the inhomogeneous case, where the squared modulus we need is the one given in (2.5). As usual in the thermodynamic limit we trade the sum over n for a integral and compute:

$$\rho_0(j,\omega) = \frac{2}{\pi}\int_0^\pi dk \sin^2\big(kj\big)\delta\big(\omega + 2t\cos k\big) = \frac{2}{\pi}\frac{\sin^2\big(k(\omega)j\big)}{|2t\sin\big(k(\omega)\big)|} = \frac{2}{\pi}\frac{\sin^2\big(k(\omega)j\big)}{2t\sqrt{1-\cos^2\big(k(\omega)\big)}}$$

so that

$$\rho_0(j,\omega) = \frac{2}{\pi}\frac{\sin^2\big(k(\omega)j\big)}{\sqrt{4t^2-\omega^2}} \tag{3.15}$$

Here we introduced the inverse function of the dispersion relation $k(\omega) = \arccos(-\frac{\omega}{2t})$. Up to this point the spectral function is fully *exact* for every value of ω and site j. For our future purpose though, it is enough to evaluate this function close to the Fermi energy, which coincides with the chemical potential μ since we are working at $T = 0$. Reminding the definition of Fermi velocity

$$v_F = \omega'(k_F) = 2t\sin(k_F) = 2t\sqrt{1-\frac{\mu^2}{4t^2}} = \sqrt{4t^2-\mu^2} \tag{3.16}$$

we approximate the spectral density with

$$\rho_0(j,\omega) = \frac{2}{\pi}\frac{\sin^2\big(k(\omega)j\big)}{v_F\sqrt{1-\epsilon^2}} = \frac{2\sin^2\big(k(\omega)j\big)}{\pi v_F} + O(\epsilon)$$

with ϵ being

$$\epsilon = \frac{\omega^2-\mu^2}{v_F^2}$$

Furthermore, one can expand the function $k(\omega)$ around the Fermi vector

$$k(\omega) = k_F + \frac{\omega-\mu}{v_F} + O\big((\omega-\mu)^2\big)$$

to obtain

$$\rho_0(j,\omega\simeq\mu) \simeq \frac{2\sin^2\big(k_F j\big)}{\pi v_F} \tag{3.17}$$

In this work we are mainly focused on the spectral density function at the boundary of the chain, namely on the site $j = 1$. Directly from equation (3.15) without any approximation, for every value of ω we have the simple expression

$$\rho_0(1,\omega) = \frac{\sqrt{4t^2-\omega^2}}{2\pi t^2} \tag{3.18}$$

In figure 3.1 we plot this result for different values of j.

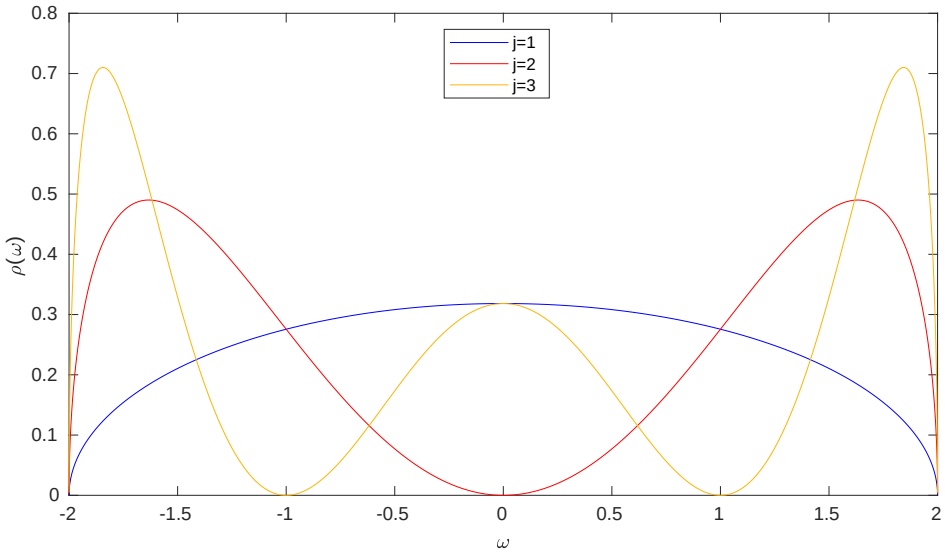

Figure 3.1: *Spectral function for the first sites close to the boundary in the free spinless fermions model.*

3.2.2 Interacting spinless fermions: suppression of the spectral weight

When the interaction is turned on, the spectral density function exhibits a very peculiar behaviour. In this case a suppression of the spectral weight sets in, at an energy close to the Fermi energy, or chemical potential $\omega = \mu$, and at an energy [4] $\omega = -\mu$. This result has been obtained numerically through the implementation of equation (3.13), using the eigenvectors and eigenenergies previously computed. We perform now an accurate analysis and characterization of the features of the dips appearing in this spectral function. From figures 3.2 and 3.3 we see the emergence of the two dips in the spectral density for different sites close to the boundary. These dips indicate a suppression of the spectral weight due to the repulsion between fermions. On the contrary, for attractive interactions $v < 0$, we notice the appearance of two peaks, denoting an enhancement at the energy mentioned above (figure 3.4). These peaks and dips have been long explored numerically, the main focus being on the repulsive case.

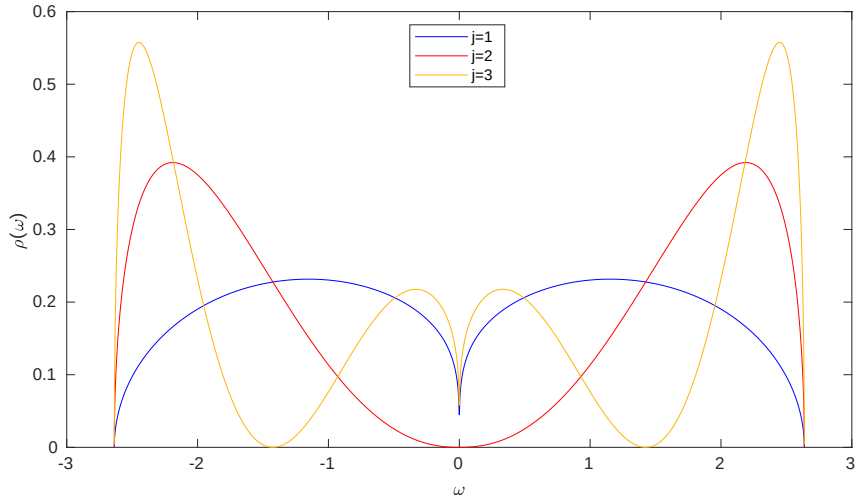

Figure 3.2: *Spectral function for sites close to the boundary with* $v = 1$, $\eta = 0.5$ *and* $L - 1 = 4000$.

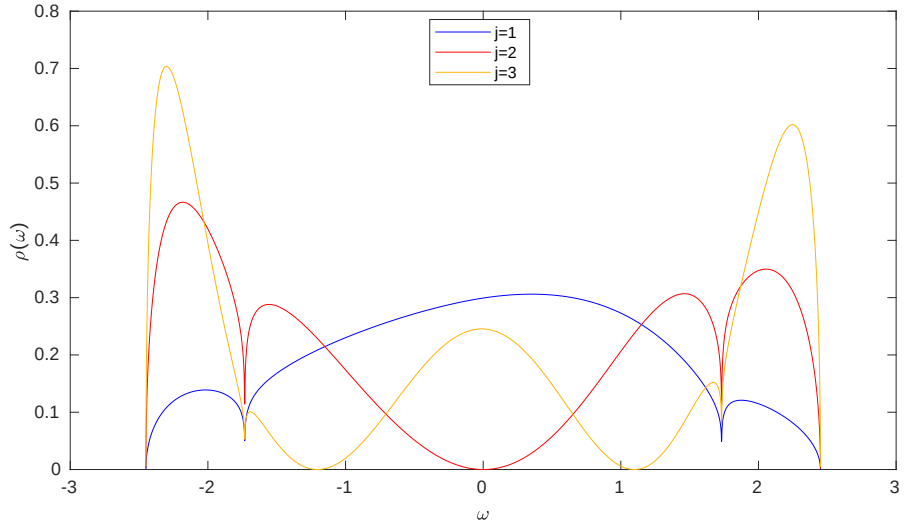

Figure 3.3: *Spectral function for sites close to the boundary with* $v = 1$, $\eta = 0.25$ *and* $L - 1 = 4000$.

[4] The shift in the chemical potential $\delta\mu$ is always set to zero in this work. See footnote 3 in section 2.2.1

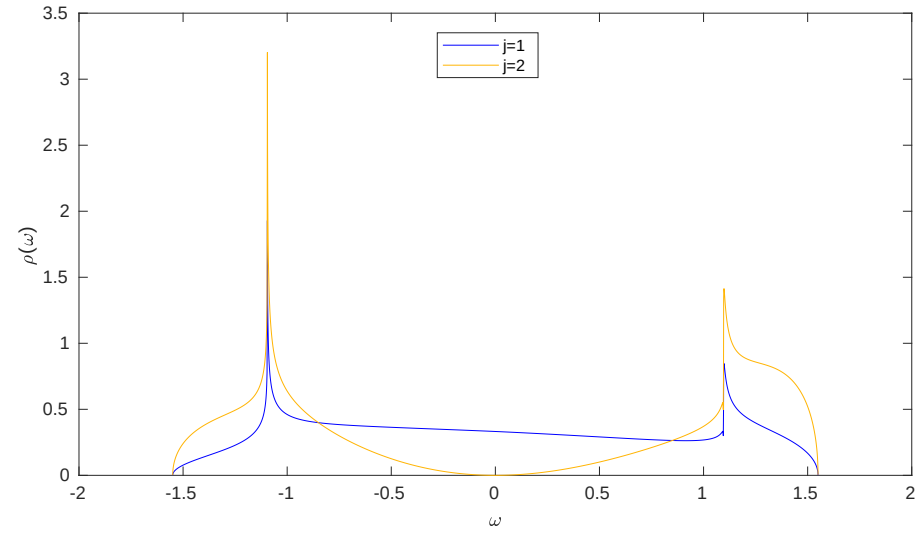

Figure 3.4: *Spectral function for sites close to the boundary with attractive interaction. Here* $v = -1$, $\eta = 0.25$ *and* $L - 1 = 4000$.

The next characterization has been made by keeping a fixed site j and exploring the behaviour of the dips with respect to different values of filling factor η. This analysis is plotted in figure 3.5. For systems of finite size L, as the number density increases from 0.2 to 0.4, the suppression in $\omega = \mu$ outlives and slides towards the centre in our plots, while its counterpart in $\omega = -\mu$ fades away and eventually disappears for half filling $\eta = 0.5$.

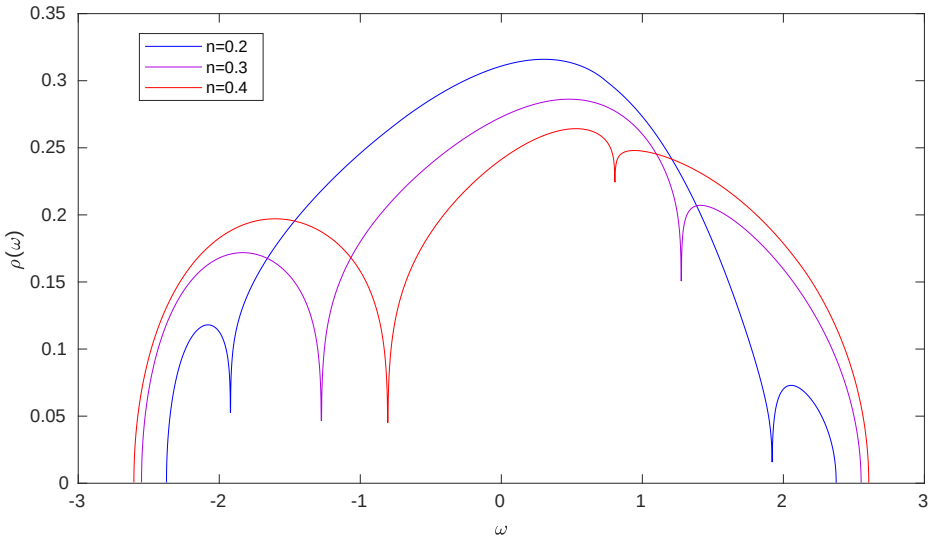

Figure 3.5: *Spectral function for different value of the filling factor* η, *with* $v = 1$, $j = 1$ *and* $L - 1 = 4000$.

We now investigate the symmetry of the spectral density function within the HF approximation. In figure 3.6 and 3.7 we compare the function for the two value η and $1 - \eta$. As we expected since the system is not invariant under this mapping, its spectral density is not invariant either. Notice that the two function would perfectly coincide provided we swap ω with $-\omega$, or more formally the spectral function satisfies $\rho(j, \omega, \eta) = \rho(j, -\omega, 1 - \eta)$.

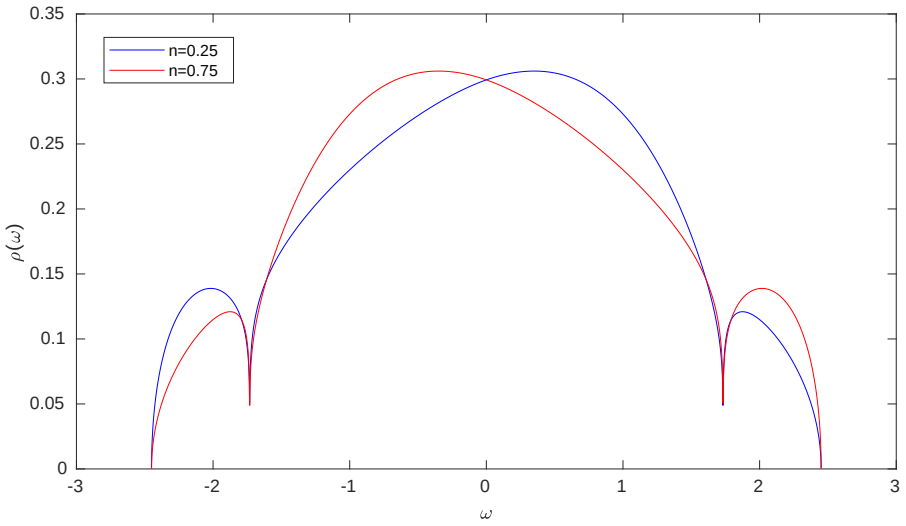

Figure 3.6: *Spectral function under the mapping* $\eta \to 1-\eta$, *for* $j=1$, $v=1$, $L-1=4000$.

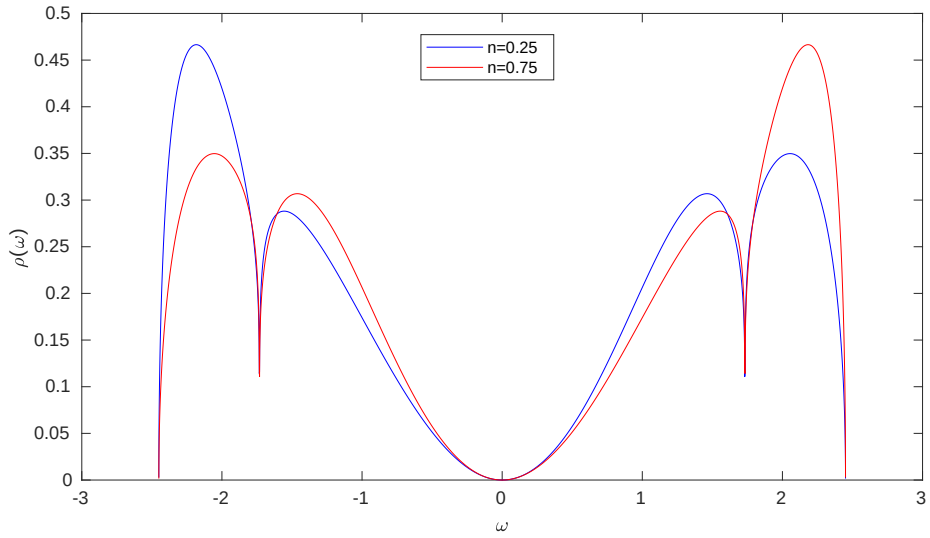

Figure 3.7: *Spectral function under the mapping* $\eta \to 1-\eta$, *for* $j=2$, $v=1$, $L-1=4000$.

The last analysis to be done concerns the dependence of this dips on the interaction strength v. To do this, we set a fixed value for j and η and compute the spectral function for increasing value of v. The results are shown in figures 3.10, 3.11 and 3.12.
The property we are mainly focused in this work is the *power-law* behaviour of the dips appearing in the local spectral function for sites close to the boundary. For the suppression in $\omega=\mu$ the power law is characterized by an exponent which differs from the one of the bulk [6]. This behaviour has been successfully checked as shown in figure 3.8. The HF exponent α_B^{HF} is extracted by taking the numerical log-log derivative of the spectral function close to the chemical potential, and evaluating the function we obtained in the point of least derivative. The spectral function then behaves as $\rho(\omega) \sim |\omega-\mu|^{\alpha_B^{HF}}$, where α_B^{HF} depends on v. Our result are in great agreement with the ones presented in [6] and are to be compared with the predictions of bosonization. From this method the LL parameter K_ρ can be computed and the boundary exponent follows through the relation

$$\alpha_B = {K_\rho}^{-1} - 1 \tag{3.19}$$

For example, this relation yields [6] $\alpha_B = 0.1838$ for $v=1$ and $\eta=0.25$, $\alpha_B = 0.0319$ for $v=0.1$ and

$\eta = 0.5$. The exponents we obtained are respectively $\alpha_B^{HF} = 0.1834$ and $\alpha_B^{HF} = 0.0298$ for systems with $L - 1 = 4000$. We can conclude that the HF approximation for the self-energy already gives meaningful result for this energy value.
We have then performed the same analysis on the dip appearing at $\omega = -\mu$. In figure 3.9 we see that the spectral function close to $\omega = -\mu$ behaves as $\rho(\omega) \sim |\omega + \mu|^{\alpha_B^{HF}}$, where α_B^{HF} has been extracted numerically in the same way we have done before. Also at this energy value then, the spectral function shows a power-law suppression within the HF approximation for the self-energy.
Furthermore, the function $\alpha_B^{HF}(v)$ can be extracted numerically for both dips. As this point will be at the very centre of our analysis though, we postpone the plots to Chapter 5, where a deeper analytical understanding of the problem is also achieved.

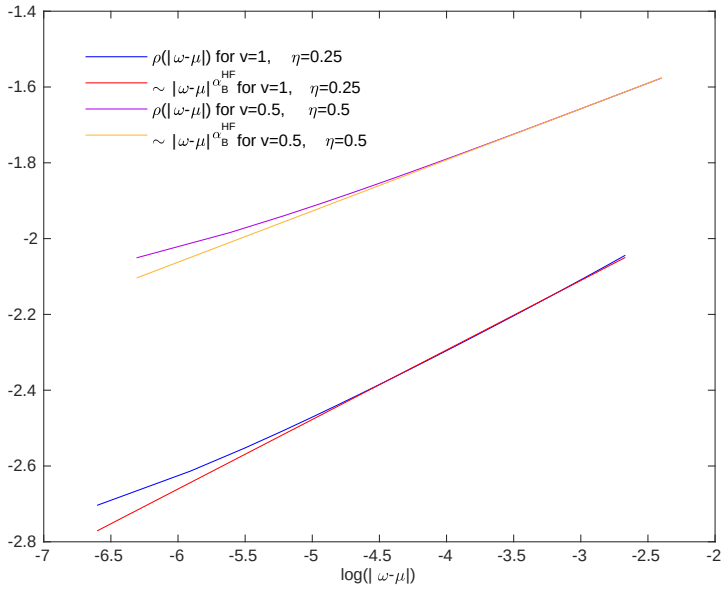

Figure 3.8: *Power-law suppression of the spectral function at $\omega = \mu$ for different values of v and η, with $L - 1 = 4000$. For details see the text.*

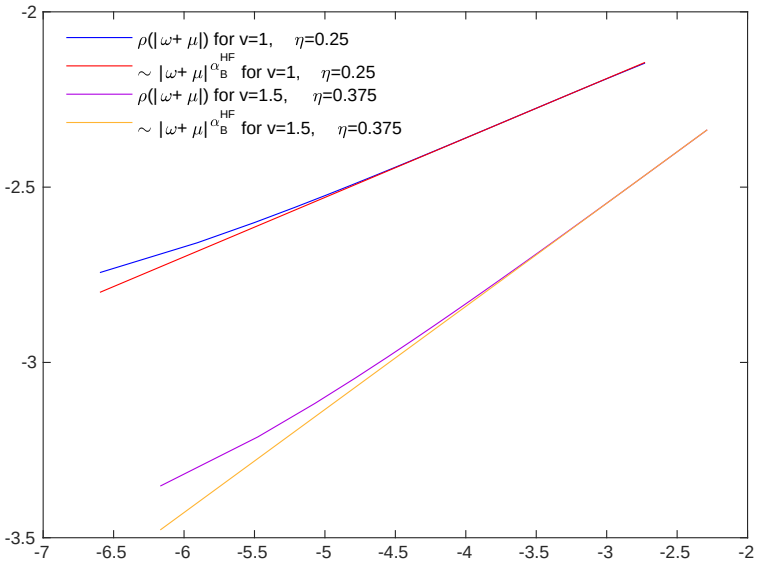

Figure 3.9: *Power-law suppression of the spectral function at $\omega = -\mu$ for different values of v and η, with $L - 1 = 4000$. For details see the text.*

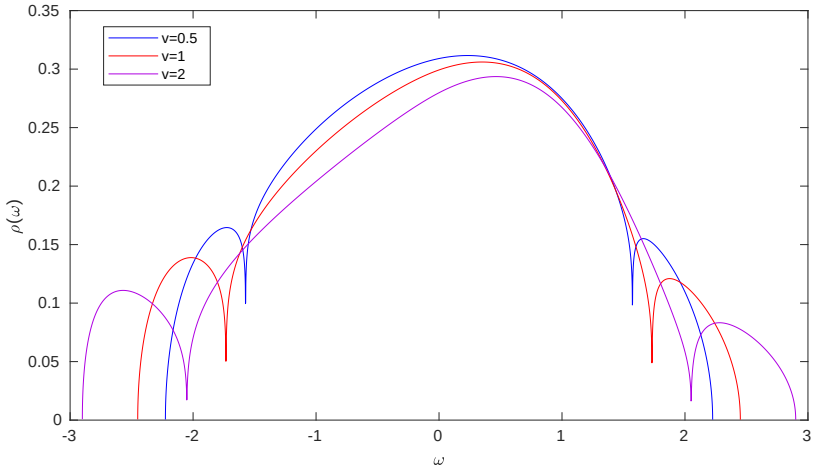

Figure 3.10: *Spectral function for different values of* v *with* $j = 1$, $\eta = 0.25$

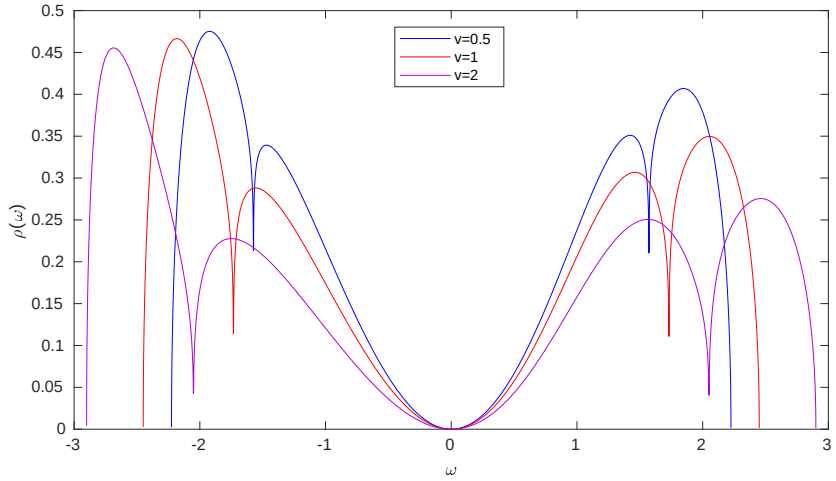

Figure 3.11: *Spectral function for different values of* v *with* $j = 2$, $\eta = 0.25$

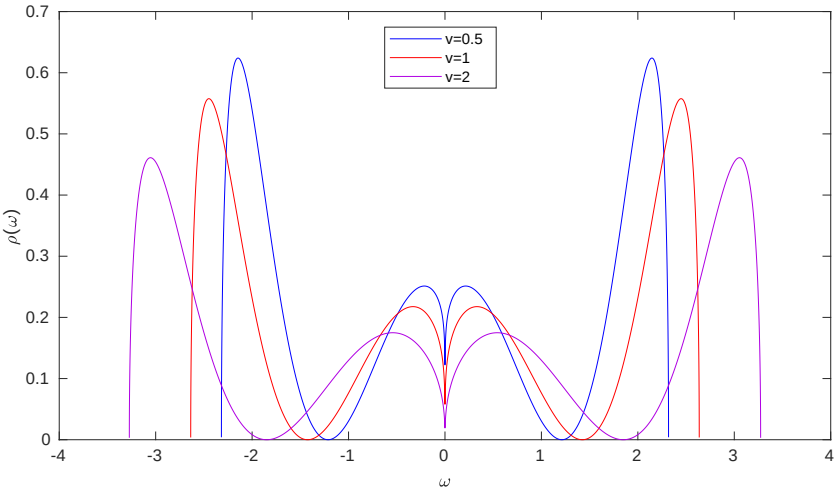

Figure 3.12: *Spectral function for different values of* v *with* $j = 3$, $\eta = 0.5$

3.3 Spectral function for the Hubbard model

We present here the analysis for the spectral function of the Hubbard model. The kinetic term in this model is identical to the previous case so that we directly focus on the interacting problem. When a comparison with the non-interacting spectral function is needed, we directly refer to figure 3.1.
The investigation has been carried out in the same way performed for the previous model, using the numerical eigenvectors and eigenvalues obtained in Chapter 2. For half-filling the spectral function in the Hartree approximation (the Fock term vanishes) does not exhibit any modifications with respect to the non-interacting case.
Things get more interesting when moving away from half-filling, where the model is known to share the features defining a LL. As in the previous model, the departure from the non-interacting case is found at energies $\omega = \mu$ and $\omega = -\mu$. In figures 3.13 and 3.14 the local spectral function for the first sites close to the boundary and different interaction potential u is given.

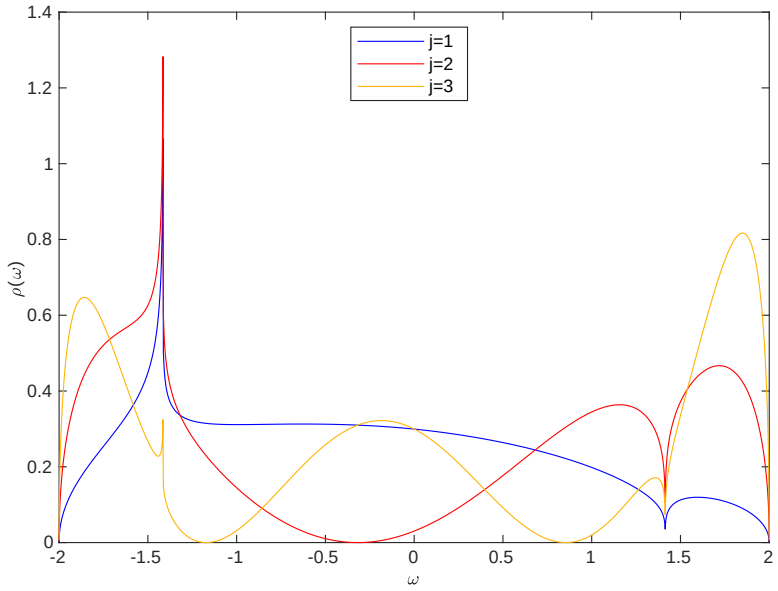

Figure 3.13: *Local spectral function of the Hubbard for the first sites close to the boundary. Here* $L-1=4000$, $\eta = 0.5$, $u = 2$.

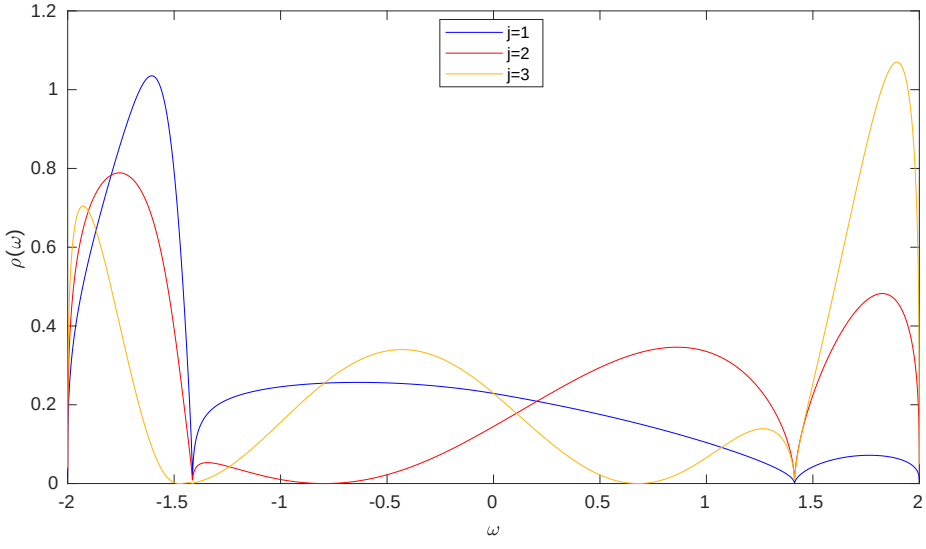

Figure 3.14: *Local spectral function of the Hubbard for the first sites close to the boundary. Here* $L-1=4000$, $\eta = 0.5$, $u = 5$.

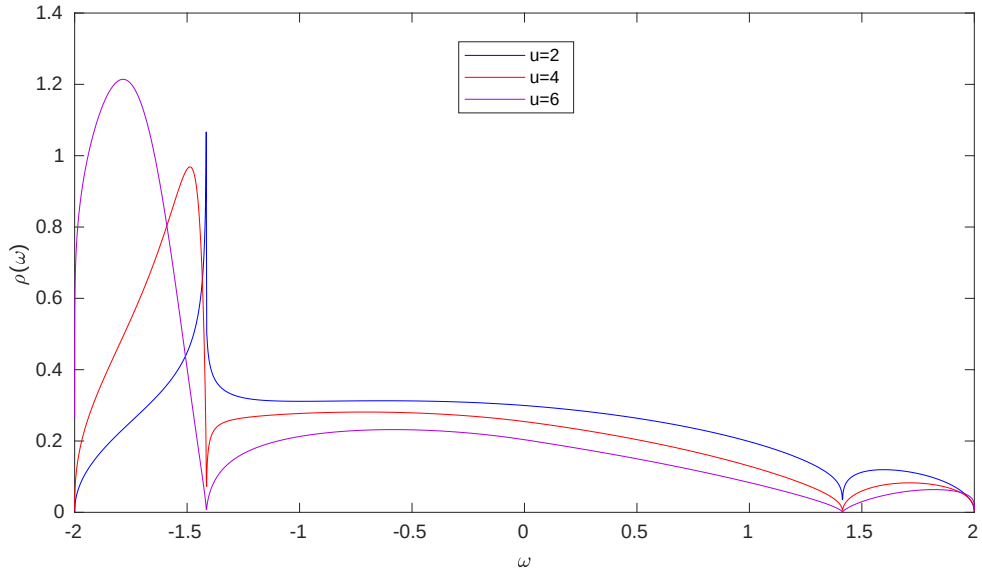

Figure 3.15: *Spectral function for the site* $j = 1$ *with* $L - 1 = 4000$, $\eta = 0.5$.

We now focus our interest on the spectral function for the site $j = 1$. This is presented for different values of u in figure 3.15. For energies approaching from below the chemical potential the spectral weight first increases as a power law (first plot of figure 3.16). With the same methods employed for the spinless fermions model the power-law exponent is extracted numerically and it is found to be $-u/(2\pi v_F)$, as shown in figure 3.17. The error has been set as an upper bound estimate, combining the numerical error and the small arbitrariness in the extraction of the exponent from the log-log derivative plots (figure 3.18).
The Hartree spectral function then exhibits a crossover and a subsequent power-law suppression as presented in the second plot of figure 3.16. The crossover is known to appear on a scale which decreases exponentially in $-1/u$ [6]. As the size $L-1$ of the systems we are investigating determines the energy resolution - which is proportional to $1/L$ - this suffices to explain why the numerical data for small u do not display the power-law suppression at the chemical potential. In our simulations the power-law suppression can only be seen for large value of u. In [6] the power-law exponent for this suppression is extracted numerically for systems of large size ($L \sim 10^6$) and reads

$$\alpha_B^H = \frac{u}{2\pi v_F} \tag{3.20}$$

This is the meaningful result to be compared with the exact exponent α_B for the power-law suppression close to the chemical potential obtained with bosonization. From [6] we have

$$\alpha_B = \frac{K_\rho^{-1} - 1}{2} \tag{3.21}$$

where the leading behaviour is given by $\alpha_B \simeq \frac{u}{4\pi v_F}$, which is one-half α_B^H. This discrepancy is already understood and further details can be found in [6]. For this reason the Hartree data only show qualitative agreement with DMRG ones, which for the suppression at the chemical potential are consistent with the exact exponent obtained with bosonization [6]. This is to be contrasted with the results obtained within the HF approximation for the self-energy for the spinless fermions model, as the exponent for the suppression at the chemical potential shows quantitative agreement with the exact boundary exponent.

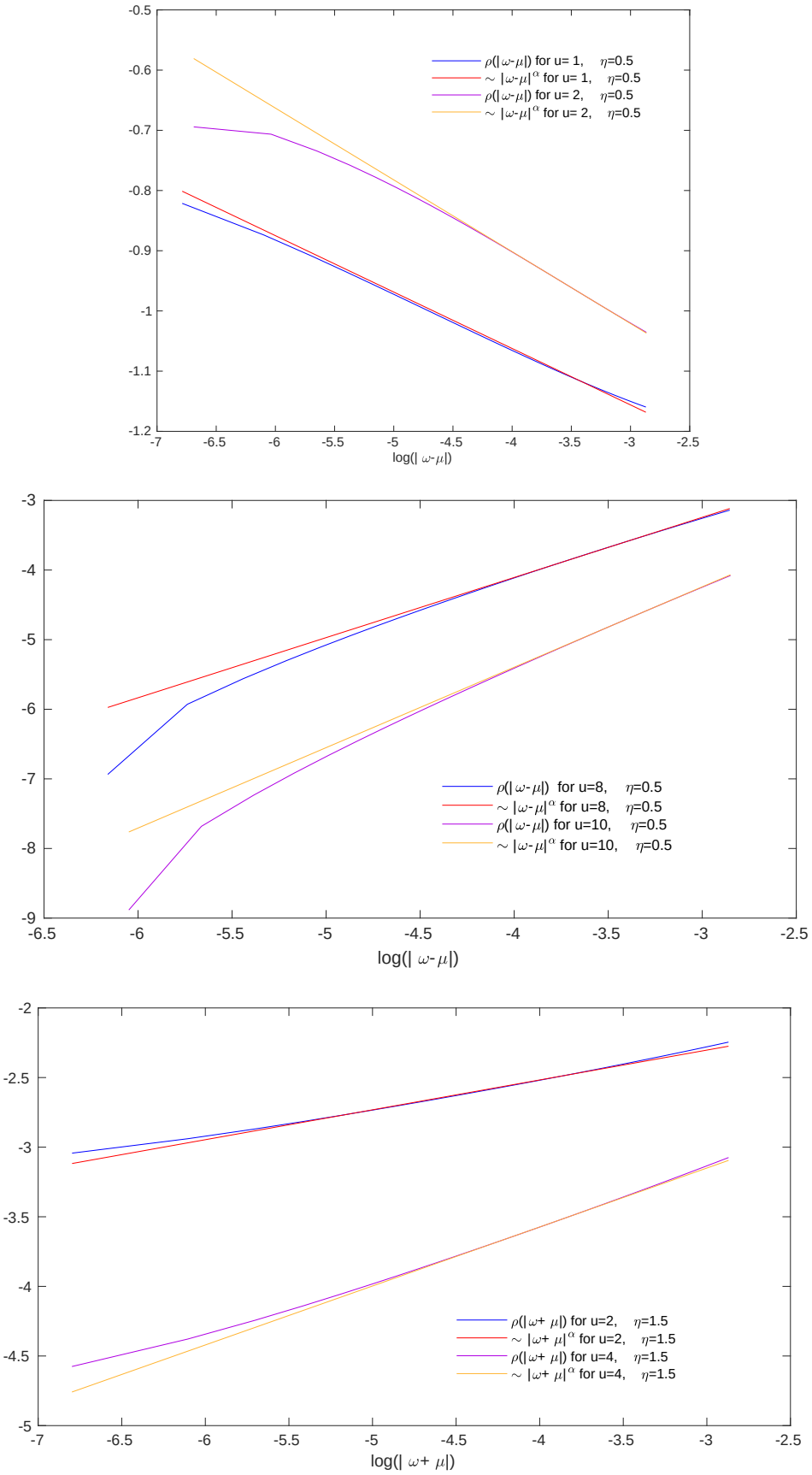

Figure 3.16: *From top to bottom: power-law increase in the spectral weight at $\omega = \mu$, power-law suppression at $\omega = \mu$ and power-law suppression at $\omega = -\mu$ in the Hubbard model, for diverse values of interaction u and filling factor η, $L - 1 = 4000$. In every plot α denotes the exponent extracted numerically. For details see the text.*

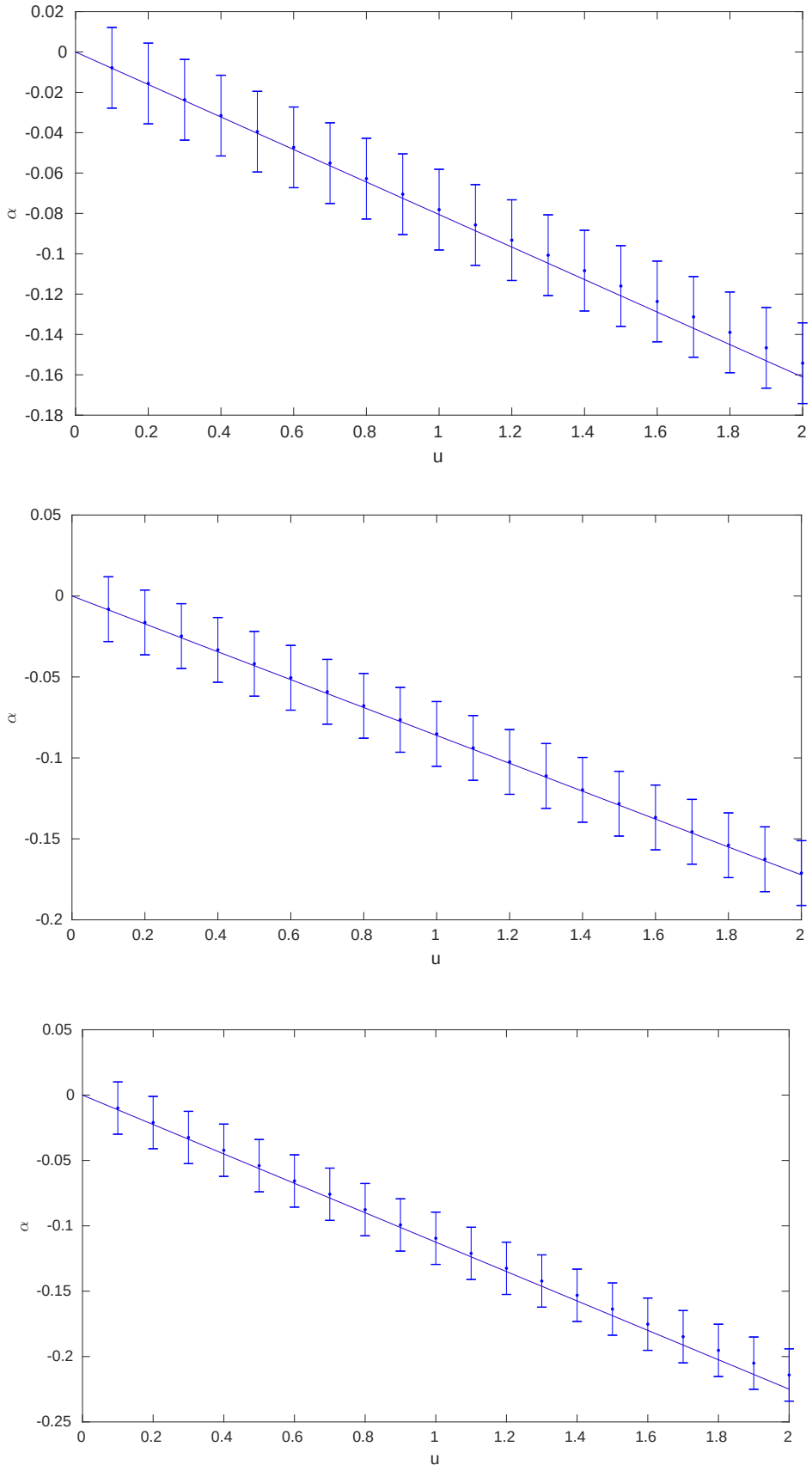

Figure 3.17: $\alpha = -u/2\pi v_F$ *(solid line) compared with* α_B^H *(numerical data). Here* $L - 1 = 4000$*, and from top to bottom* $\eta = 1.1$*,* $\eta = 1.25$*,* $\eta = 1.5$*. For details, see the text.*

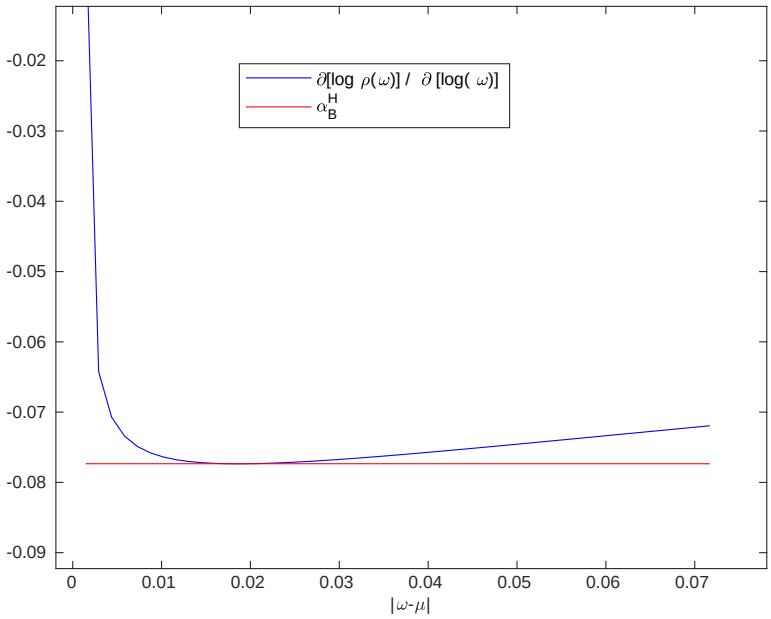

Figure 3.18: *Numerical procedure to extract the exponent of the power-law behaviour. The log-log derivative of the spectral function close to the energy value of interest ($\omega = \mu$ in this plot) is evaluated at the point of least derivative. Here $L - 1 = 4000$, $\eta = 1.5$ and $u = 2$.*

The same analysis has been performed on the power-law suppression appearing at $\omega = -\mu$ (third plot of figure 3.16), and the Hartree boundary exponent has been extracted numerically. In figure 3.19 and 3.20 we report the data for two different filling factors. It is shown that the boundary exponent is found to be $u/2\pi v_F$ for a large interval in the interaction parameter u.

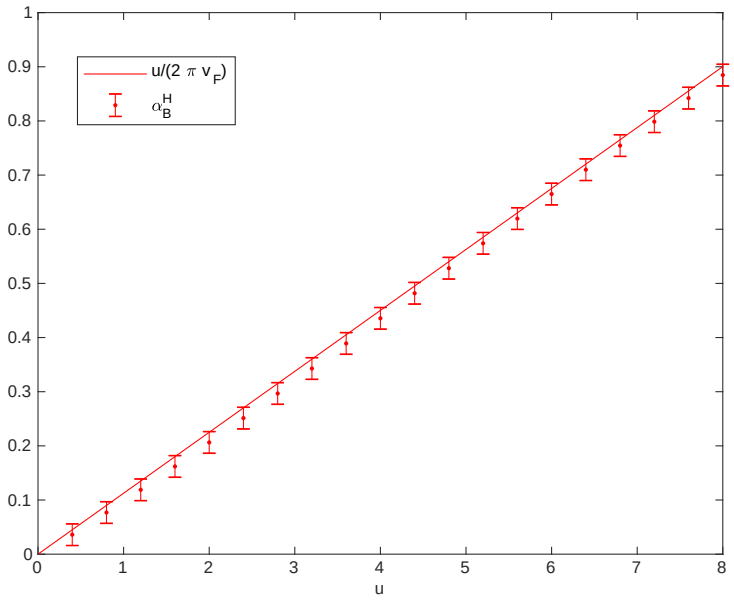

Figure 3.19: *Power-law exponent for the suppression at $\omega = -\mu$. Here $L - 1 = 4000$, $\eta = 0.5$. For details, see the text.*

On the Hartree level the local spectral function displays two important symmetries. The firs one is shown in figure 3.21. The spectral function for fixed filling and interaction u can be mapped onto the one for $-u$ and the same filling by taking the mirror image around $\omega = 0$. More formally, the local spectral function satisfies $\rho(\omega, \eta, u) = \rho(-\omega, \eta, -u)$. The spectral function for negative u is not investigated any further as the Hubbard model with attractive interaction is not a LL [6].

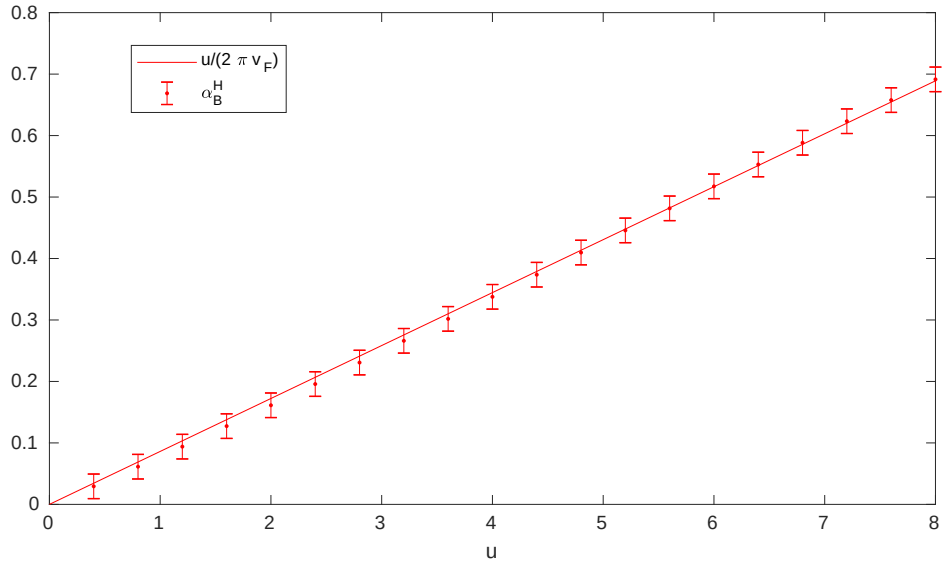

Figure 3.20: *Power-law exponent for the suppression at $\omega = -\mu$. Here $L - 1 = 4000$, $\eta = 0.75$. For details, see the text.*

The second symmetry is shown in figure 3.22. For a fixed value of interaction u the spectral function for a given η can be mapped onto the one for $2 - \eta$ by taking the mirror image around $\omega = 0$. The function satisfies then $\rho(\omega, \eta, u) = \rho(-\omega, 2-\eta, u)$. This implies that for system below half-filling $\eta < 1$, the increase in the spectral weight preceding the subsequent suppression at the chemical potential for energies which are occupied in the ground states is more pronounced compared to the analogous weight for fillings $\eta > 1$. This has to be contrasted to bosonization which always gives symmetric behaviour around the chemical potential [6]. Notice that the two aforementioned symmetries also entail that the spectral function satisfies $\rho(\omega, \eta, u) = \rho(\omega, 2 - \eta, -u)$. This is to be contrasted with the spinless fermions model where this property does not hold.

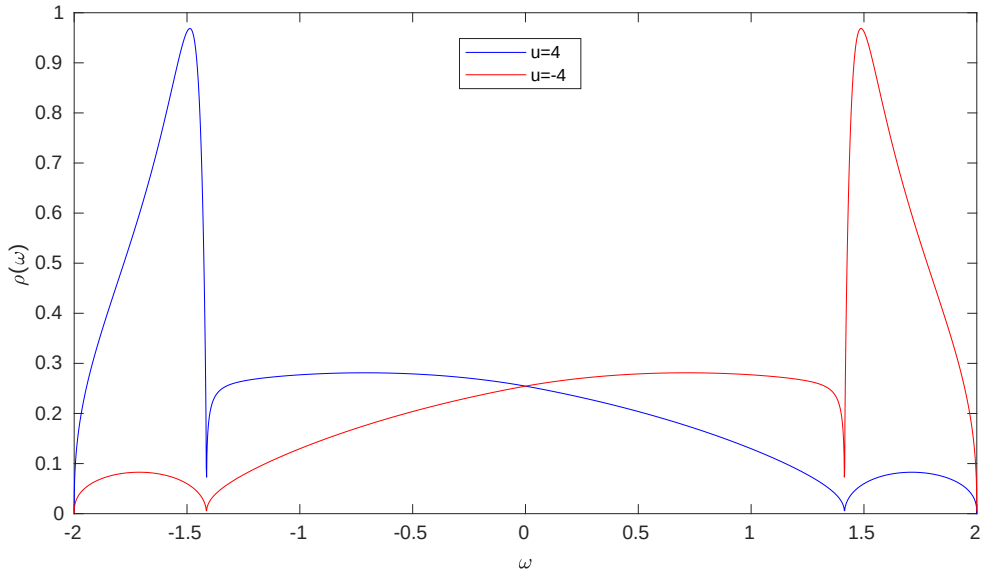

Figure 3.21: *Symmetry of the local spectral function under the mapping $u \to -u$ for $j = 1$, $\eta = 0.5$, $L-1 = 4000$.*

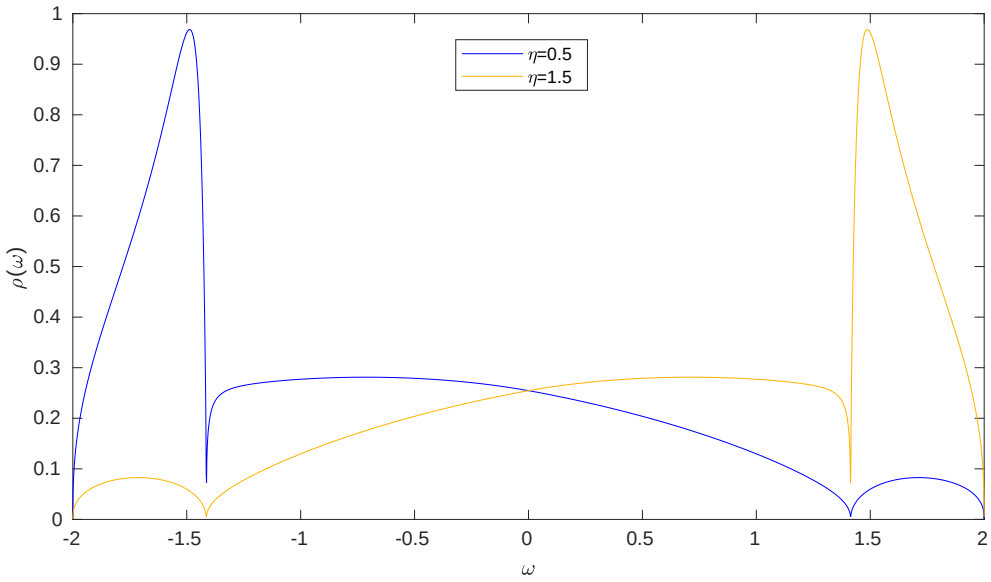

Figure 3.22: *Symmetry of the local spectral function under the mapping* $\eta \to 2-\eta$ *for* $j = 1$, $u = 4$, $L-1 = 4000$.

Closing consideration

In the last sections of this chapter we characterized the spectral function for both our model as obtained from the numerical inversion of the HF Hamiltonian. Our results for the energy value $\omega = \mu$ are in agreement with the one presented in [6]. The HF approximation for the self-energy already gives power-law behaviour. This is interesting as the same approximation for the case of PBC does not capture any of the LL features [6].
The new results involve the analysis of the power-law suppression at $\omega = -\mu$ for both the models. Up to this point though, we performed numerical simulations which offered meaningful results, but no profound physical insight is achieved. To develop a real understanding of what it is happening in the spectral density function of LLs with boundaries, we have to look at the Hartree-Fock self-energy in k-space. With some work, analytical results can then be obtained and the physics of the problem emerges more clearly. This will be the content of the next chapters.

Chapter 4

Real physics in k-space

"Of course it is happening inside your head, Harry,
but why on earth should that mean that it is not real?"
-Harry Potter and the Deathly Hallows-

4.1 Spectral density from the Green's function

In order to obtain analytical results we first explore the connection between the spectral density function and the one-particle retarded Green's function, defined for two general states $|\alpha\rangle$ and $|\beta\rangle$

$$iG^{\mathrm{R}}_{\alpha\beta}(t-t') = \Theta(t-t')\,\langle\{c_\alpha(t), c^\dagger_\beta(t')\}\rangle \tag{4.1}$$

where the expectation value is taken on the many body ground states, the curly brackets denotes the anticommutator and the operators evolve in time according to the Heisenberg picture. Our interest is on the diagonal term we denote with G^{R}_j, namely for $\alpha = \beta = j$. This function is connected to the spectral density function through the simple relation

$$\rho_j(\omega) = \lim_{\eta\to 0^+} -\frac{1}{\pi}\,\mathrm{Im}\left[G^{\mathrm{R}}_j(\omega + i\eta)\right] \tag{4.2}$$

To see this, we start from the definition of G^{R} as given in (4.1).

$$iG^{\mathrm{R}}_{\alpha\beta}(t-t') = \Theta(t-t')\,\langle c_j(t)c^\dagger_j(t')\rangle + \Theta(t-t')\,\langle c^\dagger_j(t')c_j(t)\rangle \tag{4.3}$$

We focus on the first term in the right hand side of expression (4.3), the other will be totally analogous. First of all we take advantage of the homogeneity of our system in the time variable, and set $t' = 0$. The evolution in time is governed by the interacting Hamiltonian H, and we get[1]

$$iG^{\mathrm{R}}_j(t) = \Theta(t)\,\langle e^{iHt}c_j e^{-iHt}c^\dagger_j\rangle$$

To obtain a spectral representation we introduce the resolution of identity in terms of eigenstates of the interacting Hamiltonian $|\phi_n\rangle$

[1]For simplicity, the operators at time $t = t' = 0$ carries no explicit notation, and $\hbar$ is set to 1 as usual.

$$
\begin{aligned}
iG_j^{\mathrm{R}}(t) &= \Theta(t)\,\langle\phi_0|e^{iHt}c_j\sum_n|\phi_n\rangle\,\langle\phi_n|\,e^{-iHt}c_j^\dagger|\phi_0\rangle \\
&= \sum_n \Theta(t)\,\langle\phi_0|e^{iHt}c_j\,|\phi_n\rangle\,\langle\phi_n|\,e^{-iHt}c_j^\dagger|\phi_0\rangle \\
&= \sum_n \Theta(t)e^{iE_0t}e^{-iE_nt}\,\langle\phi_0|c_j\,|\phi_n\rangle\,\langle\phi_n|\,c_j^\dagger|\phi_0\rangle \\
&= \sum_n \Theta(t)e^{i(E_0-E_n)t}|\,\langle\phi_n|c_j^\dagger|\phi_0\rangle\,|^2
\end{aligned}
$$

We can now Fourier transform this term. Setting $\xi = E_0 - E_n$ we make use of the identity[2]

$$
\int_{-\infty}^{\infty} dt\Theta(t)e^{i\xi}e^{i\omega t} = \frac{i}{\omega+\xi+i\eta} \tag{4.4}
$$

Similar computations lead to the analogous results for the second term in the anticommutator. We obtain therefore the spectral representation of the retarded Green's function we are dealing with

$$
G_j^{\mathrm{R}}(\omega+i\eta) = \sum_n \frac{|\,\langle\phi_n|c_j^\dagger|\phi_0\rangle\,|^2}{\omega+E_0^N-E_n^{N+1}+i\eta} + \sum_n \frac{|\,\langle\phi_n|c_j|\phi_0\rangle\,|^2}{\omega+E_n^{N-1}-E_0^N+i\eta} \tag{4.5}
$$

The last step is taking the imaginary part of this expression. Reminding that

$$
\lim_{\eta\to 0^+}\mathrm{Im}\,\frac{1}{\omega+\xi+i\eta} = \lim_{\eta\to 0^+} -\frac{\pi\eta}{(\omega+\xi)^2+\eta^2} = -\pi\delta(\omega+\xi) \tag{4.6}
$$

it is clear that we exactly obtain our spectral density function

$$
-\frac{1}{\pi}\lim_{\eta\to 0^+}\mathrm{Im}\left[G_j^{\mathrm{R}}(\omega+i\eta)\right] = \sum_n |\,\langle\phi_n|c_j^\dagger|\phi_0\rangle\,|^2\delta\big(\omega+E_0^N-E_n^{N+1}\big)+\sum_n |\,\langle\phi_n|c_j|\phi_0\rangle\,|^2\delta\big(\omega+E_n^{N-1}-E_0^N\big)
$$

This connection is of extreme importance for it allows us to make use of the powerful machinery of perturbation theory. Our concern is now to calculate the Green's function *analytically* for our systems within some meaningful approximation. To do this, it is useful to look back at what we have already performed in the previous chapter.

[2]For more details see [10].

4.2 Perturbative approach

4.2.1 First order for the self-energy

As a practical matter, computing the spectral function is nothing but computing the Green's function itself. The retarded Green's function we need is the diagonal matrix element of the operator [3]

$$G_j^{\mathrm{R}}(\omega + i\eta) = \langle j|G^{\mathrm{R}}(\omega + i\eta)|j\rangle = \langle j|\big[(\omega + i\eta) - H\big]^{-1}|j\rangle \tag{4.7}$$

Within the HF approximation, the full interacting Hamiltonian is split into the non-interacting part and the self-energy operator:

$$H^{\mathrm{HF}} = H_0 + \Sigma^{\mathrm{HF}} \tag{4.8}$$

In this case, due to the nontrivial expression of the matrix elements, analytical results are out of reach. Nevertheless, it has been possible to numerically invert the operator in (4.8). The Green's function we need then simply follows by change of basis:

$$\langle j|G^{\mathrm{R}}(\omega + i\eta)|j\rangle = \sum_{nn'} \langle j|n\rangle \langle n'|j\rangle \left[(\omega + i\eta) - H^{\mathrm{HF}}\right]^{-1}_{n,n'}$$

In the previous chapter we performed the first order perturbation theory in *real space* and subsequently proceeded with the numerical diagonalization of the matrix operator. This procedure is referred to as the first order perturbation for the *self-energy*.

4.2.2 First order for the Green's function

To be able to obtain analytical results we must perform an expansion to the first order in the *Green's function*. We focus on the Green's operator G

$$\begin{aligned} G &= \big[\omega - H_0 - \Sigma^{\mathrm{HF}}\big]^{-1} \\ &= \big[\big(\mathbb{I} - \Sigma^{\mathrm{HF}}(\omega - H_0)^{-1}\big)(\omega - H_0)\big]^{-1} \\ &= \big[\omega - H_0\big]^{-1}\big[\mathbb{I} - \Sigma^{\mathrm{HF}}(\omega - H_0)^{-1}\big]^{-1} \end{aligned}$$

Introducing the *non interacting Green's operator*

$$G_0 = \big[(\omega - H_0\big]^{-1} \tag{4.9}$$

one obtains

$$G = G_0\big[\mathbb{I} - \Sigma^{\mathrm{HF}} G_0\big]^{-1} \tag{4.10}$$

[3] When a scalar quantity such as $\omega + i\eta$ is added to an operator as H, the scalar is implicitly multiplied by the the identity operator.

Formally one can write

$$G = \frac{G_0}{\mathbb{I} - \Sigma^{\mathrm{HF}} G_0} = \frac{\mathbb{I}}{G_0^{-1} - \Sigma^{\mathrm{HF}}} \tag{4.11}$$

Indeed what we obtained is the famous *Dyson equation*. At this point we expand the term in the square brackets in (4.10) and truncate the expansion to the first order. Clearly the feasibility of this procedure relies on the condition of a small expansion parameter. We will return on this point later in the text. We have then

$$G = G_0\big[\mathbb{I} - \Sigma^{\mathrm{HF}} G_0\big]^{-1} \simeq G_0\big[\mathbb{I} + \Sigma^{\mathrm{HF}} G_0\big] = G_0 + G_0 \Sigma^{\mathrm{HF}} G_0 \tag{4.12}$$

To perform analytically this expansion, we project onto the basis set $|n\rangle$ where G_0 is diagonal, obtaining

$$\big[G(\omega + i\eta)\big]_{nn'} = \frac{\delta_{nn'}}{\omega + i\eta - \epsilon_n} + \sum_{mm'} \frac{\delta_{nm}}{\omega + i\eta - \epsilon_n} \langle m|\Sigma^{\mathrm{HF}}|m'\rangle \frac{\delta_{m'n'}}{\omega + i\eta - \epsilon_{n'}} \tag{4.13}$$

$$\big[G(\omega + i\eta)\big]_{nn'} = \frac{\delta_{nn'}}{\omega + i\eta - \epsilon_n} + \frac{\Sigma^{\mathrm{HF}}_{nn'}}{\big(\omega + i\eta - \epsilon_n\big)\big(\omega + i\eta - \epsilon_{n'}\big)} \tag{4.14}$$

Where we now denote the single-particle dispersion relation with ϵ_n. Once we obtain this, the spectral function follows easily through a change of basis and the relation in (4.2). The crucial point then, will be the analysis of the results this approach can offer and its consistency with the first order perturbation for the self-energy.
As it is clear from equation (4.13), our main task now turns out to be the analytical computation of the self-energy matrix elements in k-space. As a first idea, one can think of transforming the real space matrix elements we worked out in Chapter 2 into k-space. Again, due to the nontrivial behaviour in real space, this path is not feasible. Conversely, we need to represent the original interacting Hamiltonian given in Chapter 1 in k-space, and then to perform the first order perturbation theory for the interacting part.
Contrary to what we have done in the previous chapters, we start our analysis with the Hubbard model. In fact, the nature of the onsite interaction employed in this model yields to a simpler structure for the HF self-energy when compared to the spinless fermions model. Moreover, the Fock contribution vanishes for this model and we only need to evaluate the Hartree term. In this way the physical meaning emerges in a more elegant way and we will be able to point out the main source leading to the power-law suppression in the local density of state. It will then serve as a solid ground to successively perform the same procedure for the spinless fermions model, where the structure of the HF self-energy operator in k-space is more complicated. In the rest of this chapter we are going to compute and analyse this structure for both models, while underlining similarities and differences.

4.3 Hubbard model

4.3.1 Self-energy operator in k-space

As mentioned above, we now face the task of representing the Hubbard Hamiltonian in the basis of non-interacting eigenstates. With the same notation we already used we have

$$H = -2t \sum_{\sigma} \sum_{n=1}^{L-1} \cos\Big(\frac{\pi}{L} n\Big) c^{\dagger}_{n\sigma} c_{n\sigma} + \frac{4u}{L^2} \sum_{n_1 n_2 n_3 n_4} \sum_{j} \sin(k_1 j) \sin(k_2 j) \sin(k_3 j) \sin(k_4 j) c^{\dagger}_{n_1\uparrow} c^{\dagger}_{n_2\downarrow} c_{n_4\downarrow} c_{n_3\uparrow}$$

where $k_i = \frac{\pi}{L} n_i$. We now focus on the interaction term in k-space

$$V_{k_1 k_2 k_3 k_4} = \frac{4u}{L^2} \sum_j \sin(k_1 j) \sin(k_2 j) \sin(k_3 j) \sin(k_4 j) \tag{4.15}$$

To tackle this computation we first make use of Werner formula

$$\sin(x)\sin(y) = \frac{1}{2}[\cos(x-y) + \cos(x+y)]$$

for generic x and y. Plugging this into equation (4.15) and working out some algebra one gets:

$$\begin{aligned} V_{k_1 k_2 k_3 k_4} = \frac{u}{L^2} \sum_{j=1}^{L-1} \Big[& \cos\big((k_1 - k_3)j\big) \cos\big((k_2 - k_4)j\big) + \cos\big((k_1 + k_3)j\big) \cos\big((k_2 + k_4)j\big) \\ & - \cos\big((k_1 - k_3)j\big) \cos\big((k_2 + k_4)j\big) - \cos\big((k_1 + k_3)j\big) \cos\big((k_2 - k_4)j\big) \Big] \end{aligned}$$

We now define the auxiliary function:

$$f(q, q') = \frac{u}{L} \sum_{j=1}^{L-1} \cos(q)\cos(q') = \frac{u}{4L} \sum_{j=1}^{L-1} \left[e^{i(q+q')} j + e^{i(q-q')j} + \text{c.c.} \right] \tag{4.16}$$

which will be extremely helpful in the following. Let us perform the sum over the index j to give this function a more attractive look

$$\begin{aligned} f(q, q') &= \frac{u}{4L} \left[-4 + 2L\delta_{q,q'} + 2L\delta_{q,-q'} + (1 - \delta_{q,q'}) \frac{1 - e^{i(q-q')L}}{1 - e^{i(q-q')}} + (1 - \delta_{q,-q'}) \frac{1 - e^{i(q+q')L}}{1 - e^{i(q+q'} } + \text{c.c.} \right] \\ &= \frac{u}{4L} \left[-4 + 2L\delta_{q,q'} + 2L\delta_{q,-q'} + (1 - \delta_{q,q'}) \frac{1 - (-1)^{n-n'}}{1 - e^{i(q-q')}} + (1 - \delta_{q,-q'}) \frac{1 - (-1)^{n+n'}}{1 - e^{i(q+q'} } + \text{c.c.} \right] \\ &= -\frac{u}{L} + \frac{u}{2} \big(\delta^{2\pi}_{q,q'} + \delta^{2\pi}_{q,-q'} \big) + \frac{u}{4L} \Big[\big(1 - \delta^{2\pi}_{q,q'}\big) \big(1 - (-1)^{n-n'}\big) + \big(1 - \delta^{2\pi}_{q,-q'}\big) \big(1 - (-1)^{n+n'}\big) \Big] \end{aligned}$$

In the last line we explicitly used the superscript 2π on the δ-function to denote its periodicity, namely

$$\delta^{2\pi}_{q,q'} = \delta_{q,q+2\pi m}$$

with $m \in \mathbb{Z}$. It is clear that the non-δ terms vanish when taking the thermodynamic limit and the expression reduces to

$$f(q, q') = \frac{u}{2} \big(\delta^{2\pi}_{q,-q'} + \delta^{2\pi}_{q,q'} \big) \tag{4.17}$$

so that from (4.16) our interaction matrix element takes the docile form

$$V_{k_1 k_2 k_3 k_4} = \frac{1}{L} \Big[f(k_1 - k_3, k_2 - k_4) + f(k_1 + k_3, k_2 + k_4) - f(k_1 - k_3, k_2 + k_4) - f(k_1 + k_3, k_2 - k_4) \Big] \tag{4.18}$$

For the upcoming computations it is useful to "label" the terms in (4.18) as

$$V_{k_1k_2k_3k_4} = \big(V_1 + V_2\big) + \big(V_3 + V_4\big) + \big(V_5 + V_6\big) + \big(V_7 + V_8\big) \tag{4.19}$$

where the correspondence is clear when plugging (4.17) into (4.18) with the given order.

4.3.2 Hartree approximation in k-space

We succeeded in representing the interacting Hamiltonian in the basis $|n\rangle$. The first order perturbation theory requires us to work out 8 different terms, 2 δ-functions for every $f(q, q')$, as in (4.19). The Hartree approximation gives for the interacting Hamiltonian

$$H^{\mathrm{HF}} = \sum_{n_1n_2n_3n_4} V_{k_1k_2k_3k_4} c^\dagger_{n_1\uparrow} \langle c^\dagger_{n_2\downarrow} c_{n_4\downarrow}\rangle \, c_{n_3\uparrow} + \sum_{n_1n_2n_3n_4} V_{k_1k_2k_3k_4} c^\dagger_{n_2\downarrow} \langle c^\dagger_{n_1\uparrow} c_{n_3\uparrow}\rangle \, c_{n_4\downarrow} \tag{4.20}$$

Since the interaction is spin-independent, from now on we only focus on the self-energy matrix for one single spin population without further notation, the other one being perfectly identical. Moreover, given the nontrivial nature of the interaction term, the first order perturbation is better studied with the help of diagrammatic language. We start out by evaluating these terms for a system below half-filling. Within the present notation, in the matrix representation for the self-energy the rows are labelled by n_1 while the columns by n_3, as it can be understood from figure 4.1.

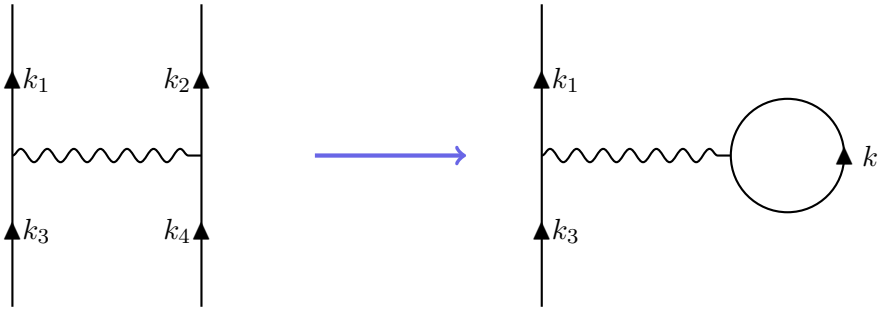

Figure 4.1: *Feynman diagram for the Hartree term in k-space.*

Let us start with the first f function in the expression (4.18). By imposing the interaction condition we get

$$k_1 - k_3 = -(k_2 - k_4) + 2\pi m$$

The Hartree approximation implies $k_2 = k_4 = k$ so that

$$k_1 - k_3 = +2\pi m$$

we then have the cases:

$$m = 0 \implies k_1 = k_3$$

$$m = \pm 1 \implies k_1 = k_3 \pm 2\pi$$

$$\implies n_1 = n_3 \pm 2L$$

The *umklapp* contribution in the second case is not possible since n_1 is not allowed to take values bigger than $2L$. We are left with the diagonal term $\delta_{k_1 k_3}$ whose value is the sum of a simple constant from zero to N_F. All together this term yields

$$V_1 = \frac{u}{2L} N_F \tag{4.21}$$

From the second δ-function we have

$$k_1 - k_3 = (k_2 - k_4) + 2\pi m$$

which takes no big effort to see it gives an identical result. The diagonal matrix elements in our Hartree self-energy matrix read:

$$\Sigma^{\mathrm{H}}_{kk} = V_1 + V_2 = u\frac{N_F}{L} \tag{4.22}$$

We proceed for the second f function with the same order.

$$k_1 + k_3 = -(k_2 + k_4) + 2\pi m = -2k + 2\pi m \implies k = -\frac{k_1 + k_3}{2} + \pi m$$

However, k must satisfy

$$0 < k \leq k_F \implies 0 < -(n_1 + n_3) + 2mL \leq 2N_F$$

We analyse the case for different values of m:

$$m = 0 \implies n_1 + n_3 < 0 \rightarrow \text{impossible!}$$

$$m = 1 \implies 0 < -(n_1 + n_3) + 2L \leq 2N_F$$

$$\implies (n_1 + n_3) > 0 \rightarrow \forall n_1, n_3 \ \wedge \ n_1 \geq 2(L - N_F) - n_3$$

$$m = 2 \implies n_1 + n_3 \geq 4L - 2N_F \text{ with } N_F^{\max} = L - 1$$

$$\implies n_1 \geq -n_3 + 2(L - 1)$$

For negative values of m one sees that there are no possible cases. In this sector of the self-energy the matrix elements are simply

$$V_3 = \frac{u}{2L} \tag{4.23}$$

The structure of this sector is illustrated in figure 4.2. Notice that this contribution is due to the umklapp scattering $m = 1$. The second δ-function gives:

$$k_1 + k_3 = k_2 + k_4 + 2\pi = 2k + 2\pi m \implies k = \frac{k_1 + k_3}{2} - \pi m$$

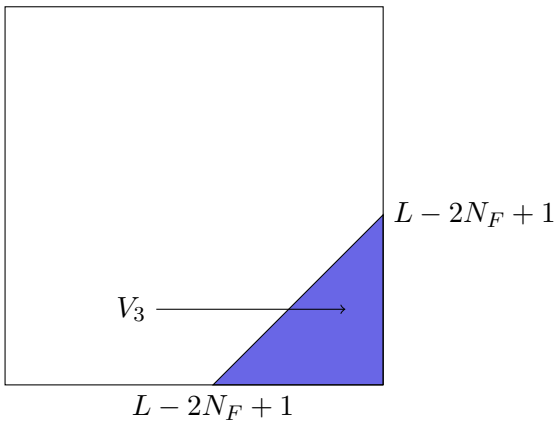

Figure 4.2: *Sector 3 of the self-energy matrix operator*

The same constrains on k lead to

$$m = 0 \implies n_1 > n_3 \wedge n_1 \leq -n_3 + 2N_F$$

$$m = 1 \implies n_1 + n_3 > 2L \rightarrow \text{impossible!}$$

$$m = -1 \implies n_1 + n_3 > -2L \rightarrow \forall n_1, n_3 \ \wedge \ n_1 \leq -n_3 + 2(L - N_F)$$

Compared to the previous case, we are now selecting the symmetric self-energy sector with respect to the antidiagonal. Here again the matrix elements are constant and equal to

$$V_4 = \frac{u}{2L} \tag{4.24}$$

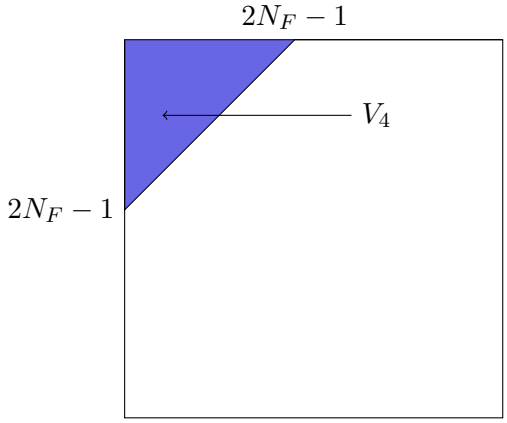

Figure 4.3: *Sector 4 of the self-energy matrix operator*

The next term in the interaction yields

$$k_1 - k_3 = -(k_2 + k_4) + 2\pi m = -2k + 2\pi m \implies k = \frac{k_3 - k_1}{2} + \pi m$$

As before, k is constrained between 0 and k_F. The only allowed cases are

$$m = 0 \implies n_1 < n_3 \wedge n_1 \geq n_3 - 2N_F$$

$$m = 1 \implies n_1 > n3 + 2L \rightarrow \forall\ n_1, n_3\ \wedge\ n_1 \geq n_3 + 2(L - N_F)$$

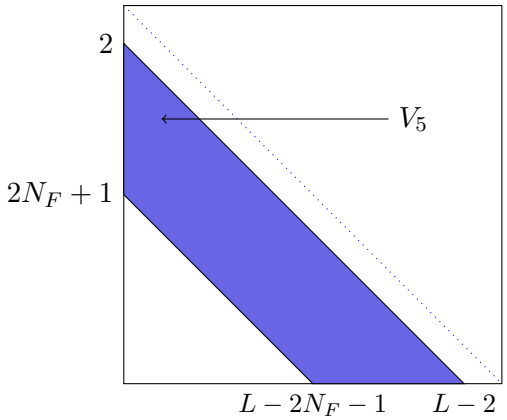

Figure 4.4: *Sector 5 of the self-energy matrix operator*

The sector obtained in this way is illustrated in figure 4.4. The matrix elements again are constant and equal to

$$V_5 = -\frac{u}{2L} \tag{4.25}$$

The next term leads to a symmetric sector with respect to the principle diagonal and it is shown in figure 4.5 . We have in fact

$$k_1 - k_3 = (k_2 + k_4) + 2\pi m = 2k + 2\pi m \implies k = \frac{k_1 - k_3}{2} - \pi m$$

$$m = 0 \implies n_1 > n_3 \wedge n_1 \leq n_3 + 2N_F$$

$$m = 1 \implies n_1 > n3 - 2L \rightarrow \forall\ n_1, n_3\ \wedge\ n_1 \leq n_3 - 2(L - N_F)$$

As before, the value of the matrix elements reads

$$V_6 = -\frac{u}{2L} \tag{4.26}$$

Furthermore, the last two terms coming from the fourth f function in (4.18) do not contribute to the structure of the self-energy matrix.

$$k_1 + k_3 = -(k_2 - k_4) + 2\pi m = +2\pi m$$

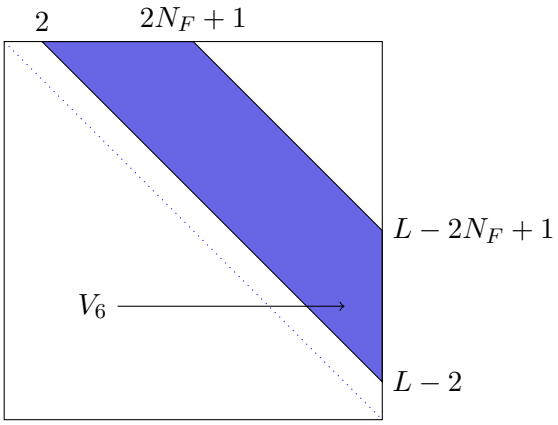

Figure 4.5: *Sector 6 of the self-energy matrix operator*

$$m = 0 \implies n_1 = -n_3 \rightarrow \text{impossible!}$$

$$m = 1 \implies n_1 > -n3 + 2L \rightarrow \text{impossible!}$$

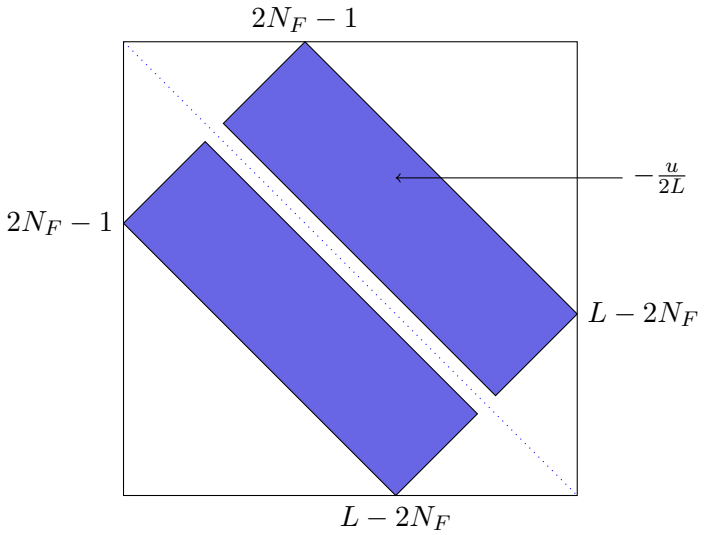

Figure 4.6: *Structure of the Hartree self-energy matrix in k-space for the Hubbard model with* $\eta < 1$.

One can easily observe that the same result holds for the last term V_8. Indeed we succeeded in computing all the matrix elements of the HF self-energy. Putting everything together we can finally have a look at the structure of the self-energy in k-space in figure 4.6.
As it is clear from our computation, we notice that only the matrix elements guaranteeing an even value for $n_1 \pm n_3$ are non vanishing in the coloured sectors. This is due to the parity symmetry with respect to the middle of the chain in OBC. We also observe that the Hartree self-energy is real and ω-independent. The nontrivial structure is due to the broken translational invariance. In the PBC case in fact, the HF self-energy matrix is diagonal thanks to momentum conservation. This can only lead to finite shifts in the chemical potential μ and the Fermi velocity v_F [6].
The peculiarity lies in the fact that the self-energy exhibits a step function crossing the diagonal *both* in (k_F, k_F) and in $(\pi - k_F, \pi - k_F)$. The diagonal contribution can only lead to a shift in the chemical potential $\delta\mu$ due to the interaction. For our purpose therefore, we can always work with a self-energy matrix where the diagonal contribution is subtracted, from now on simply denoted by Σ^{H}. For the low energy sector then one can write:

$$\Sigma^{\mathrm{H}}_{kk'} \simeq -\frac{u}{2L}\Theta(k+k'-2k_F) \tag{4.27}$$

and analogously for the "high energy" sector

$$\Sigma^{\mathrm{H}}_{kk'} \simeq +\frac{u}{2L}\Theta(k+k'-2k_F) - \frac{u}{L} \tag{4.28}$$

One could argue that this structure is responsible for the dips and peaks we observed in the spectral function, and this turns out to be exactly the case. It will be shown that this leads to the emergence of the power-law behaviour at $\omega = \mu$ and $\omega = -\mu$.

Above half-filling

We now need to perform the same analysis for the matrix elements when $k_F > \frac{\pi}{2}$. This will allow us have complete knowledge of the self-energy structure. The computations are the same and the values of the matrix elements in each sector are left untouched. However, the sectors we will end up with may differ. The combination of new matrix sectors leads therefore to a different structure. It is easy to see that the first two terms lead to identical diagonal matrix elements. We thus look at the off-diagonal terms with the same order. For V_3 nothing is changed, but the self-energy sector is illustrated in figure 4.7. Comparing this with figure 4.2 we see this is nothing but the previous sector for $m = 1$ which has been dragged and stretched back due to a different value of N_F. In a similar fashion the same holds for V_4 where the self-energy sector is pictured in figure 4.8.

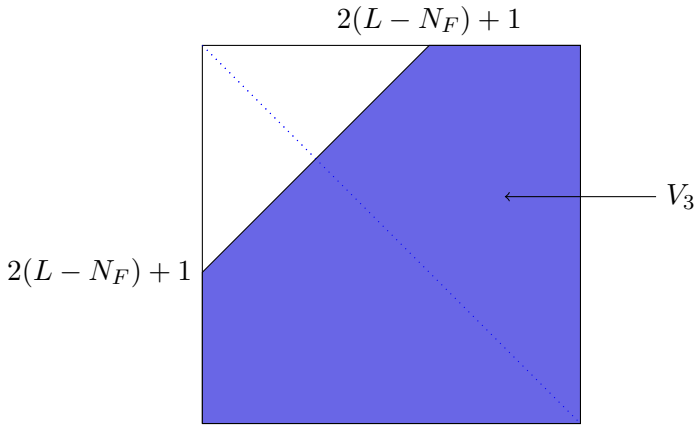

Figure 4.7: *Sector 3 for filling factor* $\eta > 1$

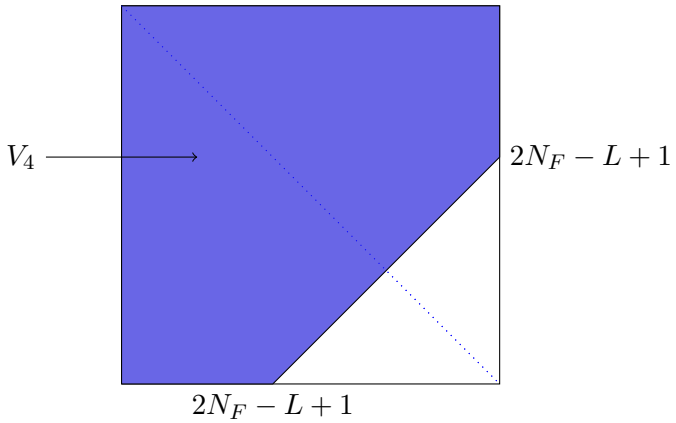

Figure 4.8: *Sector 4 for filling factor* $\eta > 1$

For the negative terms in 4.18 we have:

$$m = 0 \implies n_1 < n_3 \wedge n_1 \geq n_3 - 2N_F$$

$$m = 1 \implies n_1 < n3 + 2L \rightarrow \forall\ n_1, n_3\ \wedge\ n_1 \geq n_3 + 2(L - N_F)$$

Reminding that $n_3 - 2N_F$ is now *negative*, the case $m = 0$ reduces to the condition $n_1 < n_3$ describing the whole lower triangular part of the matrix. Comparing this with figure 4.4 we see that the same sector has stretched down to the low left corner of the matrix, and a new available sector appeared as shown in figure 4.9. Analogously the sector explored by V_6 is symmetric and illustrated in figure 4.10. Finally, The last two terms carry no contributions as happened in the first case.

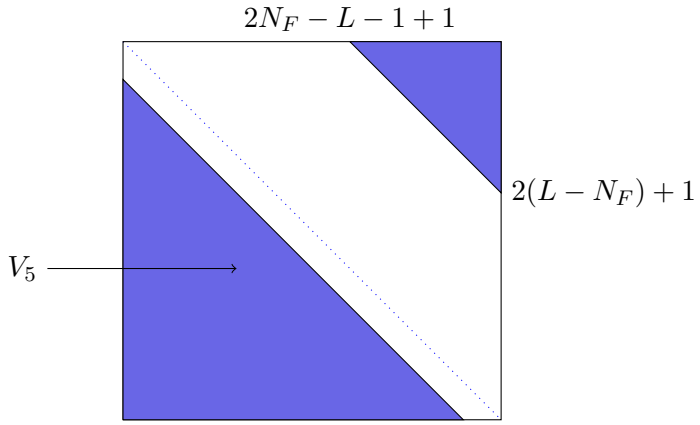

Figure 4.9: *Sector 5 for filling factor* $\eta > 1$

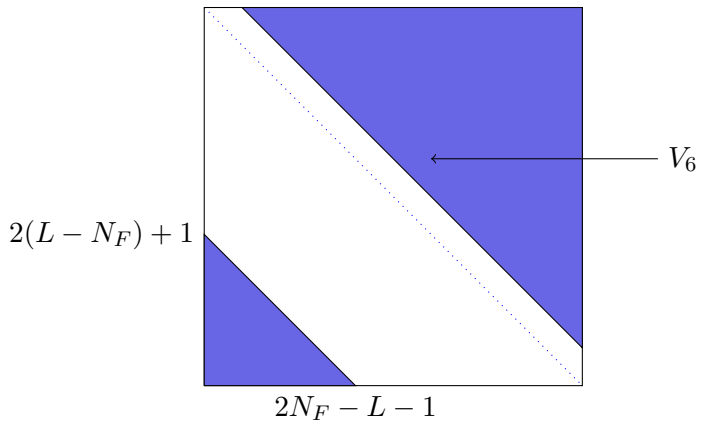

Figure 4.10: *Sector 6 for filling factor* $\eta > 1$

The overall picture of the self energy for a filling factor $\eta > 1$ is given in figure 4.11. The combination of different sectors leads again to a step function. The height of the steps in (k_F, k_F) and $(\pi - k_F, \pi - k_F)$ are however identical to the previous situation, respectively negative and positive.
We can now understand the symmetries of the spectral function discussed in section 3.3. Under the mapping $\eta \rightarrow 2 - \eta$ the two dimensional step function in Σ^{H} swaps its sign. As in our approximation the height of the step is proportional to u, we could recover an identical self-energy structure by mapping $u \rightarrow -u$. More formally, the Hartree self-energy of the Hubbard model satisfies

$$\Sigma^{\mathrm{H}}_{kk'}(\eta, u) = \Sigma^{\mathrm{H}}_{kk'}(2 - \eta, -u) \tag{4.29}$$

This leads to the symmetries of the local spectral function presented in section 3.3.

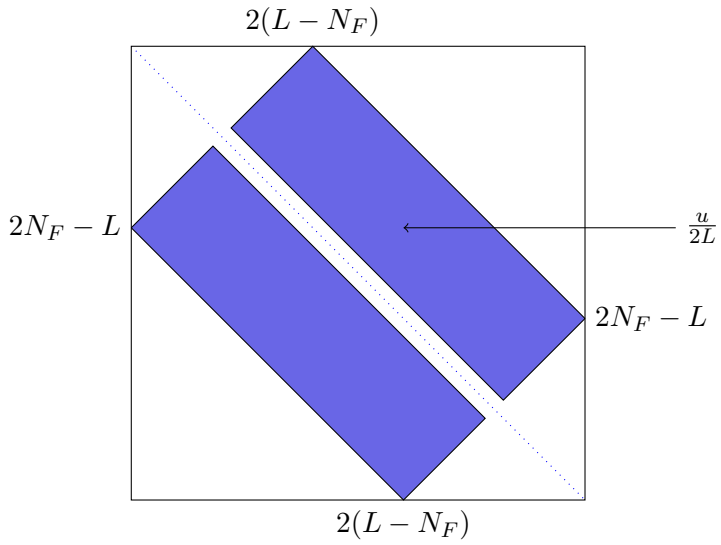

Figure 4.11: *Structure of the Hartree self-energy matrix in k-space for the Hubbard model with* $\eta > 1$

4.4 Back to spinless fermions

4.4.1 Self-energy in k-space

Moving back to our spinless fermions model, we want to represent the interaction term in k-space. The computation is similar to what we have done for the Hubbard model. In this case we have to evaluate

$$V_{k_1k_2k_3k_4} = \frac{4v}{L^2}\sum_j \sin(k_1 j)\sin(k_3 j)\sin\left[k_2(j+1)\right]\sin\left[k_4(j+1)\right] \tag{4.30}$$

As for the previous model, the last expression can be recast in the more tractable form

$$V_{k_1k_2k_3k_4} = \frac{1}{L}\Big[g(k_1-k_3,k_2-k_4)+g(k_1+k_3,k_2+k_4)-g(k_1-k_3,k_2+k_4)-g(k_1+k_3,k_2-k_4)\Big] \tag{4.31}$$

where now the auxiliary function g reads:

$$g(q,q') = \frac{v}{L}\sum_{j=1}^{L-1}\cos(qj)\cos\left[q'(j+1)\right] \tag{4.32}$$

The structure of the computation is similar to what we have already performed. We have [4]

[4]Here the starting index is stretched down to $j=0$ and we neglect the resulting constant term, since it will suffer the limit $L\to\infty$ and abandon the scene.

$$
\begin{aligned}
g(q,q')\frac{4L}{v} &= \sum_{j=1}^{L-1}\left[e^{i(q+q')j}e^{iq'} + e^{i(q-q')j}e^{-iq'} + \text{c.c.}\right] \\
&= e^{iq'}\sum_{j=1}^{L-1} e^{i(q+q')j} + e^{-iq'}\sum_{j=1}^{L-1} e^{i(q-q')j} + \text{c.c.} \\
&= e^{iq'}\left[\delta_{q,-q'}L + \big(1-\delta_{q,-q'}\big)\frac{1-(-1)^{n+n'}}{1-e^{i(q+q')}}\right] + e^{-iq'}\left[\delta_{q,q'}L + \big(1-\delta_{q,q'}\big)\frac{1-(-1)^{n-n'}}{1-e^{i(q-q')}}\right] + \text{c.c.}
\end{aligned}
$$

Focusing on the first term and its complex conjugate for simplicity, while setting $\alpha = 1-(-1)^{n+n'}$:

$$
\begin{aligned}
& e^{iq'}\left[\delta_{q,-q'}L + \big(1-\delta_{q,-q'}\big)\frac{1-(-1)^{n+n'}}{1-e^{i(q+q')}}\right] + \text{c.c.} \\
&= \big(e^{iq'} + e^{-iq'}\big)\delta_{q,-q'}L + \alpha\big(1-\delta_{q,-q'}\big)\frac{e^{iq'}(1-(e^{-i(q+q')}) + e^{-iq'}(1-(e^{+i(q+q')})}{2-2\cos(q+q')} \\
&= \big(2\cos q'\big)\delta_{q,-q'}L + \alpha\big(1-\delta_{q,-q'}\big)\frac{2\cos q' - 2\cos q}{2-2\cos(q+q')} \\
&= \big(2\cos q'\big)\delta_{q,-q'}L + \alpha\big(1-\delta_{q,-q'}\big)\frac{\cos q' - \cos q}{1-\cos(q+q')}
\end{aligned}
$$

Restoring everything we finally have

$$
g(q,q') = \frac{v}{2}\cos(q')\big[\delta_{q,-q'} + \delta_{q,+q'}\big] + \frac{1}{L}h(q,q') \tag{4.33}
$$

where $h(q,q')$ contains the non-δ terms:

$$
h(q,q') = \frac{v}{4}\frac{\cos(q')+\cos(q)}{1-\cos(q+q')}\Big[\big(1-\delta_{q,-q'}\big)\big(1-(-1)^{n+n'}\big) + \big(1-\delta_{q,q'}\big)\big(1-(-1)^{n-n'}\big)\Big] \tag{4.34}
$$

As before, the contribution in the interaction given by the terms in $h(q,q')$ is negligible when taking the thermodynamic limit and we are left with

$$
g(q,q') = \frac{v}{2}\cos q'\big(\delta_{q,-q'} + \delta_{q,q'}\big) \tag{4.35}
$$

where the 2π periodicity is now implicit in the notation. This interaction resembles the one we have already found in the Hubbard model, except from the factor $\cos q'$, which is anything but innocent.

4.4.2 Hartree-Fock approximation in k-space

Knowing the expression for the interaction term in k-space we are ready to perform the first order perturbation. In this model though, both the direct and exchange terms are present. Keeping in mind the knowledge we gained working with the Hubbard model, we start from the Hartree contribution. The matrix sectors involved for the 8 different terms are exactly the same. However, the value of the matrix elements in a specific sector is not anymore constant, since it picks up a factor $\cos(q')$. As we have seen, the first two terms lead to the matrix elements on the diagonal. In both cases we have

$$
q' = k_2 - k_4
$$

The Hartree approximation constrains $k_2 = k_4 = k$ so that

$$q' = 0 \implies V_1 = V_2 = \frac{vN_F}{2L}\cos 0 = \frac{vN_F}{2L}$$

The Hartree diagonal matrix elements are constant and read

$$\Sigma^{\mathrm{H}}_{kk} = V_1 + V_2 = \frac{vN_F}{L} \tag{4.36}$$

More interesting are the next cases 3 and 4. We set $k_2 = k_4 = k$ obtaining

$$q' = 2k \text{ with } k = -\frac{k_1 + k_3}{2} + \pi m$$

Thanks to the parity and periodicity of the cosine the matrix element is

$$V_3 = V_4 = \frac{v}{2L}\cos 2k = \frac{v}{2L}\cos(k_1 + k_3) \tag{4.37}$$

The same holds for the sector 4. The situation is sketched in figure 4.12.

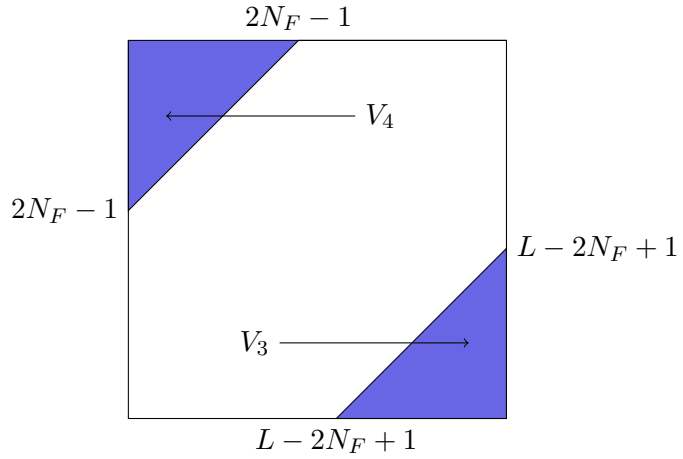

Figure 4.12: *Sectors 3 and 4 for the self-energy matrix.*

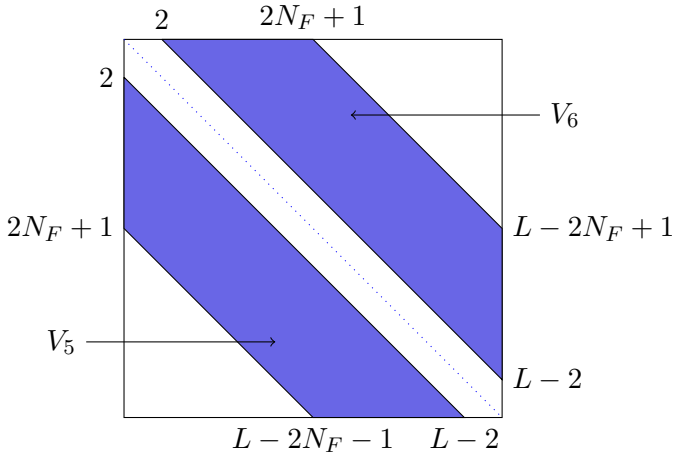

Figure 4.13: *Sectors 5 and 6 of the self-energy matrix.*

The terms 5 and 6 lead to:

$$q' = 2k = k_1 - k_3 + 2\pi m$$

In figure 4.13 we see the sector 5 and 6 with the matrix elements

$$V_5 = V_6 = -\frac{v}{2L}\cos 2k = -\frac{v}{2L}\cos(k_1 - k_3) \tag{4.38}$$

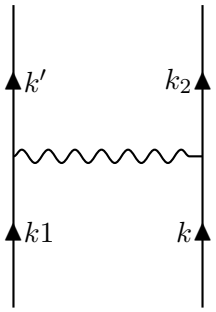

Figure 4.14: *Relabelling of the interaction diagram in k-space.*

Indeed the last terms 7 and 8 carry no contribution to the self-energy. As mentioned above, the work we have done on the Hubbard model allowed us to go through this Hartree computation for the spinless fermions model more quickly, thanks to the identical structure of the self-energy sectors involved.
We now evaluate the Fock contribution, working out the terms in the same order. Before setting off however, a slight change in the notation for the interaction is preferable, as shown in figure 4.14. In this way the incoming and outcoming k states are labelled k_1 and k_2 respectively. The exchange term force $k = k'$ and $q' = k_2 - k$. [5]

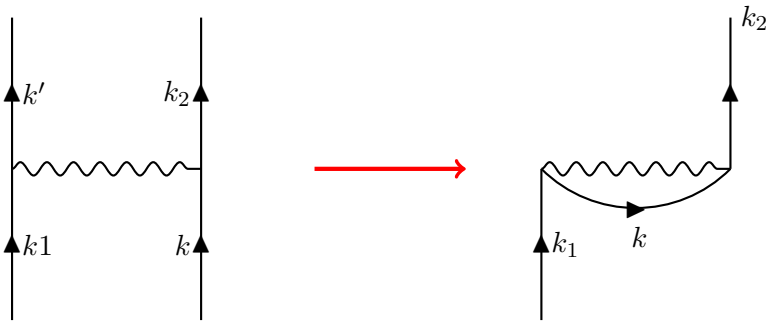

Figure 4.15: *Feynman diagram for the Fock term in k-space.*

The first δ-function gives:

$$k - k_1 = -(k_2 - k) + 2\pi m \implies k_1 = k_2$$

For the diagonal term then we have to compute

$$V_1 = \frac{v}{2L}\sum_{n=1}^{N_F}\cos\left(k_2 - \frac{\pi}{L}n\right) = \frac{v}{2L}\cos k_2 \sum_{n=1}^{N_F}\cos\left(\frac{\pi}{L}n\right) + \frac{v}{2L}\sum_{n=1}^{N_F}\sin\left(\frac{\pi}{L}n\right) \tag{4.39}$$

The sum over cosine functions leads to

[5] Although it is not very common, for the exchange term we make use of the Feynman diagram as pictured in the book of Mattuck [12]. The reasons are way too many to fit in a footnote and we refer directly to that masterpiece of didactics.

$$\sum_{n=1}^{N_F}\cos\Big(\frac{\pi}{L}n\Big) = \frac{1}{2}\Bigg[-1+\frac{1-e^{i\left(\frac{\pi}{L}(N_F+1)\right)}}{1-e^{i\frac{\pi}{L}}}+\text{c.c.}\Bigg]$$
$$= \frac{1}{2}\Bigg[-2+\frac{1-e^{-i\frac{\pi}{L}}-e^{+i\frac{\pi}{L}(N_F+1)}+e^{+i\frac{\pi}{L}N_F}+\text{c.c.}}{2-2\cos\left(\frac{\pi}{L}\right)}\Bigg]$$
$$= \frac{1}{2}\Bigg[-1+\frac{\cos\left(\frac{\pi}{L}N_F\right)-\cos\left(\frac{\pi}{L}(N_F+1)\right)}{1-\cos\left(\frac{\pi}{L}\right)}\Bigg]$$

With the help of prosthaphaeresis formulae we simplify this expression to

$$\sum_{n=1}^{N_F}\cos\Big(\frac{\pi}{L}n\Big) = \frac{1}{2}\Bigg[-1+\frac{2\sin\left(\frac{\pi}{2L}(2N_F+1)\right)\sin(\frac{\pi}{2L})}{2\sin^2(\frac{\pi}{2L})}\Bigg] = \frac{1}{2}\Bigg[-1+\frac{\sin\left(\frac{\pi}{2L}(2N_F+1)\right)}{\sin(\frac{\pi}{2L})}\Bigg]$$

In the same way we evaluate the sum of sine functions, where we are allowed to extend the index down to $n=0$

$$\sum_{n=0}^{N_F}\sin\Big(\frac{\pi}{L}n\Big) = \frac{1}{2}\Bigg[\frac{\sin\left(\frac{\pi}{L}\right)+\sin\left(\frac{\pi}{L}N_F\right)-\sin\left(\frac{\pi}{L}(N_F+1)\right)}{2\sin^2\left(\frac{\pi}{2L}\right)}\Bigg]$$
$$= \frac{1}{2}\Bigg[\frac{2\sin\left(\frac{\pi}{2L}\right)\cos\left(\frac{\pi}{2L}\right)+2\cos\left(\frac{\pi}{2L}(N_F+1)\right)\sin\left(-\frac{\pi}{2L}\right)}{2\sin^2\left(\frac{\pi}{2L}\right)}\Bigg]$$
$$= \frac{\cos\left(\frac{\pi}{2L}\right)-\cos\left(\frac{\pi}{2L}(N_F+1)\right)}{2\sin\left(\frac{\pi}{2L}\right)}$$
$$= \frac{2\sin\left(\frac{\pi}{2L}(N_F+1)\right)\sin\left(\frac{\pi}{2L}\right)}{2\sin\left(\frac{\pi}{2L}\right)}$$
$$= \sin\Big[\frac{\pi}{2L}(N_F+1)\Big]$$

Plugging the last two results into equation (4.39), one has the first diagonal contribution. As for the Hartree case, we will see that another interaction term will play a role on the diagonal matrix elements. Proceeding with the usual order we now have

$$k-k_1 = k_2-k+2\pi m \implies k = \frac{k_1+k_2}{2}+\pi m$$

The only available m is here $m=0$, defining therefore the sector sketched in figure 4.16. Reminding that now $q' = \frac{k_2-k_1}{2}$, the matrix elements read[6]

$$V_2 = \frac{v}{2L}\cos\Big(\frac{k_2-k_1}{2}\Big) \tag{4.40}$$

In a similar way for the third contribution we have

$$k = -\Big(\frac{k_1+k_2}{2}\Big)+\pi m$$

[6]We recall the fact that we are still not taking into account the overall minus sign coming from the exchange operation. This will be done once we gain complete knowledge about the self energy matrix elements.

The case with $m = 0$ is not possible, while the umklapp contribution $m = 1$ crop out the sector 3 in figure 4.16. Since $q' = k_2 + k + \pi$ in this case, the matrix elements read

$$V_3 = \frac{v}{2L}\cos\left(\frac{k_2 - k_1}{2} + \pi\right) = -\frac{v}{2L}\cos\left(\frac{k_2 - k_1}{2}\right) \tag{4.41}$$

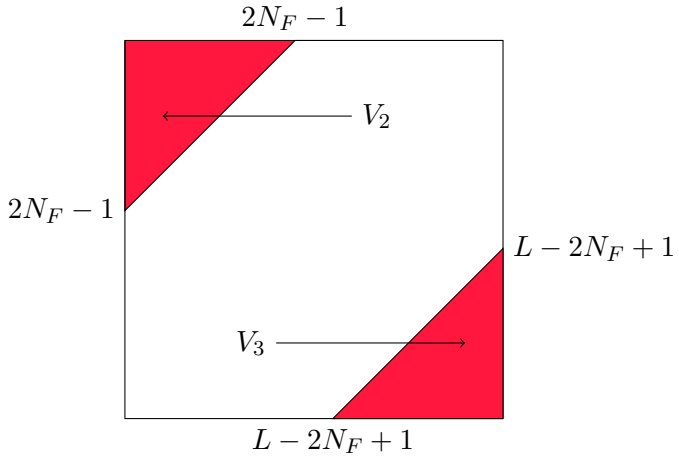

Figure 4.16: *Sector 2 and 3 in the Fock self-energy matrix.*

The fourth contribution is now setting values on the diagonal. We have in fact:

$$k + k_1 = k_2 + k + 2\pi m \implies k_1 = k_2$$

since $m = 0$ is the only acceptable case. The value of k is left to run free, leaving us to perform the sum

$$V_4 = \frac{v}{2L}\sum_{n=1}^{N_F}\cos\left(k_2 + \frac{\pi}{L}n\right) = \frac{v}{2L}\cos k_2 \sum_{n=1}^{N_F}\cos\left(\frac{\pi}{L}n\right) - \frac{v}{2L}\sum_{n=1}^{N_F}\sin\left(\frac{\pi}{L}n\right) \tag{4.42}$$

The first part is identical to the one in V_1, while the second carries opposite sign and thus cancels out when V_1 and V_4 are added together. The constant term coming from the sum of cosines vanishes in the thermodynamic limit and we finally have the expression for the diagonal Fock term

$$\Sigma^F_{kk} = \frac{v}{2L}\cos k_2 \frac{\sin\left(\frac{\pi}{2L}(2N_F + 1)\right)}{\sin(\frac{\pi}{2L})} = \cos k t_0 \tag{4.43}$$

where we recover the expression of t_0, the homogeneous hopping term we found in Chapter 2. Moving on to the fifth contribution we find:

$$k - k_1 = -(k_2 + k) + 2\pi m \implies k = \frac{k_1 - k_2}{2} + \pi m$$

The only possible case is here with $m = 0$ defining sector 5 in figure 4.17. Since $q' = k_2 + k = \frac{k_1 + k_2}{2}$ the matrix elements read

$$V_5 = -\frac{v}{2L}\cos\left(\frac{k_1 + k_2}{2}\right) \tag{4.44}$$

One can easily see that in the Fock case the terms 6 and 7 give no contribution in the same way the terms 7 and 8 did in the Hartree case. The last term then gives us

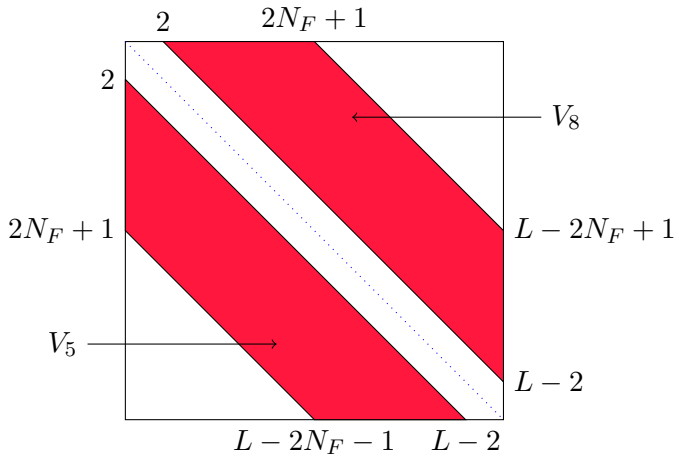

Figure 4.17: *Sectors 5 and 6 of the Fock self-energy matrix.*

$$k + k_1 = k_2 - k + 2\pi m \implies k = \frac{k_2 - k_1}{2} + \pi m$$

Again $m = 0$ is the value defining the sector 8 and being $q' = k_2 - k = \frac{k_1+k_2}{2}$ we have

$$V_8 = -\frac{v}{2L}\cos\Big(\frac{k_1+k_2}{2}\Big) \tag{4.45}$$

Self-energy matrix

We are finally able to put together every term we computed, in order to have a look at the whole structure of the self-energy matrix operator for $\eta < \frac{1}{2}$. We add up every term within its right sector and we end up with the self-energy matrix pictured in figure 4.18. As in the previous case, shift in the chemical potential due to the interaction has already been subtracted, and only the matrix elements guaranteeing an even value of $n \pm n'$ in the coloured sectors are non vanishing. We have

$$A = -\frac{v}{2L}\cos(k_1 - k_2) + \frac{v}{2L}\cos\Big(\frac{k_1+k_2}{2}\Big) \tag{4.46}$$

$$B_1 = A - \frac{v}{2L}\cos\Big(\frac{k_2-k_1}{2}\Big) + \frac{v}{2L}\cos(k_1+k_2) \tag{4.47}$$

$$B_2 = A + \frac{v}{2L}\cos\Big(\frac{k_2-k_1}{2}\Big) + \frac{v}{2L}\cos(k_1+k_2) \tag{4.48}$$

With this information we can have an insight on some features. A sharp discontinuity is still present along the lines $\gamma_1 : k_1 + k_2 = 2k_F$ and $\gamma_2 : k_1 + k_2 = 2(\pi - k_F)$. The height of the step along γ_1 is

$$\Delta_1 = \big[A - B_1\big]\Big|_{\gamma_1} = \frac{v}{2L}\Big[\cos(k_F - k_1) - \cos(2k_F)\Big] \tag{4.49}$$

while along γ_2 we have

$$\Delta_2 = \big[B_2 - A\big]\Big|_{\gamma_2} = \frac{v}{2L}\Big[\cos(\pi - k_F - k_1) + \cos(2k_F)\Big] \tag{4.50}$$

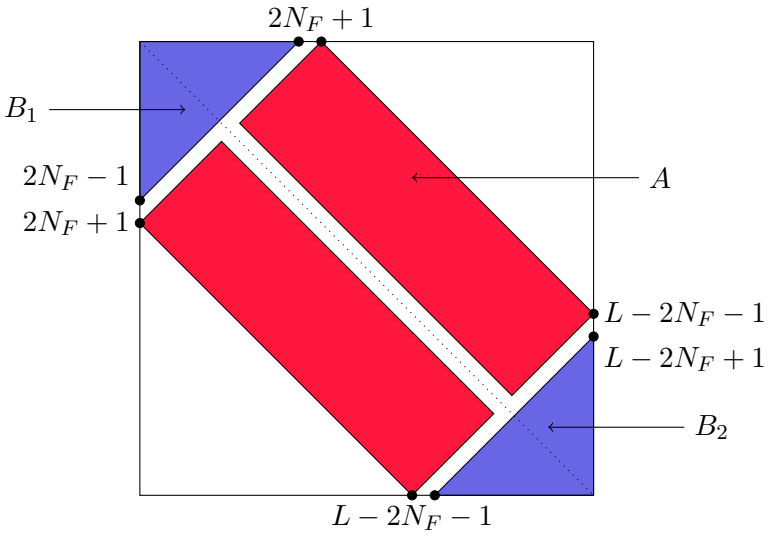

Figure 4.18: *Self-energy matrix in the Hartree-Fock approximation for the spinless fermions model with* $\eta < \frac{1}{2}$

Indeed the last expressions can be simplified and we observe that

$$\Delta_1 = \frac{v}{2L}\Big[\cos(k_F)\cos(k_1) + \sin(k_F)\sin(k_1) - \cos(2k_F)\Big] \tag{4.51}$$

$$\Delta_2 = \frac{v}{2L}\Big[-\cos(k_F)\cos(k_1) + \sin(k_F)\sin(k_1) + \cos(2k_F)\Big] \tag{4.52}$$

$$\Delta_2 = -\Delta_1 + \frac{v}{L}\sin(k_F)\sin(k_1)$$

We see from equation (4.50) that the height of the step function along γ_2 when evaluated in $k_1 = \pi - k_F$ shrinks to zero as we approach half filling, $k_F \to \frac{\pi}{2}$. Since its value is responsible for the power-law suppression in $\omega = -\mu$, we conclude this result is certainly consistent with the characterization of the spectral function we performed in Chapter 3. Notice the difference with respect to the Hubbard model: in this case the height of one step cannot be mapped onto the other one by simply swapping v to $-v$. This concludes the analysis for the case $\eta < \frac{1}{2}$.
This whole load of computations has been performed carefully also for the case $\eta > \frac{1}{2}$. As expected, it has been found that the sharp discontinuity along γ_1 slides towards the lower right corner of the matrix while the k-dependent height Δ_1 is left untouched under the mapping $\eta \to 1 - \eta$. The same fate is shared by the other discontinuity: as γ_2 moves upwards the term Δ_2 fades away when $\eta = 0.5$ but emerges with an identical value for $\eta > 0.5$.
In the next chapter we are going to employ this knowledge to extract information on the spectral density function. We will see that the first order perturbation theory is indeed capable of providing meaningful analytical results, consistently with what has been found numerically.

Chapter 5

First order perturbation for G

"And every song that I've ever heard
Is playing at the same time, it's absurd"
-Everything now, Arcade Fire-

As we understood in the previous chapter, knowing the exact structure of the self-energy operator in k-space allows us to extract analytical information about the spectral function through the relation

$$\big[G(\omega+i\eta)\big]_{nn'} = \frac{\delta_{nn'}}{\omega+i\eta+\epsilon_n} + \frac{\Sigma^{\mathrm{HF}}_{nn'}}{\big(\omega+i\eta-\epsilon_n\big)\big(\omega+i\eta-\epsilon_{n'}\big)} \tag{5.1}$$

It is therefore natural to define the quantity

$$\rho_1(j,\omega+i\eta) = -\frac{1}{\pi}\lim_{\eta\to 0^+}\mathrm{Im}\left[\sum_{nn'}\frac{1}{\omega+i\eta-\epsilon_n}\frac{1}{\omega+i\eta-\epsilon_{n'}}\langle j|n\rangle\langle n'|j\rangle\,\Sigma^{\mathrm{HF}}_{nn'}(\omega+i\eta)\right] \tag{5.2}$$

where as usual ϵ_n is the single-particle dispersion relation. This quantity denotes the first perturbative correction to the non-interacting local density of states ρ_0, already evaluated in Chapter 3. Before we dive into the maths for both models though, some considerations are needed on how to properly perform this computation.

5.1 Hubbard model

5.1.1 Effective model

Let us have a look at the terms involved in the sum in (5.2). As we have seen the structure of the self-energy is nontrivial, due to the presence of the boundaries in the system. For their nature, the other terms in the expression do not seem to make the task easier. As it is, there is no possibility to directly tackle the problem and evaluate this sum. Luckily, we also have no need to do it.
We follow the approach delineated in [6] and introduce an *effective model*. For our purpose, we consider the Hartree Hamiltonian where the diagonal contribution is subtracted, i.e. we work with

$$\tilde{\Sigma}^{\mathrm{H}} = \Sigma^{\mathrm{H}} - \delta\mu\mathbb{I} \tag{5.3}$$

where $\delta\mu$ denotes the shift in the chemical potential due to the interaction. We start by focusing on the behaviour of the spectral function close to the chemical at $\omega = \mu$. The computations will show that the appearance of a logarithmic divergence at the chemical potential in first order perturbation theory for the Green's function comes from the sharp step function crossing the diagonal in (N_F, N_F). Without modifying the low-energy properties then, the space of one-particle states can be shrunk to $n \in \{1, 2, ..2N_F\}$.
Also, for large systems, i.e $L \to \infty$, it is meaningful to work with a "coarse grained" version of $\tilde{\Sigma}^{\mathrm{H}}$, where *all* the matrix elements within the coloured area of figure 3.9 are non vanishing, but they have only half the size of the original ones. In this way, the problem of considering only even $n \pm n'$ is overcome. The effective self-energy for one spin population then reads

$$\Sigma^{\mathrm{eff}}_{nn'} = -\frac{u}{4L}\Theta(n + n' - 2N_F). \tag{5.4}$$

In order to obtain a continuous spectral function, we work in the thermodynamic limit, with non-interacting one particle eigenstates

$$\phi_{k_n}(j) = \langle j|\phi_{k_n}\rangle = \sqrt{\frac{2}{L}}\sin(k_n j)$$

and

$$\sum_n \to \frac{L}{\pi}\int dk$$

As we are interested in the spectral weight at the chemical potential, the one particle dispersion relation can be linearised around k_F

$$\epsilon(k) = v_F(k - k_F) + \epsilon(k_F) = v_F(k - k_F) + \mu \tag{5.5}$$

where μ denotes the chemical potential, heavily simplifying the computation we ought to perform. The old problem can now been recast in the more tractable form

$$\rho_1(j, \omega + i\eta) = -\frac{1}{\pi}\lim_{\eta\to 0^+}\mathrm{Im}\left[-\frac{u}{4L}\frac{2}{L}\frac{L^2}{\pi^2}\int_0^{2k_F} dk \int_0^{2k_F} dk' \frac{\Theta(k + k' - 2k_F)}{\omega + i\eta - v_F(k - k_F) - \mu}\frac{\sin(kj)\sin(k'j)}{\omega + i\eta - v_F(k' - k_F) - \mu}\right] \tag{5.6}$$

Of course the validity of this effective model is to be discussed once we see what result it can offer. The effective model we are working with can be pictured as in figure 5.1.

5.1.2 Analytical result

We start by evaluating the term:

$$\begin{aligned} G_1(j, \omega + i\eta) &= -\frac{u}{4}\frac{2}{\pi^2}\int_0^{2k_F} dk \int_0^{2k_F} dk' \frac{\Theta(k + k' - 2N_F)}{\omega + i\eta - \mu - v_F(k - k_F)}\frac{\sin(kj)\sin(k'j)}{\omega - \mu - v_F(k' - k_F)} \\ &= -\frac{u}{2\pi^2}\int_0^{2k_F} dk \frac{\sin(kj)}{\omega + i\eta - \mu - v_F(k - k_F)} \underbrace{\int_{2k_F - k}^{2k_F} dk' \frac{\sin(k'j)}{\omega + i\eta - \mu - v_F(k' - k_F)}}_{I} \end{aligned}$$

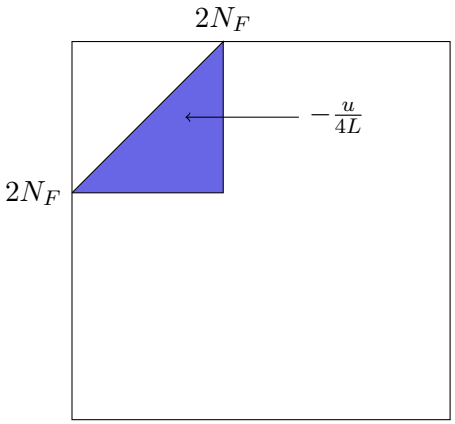

Figure 5.1: *Effective model for the Hartree self-energy in Hubbard model.*

and we first focus on the integral I. Since our interest is on the spectral weight at the chemical potential, we can approximate the sine function with its value in $k' = k_F$, and let it slide out of the integral

$$\begin{aligned} I &= \int_{2k_F-k}^{2k_F} dk' \sin(k'j)[\omega - \mu - v_F(k' - k_F)]^{-1} \\ &= \sin(k_F j) \int_{2k_F-k}^{2k_F} dk'[\omega - \mu - v_F(k' - k_F)]^{-1} \\ &= -\frac{\sin(k_F j)}{v_F} \log|\omega - \mu - v_F(k' - k_F)|\Big|_{2k_F-k}^{2k_F} \\ &= -\frac{\sin(k_F j)}{v_F}\Big[\log|\omega - \mu - v_F k_F| - \log|\omega - \mu - v_F k_F + v_F k|\Big] \end{aligned}$$

For $\omega \to \mu$ the first term in the last expression is constant. The second one leads to the aforementioned logarithmic divergence. Therefore, we can already neglect the first term and proceed with the computation. For the same reason we stated above, the second sine function is taken to be constant and we are left with

$$G_1(j, \omega + i\eta) = -\frac{u}{2\pi^2 v_F} \sin^2(k_F j) \int_0^{2k_F} dk \frac{1}{\omega + i\eta - \mu - v_F(k - k_F)} \log|\omega + i\eta - \mu - v_F k_F + v_F k|$$

We now take the limit of the imaginary part to extract the Dirac δ-function

$$\begin{aligned} \rho_1(j, \omega) &= -\frac{u}{2\pi^2 v_F} \sin^2(k_F j) \int_0^{2k_F} dk \delta\Big(\omega - \big[\mu + v_F(k - k_F)\big]\Big) \log|\omega - \mu - v_F k_F + v_F k| \\ \rho_1(j, \omega) &= -\frac{u}{2\pi^2 v_F} \sin^2(k_F j) \frac{1}{\left|\frac{d\epsilon}{dk}\right|_{k_0}} \int_0^{2k_F} dk \delta(k - k_0) \log|\omega - \mu - v_F k_F + v_F k| \\ &= -\frac{u}{2\pi^2 v_F} \sin^2(k_F j) \frac{1}{\left|\frac{d\epsilon}{dk}\right|_{k_0}} \log|\omega - \mu - v_F k_F + v_F k_0(\omega)| \end{aligned}$$

where $k_0(\omega)$ is given by

$$k_0 = k_F + \frac{(\omega - \mu)}{v_F} \tag{5.7}$$

In our linearised model, the derivative appearing in the denominator is exactly v_F, leaving us with

$$\rho_1(j,\omega) = -\frac{u}{2\pi^2 v_F^2}\sin^2(k_F j)\log|2(\omega-\mu)| \tag{5.8}$$

$$\rho_1(j,\omega) \simeq -\frac{u}{2\pi^2 v_F^2}\sin^2(k_F j)\log|\omega-\mu| \tag{5.9}$$

where in the last step we neglected a regular term. It is easy to see that the previous constant term we neglected during the computation would have led to a regular term, negligible when compared to the divergent one. To build up the total spectral density function we can simply take the last term twice, thanks to the symmetry in the spin variable. From Chapter 3 we now recall the relation

$$\rho_0(j,\omega\simeq\mu) = \frac{2\sin^2(k_F j)}{\pi v_F} \tag{5.10}$$

for the non interacting spectral density function. Moreover, being mainly interested in the site closest to the boundary $j = 1$, this expression simplifies further to

$$\rho_0(1,\omega\simeq\mu) = \frac{2\sin^2(k_F)}{\pi v_F} = \frac{v_F}{2\pi t^2} \tag{5.11}$$

and we can recast the the spectral function $\rho = \rho_0 + \rho_1$ in a more convenient form

$$\rho(1,\omega\simeq\mu) = \rho_0(1,\omega\simeq\mu)\left[1 - \frac{u}{2\pi v_F}\log|\omega-\mu|\right] + \text{regular terms} \tag{5.12}$$

5.1.3 Seizing the meaning of the divergence

In the first order perturbation theory for the Green's function then, the spectral density function presents a *logarithmic divergence* when approaching the chemical potential. The divergence is an artefact emerging in the perturbative approach to the matrix inversion, and it is not due to a singular frequency behaviour of Σ^H. We thus expect that this term and further divergent ones in the perturbative expansion can be summed to produce the power-law behaviour. For $\omega \to \mu$ in fact, the spectral function ρ^{H} obtained in the Hartree approximation for the self-energy can be written as a power-law and we observe that

$$\rho^{\mathrm{H}}(1,\omega\simeq\mu) = \rho_0(1,\omega\simeq\mu)|\omega-\mu|^{\alpha(u)} \tag{5.13}$$

$$= \rho_0(1,\omega\simeq\mu)e^{\alpha(u)\log|\omega-\mu|} \tag{5.14}$$

$$\simeq \rho_0(1,\omega\simeq\mu)\Big[1+\alpha(u)\log|\omega-\mu|\Big] \tag{5.15}$$

The prefactor of the logarithm we obtained in (5.12) is negative, and it is thus denoting an increase in the spectral weight for ω approaching μ. This is consistent with what we found in the full inversion of $\left[\omega + i\eta - \epsilon(k_n) - \Sigma^{\mathrm{H}}\right]$ presented in Chapter 3. The exponent for power-law increase was found to be

$$-\frac{u}{2\pi v_F} \tag{5.16}$$

which coincides with the prefactor of the logarithm we obtained analytically in (5.12).
On the other hand, for very small $|\omega-\mu|$ we know that ρ^{H} displays a power-law suppression with exponent

$$\frac{u}{2\pi v_F} \tag{5.17}$$

We deduce that in this model the first order perturbation theory for the Green's function at $\omega = \mu$ does not capture the eventual power-law suppression, which is known to set in at energies exponentially close to the chemical potential [6]. This is not surprising since for any perturbative approach to work, the perturbative correction must be small compared to the leading term. In our case this implies that $\log|\omega - \mu|$ must be small compared to 1, and for such $|\omega - \mu|$ one indeed finds an increase of the weight.

5.1.4 The dip at $\omega = -\mu$

From expression (3.13) the spectral weight at $\omega = -\mu$ is given by the square modulus of the matrix element $\langle j|L - N_F\rangle$ since

$$\epsilon(\pi - k_F) = -2t\cos(\pi - k_F) = +2t\cos(k_F) = -\mu \tag{5.18}$$

We then expect that the second step function in the self-energy matrix, the one crossing the diagonal in $(L - 1 - N_F, L - 1 - N_F)$, is responsible for the suppression appearing at $\omega = -\mu$. Therefore, to perform the computation we introduce an effective model in the same way it has been done in the previous case. In section 4.3.2 we analysed the symmetry of the Hartree self-energy matrix. For a fixed filling factor η, the height of the second step function can be mapped into the height of the first step by mapping $u \to -u$. For this reason, we expect that the HF approximation for the Green's function at $\omega = -\mu$ leads to the same result we obtained for $\omega = \mu$, provided we exchange u with $-u$. The effective self-energy we work with is

$$\Sigma^{\text{eff}}_{nn'} = +\frac{u}{4L}\Theta\big(n + n' - 2(L-1) + 2N_F)\big) \tag{5.19}$$

and it is restricted this time to the lower-right part of the matrix. The situation is sketched in figure 5.2.

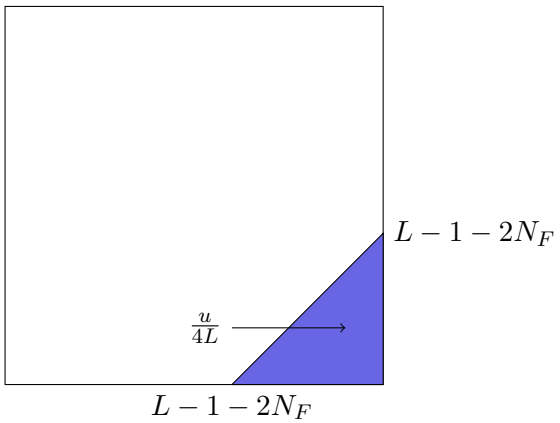

Figure 5.2: *Effective model for the Hartree self-energy in Hubbard model.*

In this case the dispersion relation can be linearised around the point $k = \pi - k_F$. Due to its symmetry, again the Fermi velocity appears

$$\epsilon(k) \simeq -\mu + 2t\sin(k)\Big|_{\pi - k_F}\big(k - (\pi - k_F)\big) = -\mu + v_F\big(k - (\pi - k_F)\big).$$

In the continuum limit, the integral to be performed reads

$$G_1(j,\omega+i\eta) = \frac{u}{4L}\frac{2}{\pi}\int_{\pi-2k_F}^{\pi} dk \int_{2\pi-2k_F-k}^{\pi} dk' \frac{\sin(kj)}{\omega+i\eta+\mu-v_F\big(k-(\pi-k_F)\big)}\frac{\sin(k'j)}{\omega+i\eta+\mu-v_F\big(k'-(\pi-k_F)\big)}$$

As we are now interested in the spectral weight at $\omega = -\mu$, the sine functions can be approximated with the value in $\sin(\pi - k_F) = \sin(k_F)$ and dragged out of the integral. As we expected, the integral is analogous to the one we already performed when μ is replaced by $-\mu$, the integration domain is shifted by $\pi - 2k_F$ in both axis k and k', and the map $u \to -u$ is performed. With the simple substitution

$$k = q + \pi - 2k_F \implies dk = dq$$

$$k' = q' + \pi - 2k_F \implies dk' = dq$$

The integration extremes are shifted back and we exactly restore the integral we worked out for the upper-left part of the matrix. It should then be clear that the result we obtain for the spectral density function close to $\omega = -\mu$ is

$$\rho(1,\omega \simeq -\mu) = \rho_0(1,\omega \simeq -\mu)\Big[1 + \frac{u}{2\pi v_F}\log|\omega-(-\mu)|\Big] + \text{regular terms} \tag{5.20}$$

The prefactor of the divergent term is in this case positive, denoting the suppression of the spectral weight instead of the increase we found for $\omega = \mu$. From (5.20) the prefactor we obtain is

$$\frac{u}{2\pi v_F}$$

which is exactly the exponent of the power-law suppression at $\omega = -\mu$ we extracted numerically from the full inversion of the HF Hamiltonian in Chapter 3. The HF approximation for the Green's function at $\omega = -\mu$ is then consistent with the HF approximation for the self-energy.
Notice that the suppression occurring at $\omega = -\mu$ can be traced down to the umklapp processes, which are responsible for of the non-analytical behaviour of Σ^{H} in $(\pi - k_F, \pi - k_F)$. We can conclude that the Hartree approximation for the Green's function is capable of providing meaningful results for the suppression appearing at an energy different from the Fermi energy.

5.2 Spinless fermions model

The work we have done on the Hubbard model for both the step functions is now helping us going through the analysis of the spinless fermions model. As in the previous case, for our purpose we work with an effective self-energy where the shift in the chemical potential due to the interaction is already subtracted. Again, we notice that the structure of the self-energy presents two lines along which the matrix elements display a sharp jump, crossing the diagonal in (N_F, N_F) and $(L-1-N_F, L-1-N_F)$. It will be shown that this lead to the suppression of the spectral weight at $\omega = \mu$ and $\omega = -\mu$. The main issue now is that we are not facing a "standard" step function, where the matrix elements assume a constant value before and after the step line. The nearest neighbour interaction in real space in this model is responsible for the appearance of a non trivial oscillating behaviour of the HF self-energy matrix elements in k-space as computed in Chapter 4. Understanding the crucial role of the non-analyticity and being guided by the successful results obtained for the Hubbard model, we introduce an effective model precisely as we already did.

5.2.1 The first dip

For the suppression appearing at $\omega = \mu$, we can shrink the integration domain to the same low-energy sector as this is not responsible for the emergence of a logarithmic divergence. To proceed we have to substitute the nontrivial expression of the the matrix elements given in (4.46) and (4.47) for a standard Θ function as in the effective self-energy for the Hubbard model. At a first glance though, it is not obvious which value one should choose for the height of the step. We are interested in the spectral weight close to $\omega = \mu$ so that the important point to be considered is (k_F, k_F). The step crossing the diagonal in this point is responsible for the appearance of the logarithmic divergence. We therefore take for the effective model a Θ function where the height is equal to the proper height of the step evaluated in (k_F, k_F). From equation (4.49) this reads

$$\Delta_1 = 1 - \cos(2k_F) \tag{5.21}$$

Once the step function is set to be formally identical to the Hubbard case, we proceed in the same way in the construction of the effective model. The effective HF self-energy we work with is

$$\Sigma^{\text{eff}}_{nn'} = \frac{v}{4L}\Delta_1 \Theta(n + n' - 2N_F). \tag{5.22}$$

A sketch is given in figure 5.3.

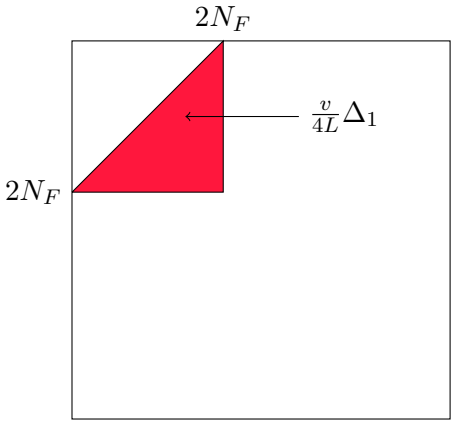

Figure 5.3: *Effective model for the Hartree-Fock self-energy in the spinless fermions model.*

Taking the thermodynamic limit we eventually want to evaluate the integral:

$$\rho_1(j, \omega + i\eta) = -\frac{1}{\pi}\lim_{\eta\to 0^+} \text{Im}\left[-\frac{\Delta_1 v}{L}\frac{2}{L}\frac{L^2}{\pi^2}\int_0^{2k_F} dk \int_0^{2k_F} dk' \frac{\Theta(k + k' - 2k_F)}{\omega + i\eta - \mu - v_F(k - k_F)} \frac{\sin(kj)\sin(k'j)}{\omega + i\eta - \mu - v_F(k' - k_F)}\right]$$

The computation is then formally identical, and for ω approaching μ we can finally obtain

$$\rho_1(1, \omega \simeq \mu) = \frac{v}{\pi v_F}\Big[1 - \cos(2k_F)\Big]\rho_0(1, \omega \simeq \mu)\log|\omega - \mu| + \text{regular terms} \tag{5.23}$$

$$\rho_1(1, \omega \simeq \mu) = \frac{v}{\pi v_F}\Big[2\sin^2(k_F)\Big]\rho_0(1, \omega \simeq \mu)\log|\omega - \mu| + \text{regular terms} \tag{5.24}$$

Thanks to the definition of v_F, the function $\rho = \rho_0 + \rho_1$ can be recast in the form

$$\rho(1, \omega \simeq \mu) = \rho_0(1, \omega \simeq \mu)\left[1 + \frac{v}{\pi t}\sin(k_F)\log|\omega - \mu|\right] + \text{regular terms} \tag{5.25}$$

Furthermore, one can define

$$|v_c| = \frac{\pi t}{\sin(k_F)} \tag{5.26}$$

to end up with the more elegant form

$$\rho(1, \omega \simeq \mu) = \rho_0(1, \omega \simeq \mu)\left[1 + \frac{v}{|v_c|}\log|\omega - \mu|\right] + \text{regular terms} \tag{5.27}$$

As we expected from an effective model formally identical to the one employed in the Hubbard case, a logarithmic divergence is found at $\omega = \mu$. In this case the prefactor of the logarithm reads

$$\alpha = \frac{v}{|v_c|} = \frac{v}{\pi t}\sin(k_F) \tag{5.28}$$

This result is to be compared with the HF exponent α_B^{HF} we can extract from the full inversion of the HF Hamiltonian. The results are shown in figure 5.4. The exponent α_B^{HF} together with its error is extracted from the numerical data with same procedure employed for the Hubbard model and presented in Chapter 3. For $v > 0$ the prefactor α is positive, correctly denoting a suppression in the spectral weight at energies approaching the chemical potential. Remarkably, α is the *exact* leading behaviour in the expansion of $\alpha_B^{\mathrm{HF}}(v)$ for small v. In figure 5.4 the solid line representing α perfectly matches the tangent of $\alpha_B^{\mathrm{HF}}(v)$ in $v = 0$. As in this computation the analytical prefactor is determined by the height of the step function crossing the diagonal in (k_F, k_F), this result validates the choice to employ Δ_1 in this effective model.
We have thus been able to compute analytically the correct leading term of the HF boundary exponent. This let us conclude that first order perturbation theory for the Green's function provides meaningful results at $\omega = \mu$. The deviation of α_B^{HF} from linear behaviour is to be traced back to the summation of higher order terms in the perturbative expansion. These terms in fact do provide $\alpha_B^{\mathrm{HF}}(v)$ with higher powers of v. A guess function has been made to fit the numerical exponent and reads

$$\alpha_B^{\mathrm{HF}}(v) = \frac{\zeta}{1+\zeta} \qquad \text{where} \qquad \zeta = \frac{v}{|v_c|}$$

This function has been proven extremely precise, and it is therefore plotted across the numerical data in figure 5.4. For the sake of completeness it is to be clarified that even the HF approximation for the self-energy can only provide the correct leading behaviour of the exact exponent α_B. This is to be obtained by the means of different techniques, e.g. DMRG or bosonization as in [6].

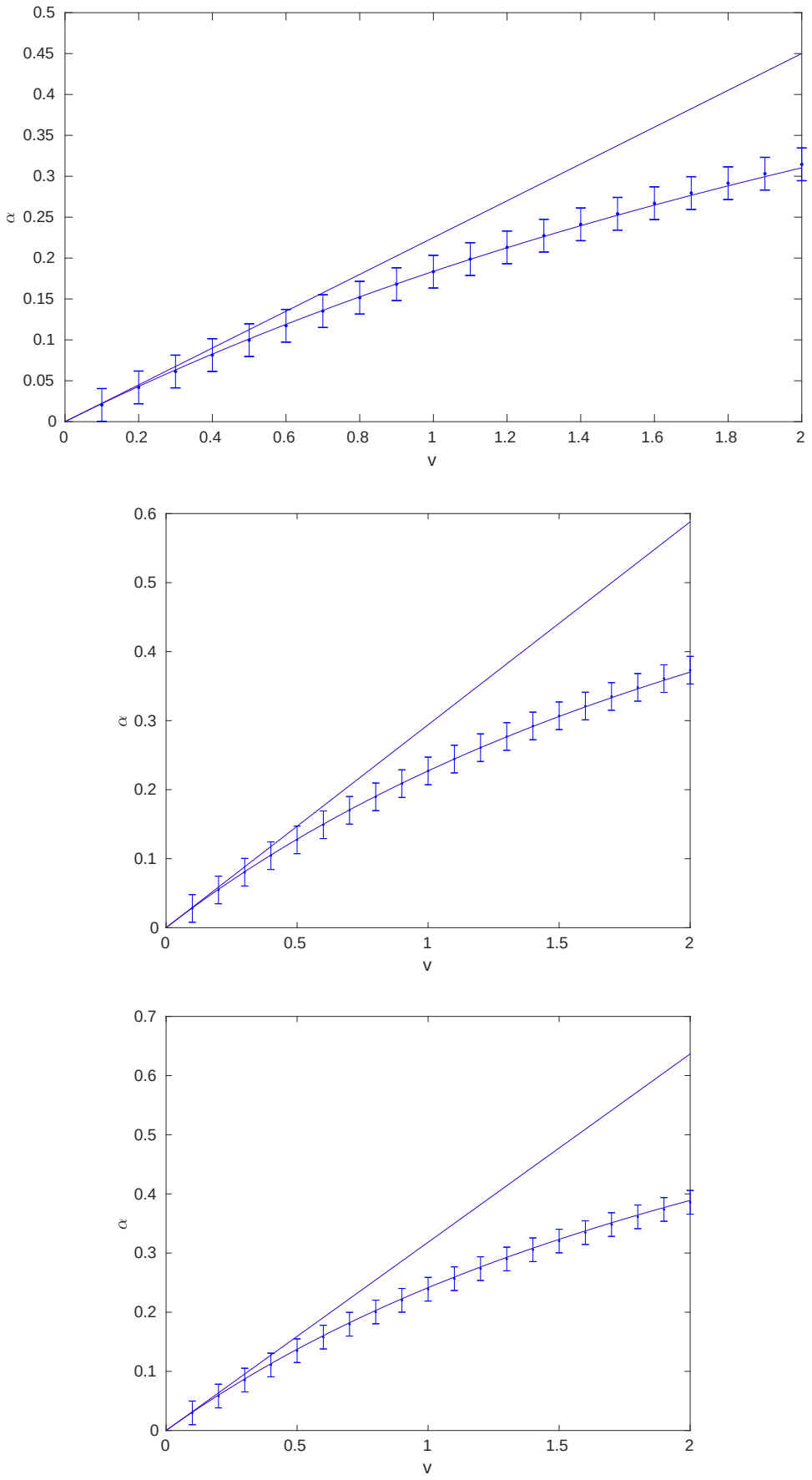

Figure 5.4: *Analytical prefactor* α *(solid straight line) compared with* α_B^{HF} *(numerical data). Here* $L-1=4000$*, and from top to bottom* $\eta=0.25$*,* $\eta=0.375$*,* $\eta=0.5$*. For details, see the text.*

5.2.2 The second dip

We now investigate the suppression of the spectral weight appearing at $\omega = -\mu$, which is caused, as in the Hubbard model, by the sharp step function in the HF self-energy matrix crossing the diagonal in $(\pi - k_F, \pi - k_F)$. We perform the HF approximation for the Green's function by introducing an effective model in analogy to the one employed for the second dip in the Hubbard model. The effective model is pictured in figure 5.5.
Motivated by the successful results obtained for the dip at $\omega = \mu$ in the spinless fermions model, a "standard" step function is used, where the height of the step is now chosen to be the proper height of the step evaluated in $(\pi - k_F, \pi - k_F)$. From the expression (4.50) evaluated in Chapter 4 we have

$$\Delta_2 = 1 + \cos(2k_F) \tag{5.29}$$

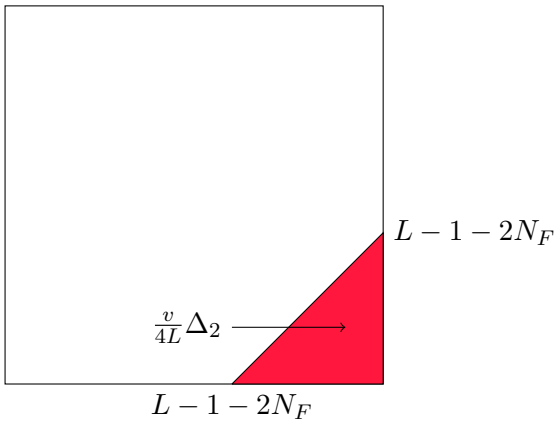

Figure 5.5: *Effective model for the Hartree-Fock self-energy in the spinless fermions model.*

The computations are formally identical and we finally obtain

$$\rho_1(1, \omega \simeq -\mu) = \frac{v}{\pi v_F}\Big[1 + \cos(2k_F)\Big]\rho_0(1, \omega \simeq -\mu)\log|\omega + \mu| + \text{regular terms} \tag{5.30}$$

Some quick rearrangements leave us with

$$\rho(1, \omega \simeq -\mu) = \rho_0(1, \omega \simeq -\mu)\left[1 + \frac{v}{\pi t}\frac{\cos^2(k_F)}{\sin(k_F)}\log|\omega + \mu|\right] + \text{regular terms} \tag{5.31}$$

To put it in more elegant form we define

$$|v_c'| = \frac{\pi t \sin(k_F)}{\cos^2(k_F)} = |v_c|\tan^2(k_F) \tag{5.32}$$

and recast our result as

$$\rho(1, \omega \simeq -\mu) = \rho_0(1, \omega \simeq -\mu)\left[1 + \frac{v}{|v_c|}\frac{1}{\tan^2(k_F)}\log|\omega + \mu|\right] + \text{regular terms} \tag{5.33}$$

Notice that the prefactor vanishes as $k_F \to \frac{\pi}{2}$, consistently with our analysis of the step along γ_2 in the self-energy. In figure 5.6 this result is compared with the HF exponent α_B^{HF} at $\omega = -\mu$ we extracted numerically from the full inversion of the HF Hamiltonian. In analogy to the previous case, the prefactor we obtained analytically is the correct leading term in the expansion of $\alpha_B^{\text{HF}}(v)$ for small v. Again, this validates the choice to employ Δ_2 as the correct effective height of the step leading to the suppression at $\omega = -\mu$.

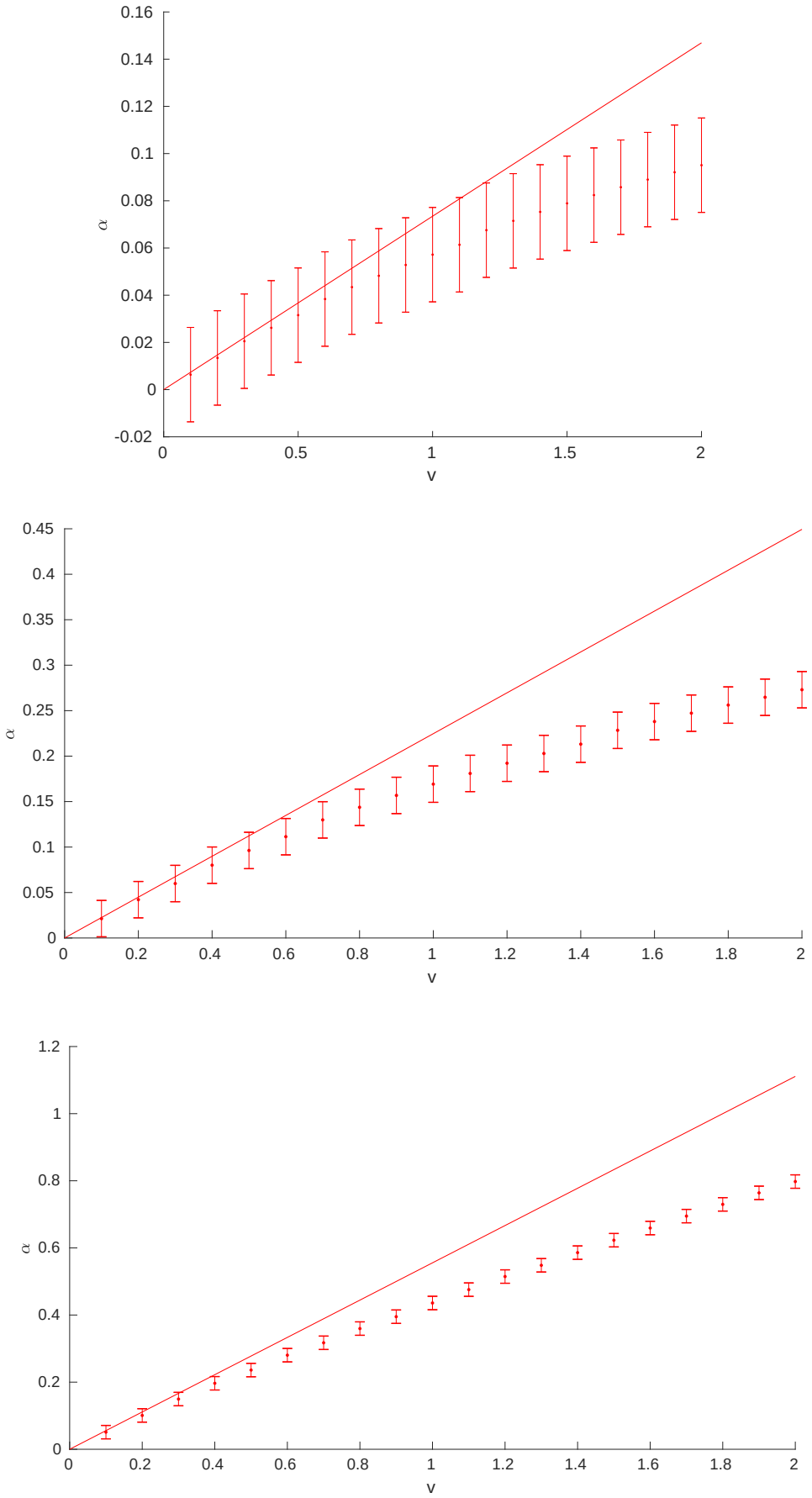

Figure 5.6: *Analytical prefactor* α *(solid line) compared with* α_B^{HF} *(numerical data). Here* $L-1=4000$*, and from top to bottom* $\eta=0.65$*,* $\eta=0.75$*,* $\eta=0.85$*. For details, see the text.*

5.3 Recursive method for exact mean field exponent

In this last section we want to provide a noticeable and clever method allowing us to extract analytically the behaviour of the exponent as a function of the interaction term. This method is taken from the Diploma thesis of Ralf Hedden.
Given the one particle nature of the problem in the mean field approximation, we can make use of a recursive method to obtain the wave function at the chemical potential

$$\phi_{k(\mu)}(j) \tag{5.34}$$

In fact, recalling the expression for the local spectral function

$$\rho(j,\omega) = \sum_k \phi_k^*(j)\phi_k(j)\delta(\epsilon(k)-\omega) \tag{5.35}$$

we notice that the quantity of our interest is

$$\rho(1,\mu) = \phi_{k(\mu)}^*(1)\phi_{k(\mu)}(1)\frac{1}{\left|\frac{d\epsilon(k)}{dk}\right|_{k=k(\mu)}} \tag{5.36}$$

Thus the knowledge of the wavefunction in (5.34) is essential. To achieve this task, we first modify the lattice spinless fermions model we used so far. We now work with a semi-infinite chain, whose sites span from $j=1$ to ∞. The nearest neighbour interaction is however limited to the first $N+1$ sites of the chain. This has two major advantages. On one hand we simplify the terms in mean field Hamiltonian for $N\to\infty$. On the other, the eigenvalues are condensed into a continuum set of values, guaranteeing us the existence of the eigenfunction at the chemical potential in (5.34). Also, this procedure is carried out for the specific case of a system at half-filling $\eta=\frac{1}{2}$. With this consideration the mean field Hamiltonian reads

$$H^{\mathrm{MF}} = -t_0\sum_{j=1}^{\infty} c_{j+1}^\dagger c_j + \text{h.c.} + \sum_{j=1}^{N}\frac{v}{\pi}\frac{(-1)^j}{2j+1}c_{j+1}^\dagger c_j + \text{h.c.} + v\sum_{j=1}^{\infty} n_j \tag{5.37}$$

where now

$$t_0 = t + \frac{v\sin(\pi\eta)}{\pi} = t + \frac{v}{\pi} \tag{5.38}$$

is the renormalized homogeneous hopping. The inhomogeneous hopping term is exactly modelling the algebraic decaying oscillation we found in Chapter 2, as for a system at half-filling

$$-t_1(j) = v\frac{\sin(2k_F j)}{\pi(2\pi+j} = v\frac{\sin(\pi j)}{\pi(2\pi+j)} = \frac{v}{\pi}\frac{(-1)^j}{2j+1} \tag{5.39}$$

For the eigenfunction we look for, the following relation holds

$$H^{\mathrm{MF}}\phi_{k(\mu)} = \mu\phi_{k(\mu)} \tag{5.40}$$

The mean field Hamiltonian is tridiagonal, and denoting $\phi_{k(\mu)}=\phi$ for simplicity, we can write

$$
\begin{aligned}
\frac{v}{2}\phi(1) - t_1\phi(2) &= \mu\phi(1) \\
-t_1\phi(1) + v\phi(2) - t_2\phi(3) &= \mu\phi(2) \\
&\vdots \\
-t_{n-1}\phi(n-1) + v\phi(n) - t_{n+1}\phi(n+1) &= \mu\phi(n) \\
&\vdots \\
-t_N\phi(N) + v\phi(N+1) - t_0\phi(N+2) &= \mu\phi(N+1) \\
\\
-t_0\phi(N+1) + v\phi(N+2) - t_0\phi(N+3) &= \mu\phi(N+2) \\
&\vdots
\end{aligned}
$$

where

$$
t_n = \frac{v}{\pi}\frac{(-1)^n}{2n+1} \tag{5.41}
$$

At half-filling the chemical potential reads

$$
\mu = v \tag{5.42}
$$

We then obtain

$$
\begin{aligned}
\phi(2) &= -\frac{v}{2t_1}\phi(1) \\
\phi(3) &= -\frac{t_1}{t_2}\phi(1) \\
&\vdots \\
\phi(n+1) &= -\frac{t_{n-1}}{t_n}\phi(n-1) \\
&\vdots \\
\phi(N+2) &= -\frac{t_N}{t_n}\phi(N) \\
&\vdots
\end{aligned}
$$

so that for $2n+1 \leq N$ we can write

$$
\phi(2n+1) = (-1)^n\phi(1)\prod_{l=1}^{l=m}\frac{t_{2l-1}}{t_{2l}} \tag{5.43}
$$

$$
\phi(2n) = (-1)^{n+1}\frac{v}{2t_1}\phi(1)\prod_{l=1}^{l=m}\frac{t_{2l-2}}{t_{2l-1}} \tag{5.44}
$$

For $2n+1 \geq N+1$ the eigenfunction does not change considerably and oscillates between the values $\pm\phi(N+1)$ and $\pm\phi(N+2)$. For large N the local spectral function at the chemical potential is approximated by

$$\left[|\phi(N+1)|^2 + |\phi(N+2)|^2\right]^{-1} \tag{5.45}$$

We can set $m = \frac{N}{2}$ and evaluate the last expression by taking the $\log_N$ of the product to obtain

$$\phi(N+1) \sim (-1)^{\frac{N}{2}} \phi(1) N^{\frac{v}{2\pi t_0}} \qquad \phi(N+2) \sim \frac{v}{2t_0}(-1)^{\frac{N}{2}} \phi(1) N^{-\frac{v}{2\pi t_0}} \tag{5.46}$$

From (5.45) we then have

$$\rho(1,\mu) \sim \left[N^{\frac{v}{\pi t_0}} + N^{-\frac{v}{2\pi t_0}}\right]^{-1} \tag{5.47}$$

As we only consider here repulsive interaction $v > 0$, for large values of N the positive exponent is dominating and results in

$$\rho(1,\mu) \sim \left[\frac{1}{N}\right]^{\frac{v}{\pi t + v}} \tag{5.48}$$

so that

$$\alpha^{\mathrm{MF}} = \frac{v}{\pi t + v} \tag{5.49}$$

We have eventually found analytically the mean field exponent for the suppression of states at site $j = 1$ for the special case $\eta = \frac{1}{2}$. This function justifies the guess we have made for the behaviour of the aforementioned exponent for every filling factor η, which has proven to be in great agreement with the numerical data. An attempt has been made in order to extend the present recursive method for different fillings. We did not succeed due to the lack of the essential simplification in (5.42).

Conclusion

The theoretical expectation that a LL chain with impurities will, at low energies, behave as if it is cut into several disconnected pieces with open ends led to the investigation of several LL models with open boundary condition. In this work we focused our attention on the particular behaviour of the local spectral function close to the open boundary.
We verified that the HF approximation for the electron self-energy already gives power-law behaviour at two distinct energies $\omega = \mu$ and $\omega = -\mu$, which is a clear signature of the LL physics. In the Hubbard model for energies approaching the chemical potential from below, the spectral weight first increases as a power law. At energies exponentially close to the chemical potential the spectral function exhibits a crossover, and a final power-law suppression sets in. On the contrary, at $\omega = -\mu$ no enhancement of the spectral weight is present, and the spectral function only exhibits a power-law suppression. Our results are in agreement with the ones presented in [6]. In the spinless fermions model the local spectral function displays power-law suppression with *different* exponents at the aforementioned energies. The HF boundary exponent at $\omega = \mu$ we extracted from the numerical data has been verified to be in perfect agreement with the one presented in [6].
The physical reason for the power-law suppression in the spectral function emerged while evaluating the HF self-energy matrix elements in k-space. For both models the self-energy displays two sharp step functions crossing the diagonal in (k_F, k_F) and $(\pi - k_F, \pi - k_F)$. These non-analytical structures respectively lead to the suppression of the spectral weight at $\omega = \mu$ and $\omega = -\mu$. This analysis also showed that the second dip is caused by the umklapp processes.
The introduction of an effective model allowed us to perform the first order perturbation theory for the Green's function, wherein a logarithmic divergence in the spectral function is found at the aforementioned energies. We demonstrated that this divergence is consistent with the power-law previously obtained numerically. In fact, the HF approximation for the self-energy is a sum over *infinitely many* diagrams in a Dyson series, which eventually develops the power law. A logarithmic divergence is the best we can expect when truncating the series to the first order, as shown in section 5.1.3.
For the repulsive Hubbard model the prefactor of the logarithm at $\omega = \mu$ is negative, denoting the increase in the spectral weight for large energies around the chemical potential. Thereafter, the HF approximation for the Green's function at $\omega = \mu$ is only correct to linear order in the interaction, and it does not capture the eventual power-law suppression setting in at energies asymptotically close to the chemical potential. The prefactor at $\omega = -\mu$ is the correct HF boundary exponent for the power-law suppression at $\omega = -\mu$. Noticeably, for the spinless fermions model at both energies the prefactor of the logarithm is the correct leading order of the HF boundary exponent for small interaction.
We therefore confirmed that perturbation theory is capable of providing meaningful results for the spectral properties of LL lattice models with open boundaries, as presented in [6]. The new results concern the analysis of the dip appearing at $\omega = -\mu$ in the spectral function for the spinless fermions model. Within the HF approximation for the self-energy, the power-law suppression has been characterized numerically for diverse sets of parameters such as interaction strength and filling factor. Furthermore, the effective model employed for the Hubbard case in [6] has been extended to the spinless fermions model successfully. This allowed us to obtain analytically the leading order of the HF exponent for both the suppression at $\omega = \mu$ and the one at $\omega = -\mu$.

Acknowledgements

I profoundly thank Professor Volker Meden for allowing this amazing experience to come to life. I thank him for all the precious help he gave me, the patience and the time spent in guiding me throughout the project.
I am grateful to Professor Maurizio Zani, whose incommensurable passion for Physics and teaching ignited mine, and for being always a role model to me, and to Professor Sandro Salsa, who showed me the beauty of Mathematics. My gratitude goes to Professor Roberto Piazza for his wonderful lectures on Statistical Physics, for the time he spent explaining things in detail to me, and for patiently answering to all my questions. He turned my interest into profound passion and motivated me to take this path. I will be always grateful for this and all the help he keeps on giving me.
I thank my flatmates in Aachen, Georgi, Ahmed and Kathy, for being always there when I needed some help. A special thank goes to Georgi and Ahmed, for the very serious discussions we had and for the less serious ones, for all the memorable moments when we cry-laughed, for sharing their path with me, and being real, exceptional friends. I thank all the incredible people I met during my time in Aachen for the strong connections we made, which will defeat time and space, the whole Capoeira group and Mestre Lagosta for his passion and enthusiasm in the trainings.
Also, I want to thank the bike the Universe kindly gave me a few days after my arrival - you know, sometimes you just need to ask -. This experience wouldn't have been the same without her.
Some things then have a life on their own in the original language, and the reader would forgive me if I present the last acknowledgements in Italian. Indeed, it could be a good motivation to start learning it.

Ringrazio tutte le persone che hanno condiviso con me una parte del percorso fatto fino a qui. Grazie alle persone che in questi anni hanno vissuto con me e mi hanno dato tantissimo. Ringrazio Luca per tutto quello che abbiamo condiviso assieme, Simone per un'amicizia unica e meravigliosa, Federico per tutto quello che mi ha insegnato e per essere sempre pronto ad aiutare. Ringrazio Martina, Stefania, Giada, Sophie e Matteo per aver vissuto con me a Padova e per i momenti meravigliosi passati assieme. In particolare Stefy per essere diventata davvero una sorella, Marty per essere sempre disponibile a dare una mano, Matte per le discussioni di fisica e non.
Ringrazio Edo, Michele, Cate, Yle, Gianluca e i vinili di Gianluca per i momenti stupendi ad Aachen, Erika per l'aiuto nei momenti difficili, Lucia, Isabella, Alberto, Leonardo, Francesca, Elena per sapermi ascoltare e per i consigli preziosi, gli amici di una vita Matteo, Francesco, Nicola, per un'amicizia grandiosa e inossidabile, Giulio Candre per la possibilità di condividere domande cosmiche, Giulio Frank che mi ha insegnato che il mondo si può cambiare e non bisogna mai mollare, e Marco Poz che mi ha insegnato a non smettere mai di sognare. Un ringraziamento speciale a Greta che ha saputo aiutarmi davvero nelle difficoltà di questi ultimi mesi, mio cugino Filippo, e tutta la mia famiglia che ha reso possibile tutto questo.

Bibliography

[1] J. Voit. One-dimensional Fermi liquids. *Reports on Progress in Physics*, 58(9):977–1116, sep 1995.

[2] T. Giamarchi. *Quantum Physics in One Dimension*. Clarendon Press, 2003.

[3] G. Vignale G. Giuliani. *Quantum Theory of the Electron Liquid*. Cambridge University Press, 2008.

[4] J. Voit. A brief introduction to Luttinger liquids. *AIP Conference Proceedings*, 544(1):309–318, 2000.

[5] Schönhammer K. Luttinger liquids: the basic concepts. *In: Baeriswyl D., Degiorgi L. (eds) Strong interactions in low dimensions. Physics and Chemistry of Materials with Low-Dimens*, 25, 2004.

[6] U. Schollwöck O. Schneider T. Stauber K. Schönhammer V. Meden, W. Metzner. Luttinger liquids with boundaries: Power-laws and energy scales. *Eur. Phys. J. B*, 16:631, (2000).

[7] Dongxiao Yue, L. I. Glazman, and K. A. Matveev. Conduction of a weakly interacting one-dimensional electron gas through a single barrier. *Phys. Rev. B*, 49:1966–1975, Jan 1994.

[8] Alexander Altland and Ben D. Simons. *Condensed Matter Field Theory*. Cambridge University Press, 2 edition, 2010.

[9] A.L. Fetter and J.D. Walecka. *Quantum Theory of Many-particle Systems*. Dover Books on Physics. Dover Publications, 2003.

[10] J.W. Negele and H. Orland. *Quantum many-particle systems*. Frontiers in physics. Addison-Wesley Pub. Co., 1988.

[11] T. Giamarchi. Some experimental test of Tomonaga-Luttinger liquids. *International Journal of Modern Physics B*, 26(22):1244004, 2012.

[12] R.D. Mattuck. *A Guide to Feynman Diagrams in the Many-body Problem*. Dover Books on Physics Series. Dover Publications, 1992.

[13] V. Meden K. Schönhammer X. Barnabé-Thériault, A. Sedeki. Junctions of one-dimensional quantum wires: Correlation effects in transport. *Phys. Rev. B*, 71, (2005).

[14] V. Meden D. Schuricht, S. Andergassen. Local spectral properties of Luttinger liquids: scaling versus nonuniversal energy scales. *J. Phys.: Condens. Matter*, 25, (2012).

[15] Jun Sato Masanori Kohno, Mitsuhiro Arikawa and Kazumitsu Sakai. Spectral properties of interacting one-dimensional spinless fermions. *J. Phys. Soc. Jpn.*, 79, (2010).

[16] Jean-Sébastien Caux and Cristiane Morais Smith. Celebrating Haldane's 'Luttinger liquid theory'. *Journal of Physics: Condensed Matter*, 29(15):151001, mar 2017.

[17] V. Meden, W. Metzner, U. Schollwöck, and K. Schönhammer. Scaling behavior of impurities in mesoscopic Luttinger liquids. *Phys. Rev. B*, 65:045318, Jan 2002.

[18] G. Grosso and G.P. Parravicini. *Solid State Physics*. Elsevier Science, 2000.